DLR-IB-AS-BS-2020-25

Coupling strategies for solving the RANS equations

Forschungsbericht

Autor
Guillermo Suárez Martínez

Deutsches Zentrum
DLR für Luft- und Raumfahrt

Bericht des Instituts für Aerodynamik und Strömungstechnik
Report of the Institute of Aerodynamics and Flow Technology

DLR-IB-AS-BS-2020-25

Coupling strategies for solving the RANS equations

Guillermo Suárez Martínez

Herausgeber:
Deutsches Zentrum für Luft- und Raumfahrt e.V.
Institut für Aerodynamik und Strömungstechnik
Lilienthalplatz 7, 38108 Braunschweig

ISSN 1614-7790

Stufe der Zugänglichkeit: 1
Braunschweig, im Februar 2020

Institutsdirektor:
Prof. Dr.-Ing. habil. C.-C. Rossow

Verfasser:
Guillermo Suárez Martínez

Abteilung: Center of Computer Applications in Aerospace Science and Engineering

Abteilungsleiter:
Prof. Dr. S. Görtz

Der Bericht enthält:
92 Seiten
27 Bilder
13 Tabellen
43 Literaturstellen

Coupling strategies for solving the RANS equations

BY

Guillermo Suárez Martínez

DIPLOMA THESIS FOR DEGREE

Master in Aerospace Science and Technology

AT

Universitat Politècnica de Catalunya

SUPERVISED BY:

PD Dr. Stefan Langer

Dr. Fernando Mellibovsky

Physics Department, Aerospace Engineering Division

Acknowledgments

First of all, I would like to express my gratitude to my supervisor Dr. habil. Stefan Langer at the Center for Computer Applications in AeroSpace Science and Engineering located in the Institute of Aerodynamics and Flow Technology within the Deutschen Zentrums für Luft- und Raumfahrt (DLR). I thank him for giving me this opportunity to work on this project and for making this highly enriching and valuable experience possible.

Finally, I gratefully acknowledge the DLR for the funding I received during this period.

Abstract

For the present work two implicit methods of coupling the compressible Reynolds Averaged Navier-Stokes equations in conjunction with the one equation Spalart-Allmaras turbulence model have been developed. The first approach, known as fully coupled technique, strongly couples the two different systems of equations, and accordingly solves for a single system. The second technique has been defined as weakly coupled approach. On the one hand, it also solves for a single set of equations. On the other hand, the full Jacobian is not build by excluding the evaluation of the cross derivatives. The latter approach must be understood in the sense of an intermediate step between the loosely and fully coupled techniques, allowing to evaluate the coupling solution strategy. The subject of this thesis is to examine whether it is advantageous to solve the systems of equations in a mathematically consistent coupled manner or loosely coupled. For the space discretization, an unstructured finite volume scheme based on node-centered dual mesh is used. The solution procedure is based on a nonlinear agglomeration multigrid technique combined with a multistage line implicit Runge-Kutta smoother. The inner system of equations is solved through a Block Symmetric Gauss-Seidel scheme. The assessment of the newly developed methodologies is obtained by a comparative study with a loosely coupled solution strategy along with experimental data. The attention is focused on the accuracy of the results, the number of overall cycles and convergence rates of the solution method. Several numerical computations have been carried out in four two-dimensional and three-dimensional well known benchmark test cases: the CASE 9, MDA30P30N, DPW5CRM and the NASA Trap Wing. The obtained results evidence that no improvement is obtained regarding accuracy but demonstrate superiorities and inferiorities in the convergence rate for the weakly coupled and fully coupled strategies.

Contents

List of Figures

List of Tables

Chapter 1

INTRODUCTION

Computational Fluid Dynamics (CFD) is a key technology for future aircraft development. The capabilities of this numerical simulation tool allow to accurately predict the fluid properties surrounding an aircraft with relative little costs when compared to wind-tunnel testing or even real physical tests. Therefore, CFD allows for more flexibility, and consequently larger number of design studies, analysis and further improvements can be carried out, such as noise reduction, flight envelope optimization and design of critical concepts. That is the reason why its usage in industry has considerably grown during the last decades.

However, CFD codes are rather far from being consolidated as a rigorous design tool, i.e., make use of wind tunnels merely for verification. One of the main contributors are the several limitations inherent in CFD codes. Because of that, there is a challenge to develop more efficient and robust codes for foreseeable complex applications. The design of such solvers is strictly achieved by the understanding of the governing equations describing the motion of fluid flows as well as the implemented numerical techniques to approximately solve them. With that knowledge, major work can be done to improve the solution procedures to overcome the difficulties of the CFD techniques. For example, something to consider is the implementation of assumptions and advanced reliable techniques for the solution algorithms which allow to develop faster and/or more robust codes. Nevertheless, still exists a lack of knowledge regarding these aspects. In particular, the topic concerning the different perspectives to solve the governing equations is still unclear and under discussion.

1.1. Problem description

The vast majority of applications in the aerospace industry are subject to complex flow conditions with high associated Reynolds numbers, and consequently they are dominated by turbulent flows. Turbulence is characterized by an irregular and highly random motion driven by complex turbulent structures. These structures describe a highly irregular flow field in space and unsteady behavior in time.

Naturally, in order to achieve a level of accuracy when numerically solving the conservation equations, known as Navier-Stokes (NS) equations, on the aforementioned situations, it is imperative to capture the smallest length and time scales from these structures. The direct approach for solving those equations is the Direct Numerical Simulation (DNS). This technique allows for straightforward procedures when resolving the NS equations, however, it presents several issues and limitations for dealing with turbulent flows. Its main drawback is the required spatial and time resolutions. They have to be sufficiently small to capture the essential characteristics of the flow, resulting in high computational resources demand, even for present day high performance computers. As an overall, this makes DNS an inefficient approach to solve turbulent flows for practical engineering applications.

Considering the complexity and nature of the flow, different mathematical techniques such as Detached- and Large-Eddy Simulation (DES and LES) and Reynolds Averaged Navier-Stokes (RANS) equations have been developed as an alternative solution. Reynolds Averaging is a very well known approach which allows for a practical implementation of numerical techniques when dealing with turbulent flows. Within this procedure, the flow variables are decomposed into a mean and a fluctuating component. Then, the averaging process is applied to the resulting equations whereby the fluctuations are removed, which allows to treat the equations as a mean continuum flow. As a counterpart, the averaging process gives rise to more unknowns, the turbulent kinetic energy and eddy viscosity, resulting in an undefined system of equations, i.e., more unknowns than equations. Because of these additional unknowns, further equations are required for closing the problem, the so-called closure of the problem. These additional amended equations are provided by a turbulence model.

A turbulence model is a conceptual model that approximates the essence of the turbulent flow behavior, and accordingly introduces and accounts for the turbulent effect into the Reynolds Averaged Navier-Stokes equations. Although it has been derived by an heuristic process, it is suffice accurate to describe the flow field for the desired range of applicability. Mathematically, it formulates an additional system of governing equations employing a set of artificial variables, which are then related to the RANS equations for the determination of the emerged unknowns.

Going into more details about this problem and accordingly to the previous exposition, from a mathematical point of view the Reynolds Averaged Navier-Stokes equations consists of two systems of equations:

a) The averaged flow equations of fluid dynamics (mean flow equations).

b) Equations representing the turbulent effects (turbulence equations).

Both systems form a coupled system of nonlinear equations that can be expressed abstractly by discretization,

$$\frac{d}{dt}\begin{pmatrix} W_{\text{mean}}(t) \\ W_{\text{turb}}(t) \end{pmatrix} = \begin{pmatrix} -M_{\text{mean}}^{-1} R_{\text{mean}}(W_{\text{mean}}(t), W_{\text{turb}}(t)) \\ -M_{\text{turb}}^{-1} R_{\text{turb}}(W_{\text{turb}}(t), W_{\text{mean}}(t)) \end{pmatrix}, \tag{1.1}$$

where W stands for the flow variables, R for the residual, and M for the mass matrix, and the sub-indices "mean" and "turb" refer to the mean and turbulent systems of equations respectively.

However, as we will demonstrate further in this thesis, both systems can presumably be related by a loosely interaction. Indeed, inspired by the large flexibility and the reduced associated complexity, possibly the widespread solution technique is to neglect their interaction and then solve the turbulent and mean flow equations in a segregated approach, i.e., equation (1.1) is formally replaced by,

$$\begin{aligned} \frac{d}{dt} W_{\text{mean}}(t) &= -M_{\text{mean}}^{-1} R_{\text{mean}}(W_{\text{mean}}(t); W_{\text{turb}}(t)) \\ \frac{d}{dt} W_{\text{turb}}(t) &= -M_{\text{turb}}^{-1} R_{\text{turb}}(W_{\text{turb}}(t); W_{\text{mean}}(t)), \end{aligned}$$

where the equations are independently solved by loosely coupling. Such an approach has proved successful for a variety of examples, taking into account the fact that the two equations often behave differently in the solution process.

From a mathematical point of view, however, (1.1) forms a coupled system of equations which can also be solved fully coupled,

$$\frac{d}{dt}W(t) = -M^{-1}R(W).$$

with $W = (W_{\text{mean}}, W_{\text{turb}})$ and $R = (R_{\text{mean}}, R_{\text{turb}})$. As it will be reviewed further in this thesis, the treatment of the coupled system of equations is an open problem. So far, comparative studies concerning the advantages and disadvantages of the two different approaches are missing. Furthermore, the existing literature on the topic is somehow contradictory [1, 2, 3, 4].

1.2. Objective

Motivated by the lack of understanding and agreement in the literature regarding whether the mean and turbulent flow equations should be solved fully or loosely coupled, the purpose of the present work is to develop a fully coupled solver for the RANS equations restricted to the one equation turbulence model of Spalart-Allmaras in order to shed light into the discussion of the coupling strategies.

Furthermore, we propose a further strategy, defined throughout this thesis as *weakly coupled* manner. From a mathematical perspective it is identical to the loosely coupled technique. However, the method of resolving the set of equations is the same as for the fully coupled, i.e., coupling the turbulent equations to the mean flow. Thereby, it must be interpreted as an intermediate step between both methods. A particular advantage of this strategy when compared to the loosely coupled approach is its inherent characteristic to assess the coupling strategy.

This work aims to develop and investigate a methodology for the numerical solution of the RANS equations. Although the coupling strategy tends to be more costly to implement, its formulation is more consistent and accordingly better convergence rates are expected. First, the mathematical model is derived. One of the main focus of this work is the computation of the full Jacobian, encompassing for the so-called cross terms, i.e., the derivative of the mean flow equations with respect to the turbulent variables, and the derivative of the turbulent flow equations with respect to the mean flow variables. The second main goal is the implementation, under specification of a computer code framework, of the two coupling methods for the solution strategy of the RANS equations. Finally, the assessment of the developed solvers is carried out by comparative calculations with a loosely coupled solution strategy and evaluation with experimental data for four different benchmark test cases. The attention is focused on the accuracy of the results and the overall performance. This investigation can only be carried out numerically, as the analytically investigation of such a problem is mostly an impossible task.

Given an initial condition, the Navier-Stokes equations describe the time evolution of the flow field. However, for validation purposes we are not interested in the accurate

time approximation of the equations, only on predicting the statistically steady state solution. Therefore, we assume that after certain time, the solution converges to the steady state condition and hence, only time-independent solutions are sought. These computations have been performed in a parallel computer system and carried out in a High-Performance-Computational environment. Because they are highly time and resources consuming, trying to conduct an analysis based on the full unsteady RANS equations for one of these examples is almost unfeasible for the purposes for this thesis.

1.3. Framework

Throughout this thesis, the most crucial aspects of the software are introduced. The details and properties of the mathematical framework are not discussed in detail, only the major points. For an exhaustive and in-depth presentation we refer to [5, 6]. In the current section we present a brief overview of the software framework.

Developed at the Deutschen Zentrums für Luft- und Raumfahrt (DLR), the software is a research code written in the program language C [7], developed to explode algorithm strategies for solving numerically the RANS equations in an efficient way. It combines advanced solutions strategies to deal with stiffness and nonlinear partial differential equations arising from the discretization of the Navier-Stokes equations. In the current framework, a loosely coupled solver for different turbulence models is implemented. For the solution strategy of the nonlinear equations, an implicit Runge-Kutta smoother, which can be considered as a generalization of Newton's method, combined with Full-Approximation Storage (FAS) multigrid is employed, supporting wide bandwidth ranges, from very slow to supersonic inflow conditions.

Moreover, it is often the case that the structure of full stencil represents a large sparse matrix. The implementation of these matrices on the code is of major importance as may result in low performance algorithms. To efficiently deal with such matrices, the code has been designed to work (block) Compressed Sparse Row matrices. This significantly reduces the memory requirement for its storage. Furthermore, the code is designed to work for industrial and research applications, where high computational resources are required. In this context, the software has been exploded to efficiently work in parallel based on Message Passing Interface (MPI).

1.4. Thesis outline

The structure of the present thesis is as follows. Chapter 2 introduces the governing equations. It comprises both the Reynolds Averaged Navier-Stokes as well as the turbulence model equations. Chapter 3 is devoted to the numerical methods applied to these equations. It includes an exposition of the most relevant theory for the spatial and temporal discretization. This is one of the main goals of the current work, as the mathematical background of the fully coupled method is derived in there. It is supported with two appendices deepen the theory. Then, chapter 4 presents a detailed discussion and explanation for the motivation of this investigation. Chapter 5 presents the results from the numerical computations used for the investigation. Finally, a discussion based on these results, conclusions and future work are drawn in chapter 6.

Chapter 2

GOVERNING EQUATIONS

In this chapter we introduce the mathematical model of the governing equations. We consider the steady Reynolds Averaged Navier-Stokes (RANS) equations for three-dimensional, compressible and viscous fluids. Specifically, we will review and present the relevant aspects in the formulation of the RANS equations for a fully coupled solver. Firstly the RANS equations are introduced and presented at the beginning of the chapter. The full set of equations are not derived here, but the main concepts concerning the hypothesis and approximations introduced in its formulation are described. Finally, the chapter is enclosed with a description of the implemented turbulence model, the Negative Spalart-Allmaras model.

2.1. Favre- and Reynolds-Averaged Navier-Stokes Equations

The Navier-Stokes (NS) equations [8, 9] result from the fundamental conservation laws for mass, momentum and energy. They provide a general and highly accurate model of the time and space evolution of three-dimensional, compressible, viscous and continuous fluids. In order to consider the turbulence effects into the Navier-Stokes equations, we use of the Reynolds Averaged Navier-Stokes equations approach [8, 10].

The fundamental methodology of the RANS equations is to decompose the flow field variables of the Navier-Stokes equations into mean or averaged and fluctuating or turbulent parts. Then, this decomposition is inserted into the governing equations. The resulting set of equations are averaged and solved for the mean values. Among the different forms of the Reynolds averaging, the one of interest for application in the problem is the time averaging technique. Within this approach, the mean value is considered to be statistically steady turbulence and do not vary in time, only in space. For high speed flows where compressibility effects, i.e., density fluctuations, need to be considered, such as in the examples considered to investigate in this thesis, the Reynolds averaging is applied to density and pressure, whereas density (mass) weighted, also known as Favre-averaged, is applied for the rest of variables.

After the introduction of the Reynolds and Favre decomposition into the Navier-Stokes equations, the resulting system of equations is the so-called Favre- and Reynolds-averaged Navier-Stokes equations, or simply RANS equations for abbreviation. The integral formulation within a generic Cartesian coordinate system for an arbitrary open region $\Omega \in \mathbb{R}^3$ with boundary $\partial\Omega$ reads,

$$\frac{d}{dt}\int_{\Omega} W \,\mathrm{d}\Omega + \int_{\partial\Omega} (f_c \cdot n - f_v \cdot n)\,\mathrm{d}\partial\Omega = \int_{\Omega} Q \,\mathrm{d}\Omega, \tag{2.1}$$

where $n = (n_1, n_2, n_3)^{\mathrm{T}}$ denotes the outer unit normal vector of the control volume and W stands for the characteristic properties of the fluid, the conserved variables, i.e., the

flow unknowns, defined as,

$$W = (\rho, \rho u_1, \rho u_2, \rho u_3, \rho E)^T, \tag{2.2}$$

which components are given by the fluid density ρ, the velocity field $u = (u_1, u_2, u_3)$ and the total energy E. In equation (2.1), f_c is the vector of convective or inviscid fluxes, f_v is the vector of viscous fluxes, and Q stands for the source terms. However, we note that for the problems formulated in this thesis, no source terms are considered for the mean flow. The inviscid and viscous fluxes are defined as,

$$f_c \cdot n = \begin{Bmatrix} \rho V \\ \rho u_1 V + p n_1 \\ \rho u_2 V + p n_2 \\ \rho u_3 V + p n_3 \\ \rho H V \end{Bmatrix}, \quad f_v \cdot n = \begin{Bmatrix} 0 \\ n_1\tau_{11} + n_2\tau_{12} + n_3\tau_{13} \\ n_1\tau_{21} + n_2\tau_{22} + n_3\tau_{33} \\ n_1\tau_{31} + n_2\tau_{32} + n_3\tau_{33} \\ n_1\theta_1 + n_2\theta_2 + n_3\theta_3 \end{Bmatrix}, \tag{2.3}$$

V is the normal velocity of the flow, computed as the scalar product in $\mathbb{R}^3$ of the velocity and the normal vector, $V = \langle u, n \rangle$. By definition, the total enthalpy H reads as,

$$H = E + p/\rho. \tag{2.4}$$

Thermally perfect gas is assumed, $p = \rho \mathfrak{R} T$, and thus the pressure is determined from expression,

$$p = (\gamma - 1)\rho\left(E - \frac{\|u\|_2^2}{2}\right), \tag{2.5}$$

enclosing the system of equations. For the previous derivations, $\mathfrak{R}$ stands for the specific gas constant, T for the temperature and γ for the gas dependent ratio of specific heats $\gamma = \frac{c_p}{c_v}$. c_v and c_p are the specific-heat coefficients for constant volume and pressure processes, respectively. Calorically perfect fluid is assumed and thus they are set to constant value, $\gamma = 1.4$ for air.

With the Boussinesq' eddy viscosity hypothesis together with Stokes hypothesis [8, 10], a significant simplification is attained on the formulation, and the components of the viscous stress tensor τ for a Newtonian fluid are given by:

$$\tau_{ii} = 2\mu_{\text{eff}}\frac{\partial u_i}{\partial x_i} + \lambda_{\text{eff}}\nabla \cdot u - \frac{2}{3}\rho\tilde{K}, \qquad \lambda_{\text{eff}} = -\frac{2}{3}\mu_{\text{eff}}, \qquad i = 1,2,3, \tag{2.6a}$$

$$\tau_{ij} = \mu_{\text{eff}}\left(\frac{\partial u_i}{\partial x_j} + \frac{\partial u_j}{\partial x_i}\right), \qquad \tau_{ji} = \tau_{ij}, \qquad 1 \leq i < j \leq 3, \tag{2.6b}$$

where τ_{ij} is the viscous stress in the $j-$direction acting on a surface with normal in the $i-$direction. For the heat conduction θ we have,

$$\theta_j = \left(\sum_{k=1}^{3} u_k \tau_{jk}\right) + q_j, \qquad j = 1,2,3, \tag{2.7a}$$

$$q = \kappa_{\text{eff}}\nabla T, \qquad q = (q_1, q_2, q_3). \tag{2.7b}$$

In previous definitions λ_{eff} represents the second viscosity coefficient, μ_{eff} the effective dynamic viscosity coefficient and κ_{eff} the effective thermal conductivity. $\tilde{K}$ denotes the

Favre-averaged turbulent kinetic energy [8]. Its definition involves triple products of the fluctuating components which are typically much smaller than the other terms and for simplification purposes they are simply neglected, leading to,

$$\tilde{K} = \frac{1}{2}\widetilde{u_i'' u_i''}, \tag{2.8}$$

with $\widetilde{u_i'' u_i''}$ denoting the mean value of the fluctuating parts of the instantaneous velocity computed using Favre-averaging.

The effective viscosity and the effective thermal conductivity are computed by,

$$\mu_{\text{eff}} = \mu_l + \mu_t, \qquad \kappa_{\text{eff}} = \kappa_l + \kappa_t, \tag{2.9}$$

and the laminar viscosity μ_l is assumed to follow the Sutherland's law,

$$\mu_l = \mu_{l,\infty}\left(\frac{T}{T_\infty}\right)^{3/2}\frac{T_\infty + \bar{T}}{T + \bar{T}}, \qquad \kappa_l = \frac{c_p \mu_l}{Pr_l}, \tag{2.10}$$

whereby $\mu_{l,\infty}$ denotes a constant reference laminar viscosity value, T_∞ the reference temperature, $\bar{T}$ is the Sutherland's constant, and with the Prandtl number $Pr_l = 0.72$ for air. Meanwhile, the turbulent thermal conductivity coefficient κ_t is formulated as,

$$\kappa_t = \frac{c_p \mu_t}{Pr_t}, \tag{2.11}$$

with the turbulent Prandtl number $Pr_t = 0.92$ for air.

We introduce the laminar kinematic viscosity, which by definition is given by,

$$\nu_l = \frac{\mu_l}{\rho}. \tag{2.12}$$

Finally, the turbulent kinematic viscosity is analogously defined as in previous expression and reads,

$$\nu_t = \frac{\mu_t}{\rho}. \tag{2.13}$$

The system of equations defined by equation (2.1) results in two new unknowns, the eddy viscosity also named as turbulent viscosity μ_t, and the turbulent kinetic energy $\tilde{K}$. For their definition, the turbulent flow equations are required, the so-called closure of the problem. The turbulence model, by means of additional equations and unknowns, is the responsible of providing an approximation to μ_t and $\tilde{K}$. Hereon, we will also refer to the turbulent additional unknowns as W_{t}, whereas to the already presented mean flow variables by W_{m}.

2.2. Turbulence Model Equations

There is a lack of understanding of turbulence which hampers the criterion for selection of a turbulence model. There are several well known turbulence models in the literature,

e.g., the Spalart-Allmaras, $k-\omega$ and $k-\varepsilon$ [11, 12] but they only provide a valid solution over a restricted range of applications. In that sense, a suitable turbulence model is required in order to accurately approach to a solution of turbulent flow with a considerable amount of time and for the desired application.

For this thesis, the chosen model is the modified one equation Spalart-Allmaras turbulence model [13]. The criterion for the selection is because it presents a low computational cost and relative simplified implementation. Furthermore, it exhibits accurate modelization of complex turbulent flows such as massive flow separation and supersonic flows with the appearance of compression shocks.

2.2.1. Spalart-Allmaras type turbulence model

The Spalart-Allmaras (S-A) model is an eddy viscosity one-equation turbulence model that has been satisfactorily and widely used for different kind of applications. As stated in [13] the formulation of the Spalart-Allmaras is applicable to both, incompressible and compressible flows.

The turbulent kinetic energy $\tilde{K}$ appearing in equation (2.6a) is simply ignored [14], reducing the number of turbulent unknowns. In that sense, the eddy viscosity μ_t is prescribed by the additional introduced local transport variable $\tilde{\nu}$ from the Spalart-Allmaras model. So, in accordance,

$$W_t = \tilde{\nu}. \tag{2.14}$$

Although this model used to be more robust when compared to other turbulent models, such as the $k-\omega$, it presents numerical issues near the interface between turbulent and irrotational regions [13]. In order to improve numerical robustness, a modification to the original model was introduced, deriving the Negative Spalart-Allmaras one-equation model. In our approach the exact recommendations and modifications given in [13] are followed to implement the Negative S-A model.

2.2.1.1. The negative Spalart-Allmaras one-equation model

The value of $\tilde{\nu}$ is computed by means of the transport equation of the form,

$$\frac{D\tilde{\nu}}{Dt} = P_n - D_n + \frac{1}{\sigma}\nabla\cdot[(\nu+\tilde{\nu}f_n)\nabla\tilde{\nu}] + \frac{c_{b2}}{\sigma}(\nabla\tilde{\nu})^2, \tag{2.15}$$

which, in order to be in accordance with the formulation of equation (2.1) can be rewritten in integral form as,

$$\frac{d}{dt}\int_\Omega \tilde{\nu}\,\mathrm{d}\Omega + \int_{\partial\Omega}(f_c\cdot n - f_v\cdot n)\,\mathrm{d}\partial\Omega = \int_\Omega Q\,\mathrm{d}\Omega, \tag{2.16}$$

with the convective and viscous fluxes formulated as,

$$f_c\cdot n = \{V\tilde{\nu}\} \qquad f_v\cdot n = \begin{cases} \left(\frac{\nu_l+\tilde{\nu}}{\sigma}\right)\left(\sum_{j=1}^3 n_j\frac{\partial\tilde{\nu}}{\partial x_j}\right), & \tilde{\nu}\geq 0 \\ \left(\frac{\nu_l+f_n\tilde{\nu}}{\sigma}\right)\left(\sum_{j=1}^3 n_j\frac{\partial\tilde{\nu}}{\partial x_j}\right), & \tilde{\nu}<0 \end{cases} \tag{2.17}$$

with,

$$f_n = \frac{c_{n1}+\chi^3}{c_{n1}-\chi^3}, \qquad c_{n1} = 16. \tag{2.18}$$

The term $\sum_{j=1}^{3} n_j \frac{\partial \tilde{\nu}}{\partial x_j}$ in equation (2.17) represents the viscous stress tensor for the Negative S-A model. The main feature of this model is that the turbulent viscosity μ_t is computed as in the standard Spalart-Allmaras model [15] when the transport variable $\tilde{\nu}$ is greater or equal zero, meanwhile μ_t is set to zero when $\tilde{\nu}$ is negative,

$$\mu_t = \begin{cases} \rho\tilde{\nu} f_{v1}, & \tilde{\nu} \geq 0 \\ 0, & \tilde{\nu} < 0 \end{cases}, \qquad f_{v1} = \frac{\chi^3}{\chi^3 + c_{v1}^3}, \qquad \chi = \frac{\tilde{\nu}}{\nu_l}, \tag{2.19}$$

with the value of the constant c_{v1} provided in equation (2.21). The source terms, described by Q, can be expressed as $Q = Pr - De + Di$, which are called production, wall destruction and diffusion of source terms respectively. They are given by,

$$Pr = \begin{cases} c_{b1}\,(1-f_{t2})\,\tilde{S}\tilde{\nu}, & \tilde{\nu} \geq 0 \\ c_{b1}\,(1-c_{t3})\,S\tilde{\nu}, & \tilde{\nu} < 0 \end{cases}, \tag{2.20a}$$

$$De = \begin{cases} \left(c_{w1} f_w - \frac{c_{b1}}{\kappa^2} f_{t2}\right)\left(\frac{\tilde{\nu}}{d}\right)^2, & \tilde{\nu} \geq 0 \\ -c_{w1}\left(\frac{\tilde{\nu}}{d}\right)^2, & \tilde{\nu} < 0 \end{cases}, \tag{2.20b}$$

$$Di = \frac{c_{b2}}{\sigma} \sum_{k=1}^{3} \left(\frac{\partial \tilde{\nu}}{\partial x_k}\right)^2, \tag{2.20c}$$

with,

$$\begin{aligned}
&f_{t2} = c_{t3} \exp\left(-c_{t4}\chi^2\right), \qquad f_w = g\left(\frac{1+c_{w3}^6}{g^6+c_{w3}^6}\right)^{1/6}, \\
&S = \|\mathrm{curl}\,(u)\|_2, \qquad \bar{S} = \frac{\tilde{\nu}}{\kappa^2 d^2} f_{v2}, \qquad \tilde{S} = \begin{cases} S + \bar{S}, & \bar{S} \geq -c_{v2}S \\ S + \frac{S(c_{v2}^2 S + c_{v3}^2 \bar{S})}{(c_{v3}-2c_{v2})S - \bar{S}}, & \bar{S} < -c_{v2}S \end{cases}, \\
&g = r + c_{w2}\, r\left(r^5 - 1\right), \qquad r = \min\left\{\frac{\tilde{\nu}}{\kappa^2 d^2 \tilde{S}}, 10\right\}, \qquad f_{v2} = 1 - \frac{\chi}{1+\chi f_{v1}}, \\
&c_{b1} = 0.1355, \qquad c_{b2} = 0.622, \qquad \sigma = \frac{2}{3}, \qquad \kappa = 0.41, \\
&c_{w1} = \frac{c_{b1}}{\kappa^2} + \frac{1+c_{b2}}{\sigma}, \qquad c_{w2} = 0.3, \qquad c_{w3} = 2, \\
&c_{t3} = 1.2, \qquad c_{t4} = 0.5, \qquad c_{v1} = 7.1, \qquad c_{v2} = 0.7, \qquad c_{v3} = 0.9,
\end{aligned} \tag{2.21}$$

and d stands for the distance to the closest wall.

At this point we have introduced the conservative variables for the mean flow W_{m}, equation (2.2), and the turbulent variables W_{t}, equation (2.14). For convenience, both systems of equations have been introduced separately. However, for a fully coupled approach the RANS equations in conjunction with the Negative S-A turbulence equation define a single system of equations. Thus, hereafter we will express the vector of

variables as a single vector comprising the mean and turbulent flow variables, i.e.,

$$W = (\rho, \rho u_1, \rho u_2, \rho u_3, \rho E, \tilde{\nu})^T. \tag{2.22}$$

This consideration also applies for the viscous, inviscid flux vectors and source terms, however they are not explicitly rewritten in here.

It is worth mentioning that the code works with non-dimensional parameters. The reader is referred to [5, Section 2.3] for a complete derivation of the non dimensionalization of the presented physical laws as well as for the physical domain. For the rest of this thesis, the dimensional quantities are replaced by the their non-dimensional variables.

Chapter 3

NUMERICAL TREATMENT

This chapter describes the numerical discretization strategy, both in space and time (the so-called method of lines), used for the governing equations described in chapter 2. The spatial discretization is performed by means of second order finite volume, introduced in section 3.1.. Then, a detailed description of the solution algorithms along with the different techniques employed to speed-up the convergence of the solution are covered in section 3.2.. Finally, the chapter is enclosed with the theoretical approach used to construct the preconditioner required for the solution algorithm, section 3.3..

3.1. Finite Volume Method

The spatial discretization is done through a Finite Volume Method (FVM) approach. In a preprocessing step, the whole physical space is discretized into non overlapping and static polyhedral elements, either with a triangular or quadrilateral face shape. This is known as primary grid. The solution domain is then constructed based on a dual mesh, composed by N non overlapping elements or control volumes, each with a centroid. For this thesis, dual mesh and mesh are used as synonyms. The control volumes Ω are constructed around the vertices of the primary grid by connecting the centers of adjacent elements of the primary grid, as depicted in figure 3.1. This scheme corresponds to a node centered discretization, i.e., the flow unknowns W are located at the centroid of the control volume.

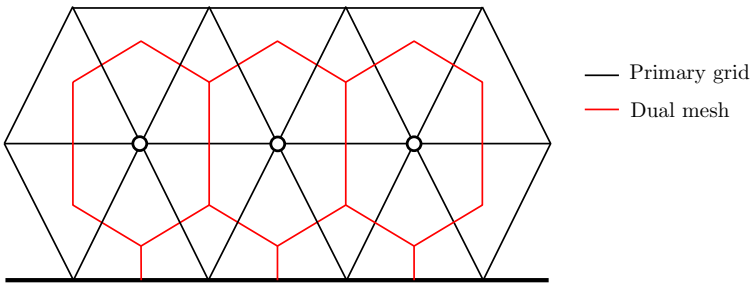

Figure 3.1: Representation of a 2D primary triangular grid and the polyhedral dual mesh.

The main characteristic of the finite volume approach is that the governing equations are solved in its conservative formulation, solving for the integral formulation inside each control volume. Within this formulation the flow field quantities are solved for its surface values of the fluxes over each control volume.

Finally note that due to the construction of the computational mesh, although the primary and dual grid share the same points, both grids have different structure. Nevertheless, there is no distinction between them regarding the discretization process. For a 3D simulation there are several choices for the shape of the elements: hexaedra,

prisms, pyramid and tetrahedra. Regarding the geometry data, we will refer to the centroid of a general control volume as point i whereas to the direct neighbors of i by j. In that sense, the group of direct neighbors will be described by $\mathcal{N}(i)$, i.e., $j \in \mathcal{N}(i)$. The corresponding face between the control volumes i and j will be represented by ij. This scheme is represented in figure 3.2.

From equations (2.1) and (2.16) we note that the flow field variables are space and time dependent,

$$W = W(x,t), \quad (x,t) \in \Omega \times (0,\infty).$$

Discontinuous Galerkin formulation with constant ansantz functions inside each control volume are used to discretize the functions representing the flow field. Thus,

$$\mathbb{L}(x) = \begin{cases} 1, & x \in \Omega_i \\ 0, & else \end{cases} . \tag{3.1}$$

Then, we approximate W by,

$$W(x,t) \approx W_h(x,t), \qquad W_h(x,t) = \sum_{i=1}^{N_{elem}} W_i(t)\mathbb{L}_{\Omega_i}(x), \tag{3.2}$$

To shorten the notation, we will return to previous notation, and simply represent the flow field by W instead of $W(x,t)$.

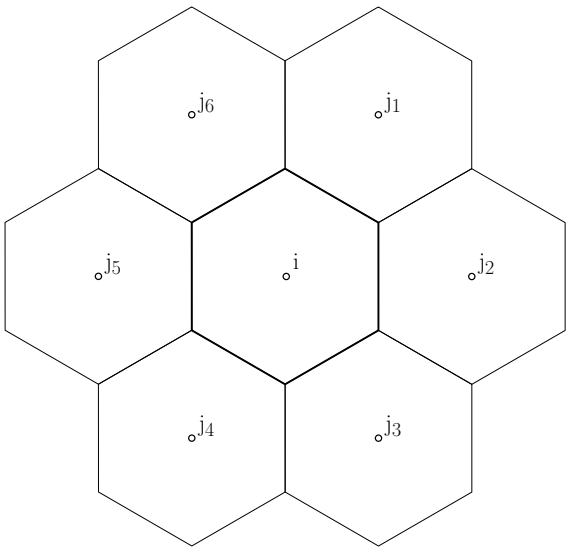

Figure 3.2: Representation of a 2D dual grid cell **i** and its direct neighbors $j \in \mathcal{N}(\mathbf{i})$.

We mention here that for the foregoing discussion of the discretization we will need to compute the distance between control volumes. The euclidean distance between two adjacent barycenters of control volumes i and j is computed as $\Delta\left(p^{(j)}, p^{(i)}\right) = \|p^{(j)} - p^{(i)}\|_2$, where $p^{(i)}$ denotes the center of each control volume.

In the following we shortly describe the relevant aspects of the spatial discretization.

3.1.1. Discrete set of equations

For a general control volume Ω_i that is fixed in space as in the case of a static grid, the integral formulation of the RANS equations, rewritten in here,

$$\frac{d}{dt}\int_{\Omega_i} W \,\mathrm{d}\Omega_i = \int_{\Omega_i} Q \,\mathrm{d}\Omega_i - \int_{\partial\Omega_i} (f_c \cdot n - f_v \cdot n)\,\mathrm{d}\partial\Omega_i, \tag{3.3}$$

can be expressed in the form,

$$\mathrm{vol}(\Omega_i)\frac{d}{dt}W_i = -R_i \qquad \text{or} \qquad \frac{d}{dt}W_i = -\frac{1}{\mathrm{vol}(\Omega_i)}R_i \tag{3.4}$$

where the volume of Ω_i is denoted by $\mathrm{vol}(\Omega_i)$, and R_i casts for the right hand side of equation (3.3) also referred to as the residual, defined by,

$$R_i = R_{c,i} - R_{v,i} - R_{Q,i}, \tag{3.5a}$$

$$R_{c,i} = \int_{\partial\Omega_i} \langle f_c, n\rangle \,\mathrm{d}\partial\Omega_i, \tag{3.5b}$$

$$R_{v,i} = \int_{\partial\Omega_i} \langle f_v, n\rangle \,\mathrm{d}\partial\Omega_i, \tag{3.5c}$$

$$R_{Q,i} = \int_{\Omega_i} Q_i \,\mathrm{d}\Omega_i, \tag{3.5d}$$

where R_c and R_v stand for the residual of the convective and viscous fluxes respectively, and R_Q for the residual of the source terms. When the discretization of equation (3.4) is applied for all control volumes it results in a system of first order ordinary differential equations,

$$\frac{d}{dt}\mathbf{W} = -\mathbf{M}^{-1}\mathbf{R}, \tag{3.6}$$

where $\mathbf{M}$ denotes the mass matrix [5, 8]. As already stated in section 3.1. the computational domain is discretized into N_{elem} non-overlapping domains also referred as control volumes. For a cell centered discretization and six variables, the mass matrix results $\mathbf{M} = \mathrm{diag}(\mathrm{diag}(\mathrm{vol}(\Omega_i))) \in \mathbb{R}^{6N_{\mathrm{elem}}\times 6N_{\mathrm{elem}}}$. Using the formulation in equation (2.22) for each of these domains, we can define,

$$\mathbf{W} = \left(W_1, \ldots, W_{N_{\mathrm{elem}}}\right), \qquad \mathbf{R} = \left(R_1, \ldots, R_{N_{\mathrm{elem}}}\right). \tag{3.7}$$

where the indices $1, \ldots, N_{\mathrm{elem}}$ denote the index of each control volume. Hence, each of these expression can be understood as a matrix $\in \mathbb{R}^{N_{\mathrm{elem}}\times 6}$, where each entry row constitutes the variables vector W or the corresponding residual for each control volume.

As already stated, we are only interested in the approximation of the steady state solution of the governing equations, i.e., a time independent solutions is assumed to exist. Accordingly we are seeking for the steady state condition of equation (3.6),

$$\frac{d}{dt}\mathbf{W} = 0,$$

which may also be interpreted as trying to drive the residual towards zero,

$$\mathbf{R} = 0. \tag{3.8}$$

However, instead of reformulating the original problem given by equation (3.6) and solving only for equation (3.8), because of stability purposes of the governing equations, the time derivative appearing in equation (3.6) is not neglected and a fictitious pseudo-time t^* is introduced instead,

$$\frac{d}{dt^*}\mathbf{W} = -\mathbf{M}^{-1}\mathbf{R}. \tag{3.9}$$

This artificial time allows to implement a time stepping method for equation (3.9). Since a physical time evolution of the solution is not desired, the temporal discretization must be understood as an implemented technique to smooth the solution towards zero, the steady state solution. It is the goal of section 3.2.2. to present such a method, the so-called smoother. The following sections are devoted to the description of the spatial discretization of equation (3.9).

For notation simplification, hereon we will drop the * superscript to represent the pseudo-time. Besides that, we will simply refer to the pseudo-time as time.

3.1.2. Spatial Discretization of Inviscid Terms

The inviscid terms of equations (2.1) and (2.16) are given by equation (3.5b), and repeated here for convenience,

$$R_{c,i} = \int_{\partial\Omega_i} \langle f_c, n\rangle \, \mathrm{d}\partial\Omega_i. \tag{3.10}$$

When using finite volume method with constant ansatz functions, the previous surface integral is understood as the spatial discretization of the net sum of convective fluxes through the face of a inner volume Ω_i. So, the spatial discretization can be directly applied to equation (3.10). For our discretization, the convective flux approximation is carried out through a central difference scheme with an added artificial matrix dissipation [16, 17]. This scheme prevents the dissipation and allows for stabilization of the solution, resulting in an accuracy improvement. A Roe solver is implemented for the solution of the Riemann problem (discontinuities in the conservative variables across the face) [18]. In addition, to handle with the oscillations in the solution, e.g., extreme large gradients in compression shocks, a pressure sensor Ψ is employed into the dissipative part, conveniently reducing the accuracy at discontinuities. Then, for an inner volume Ω_i, the evaluation of equation (3.10) is expressed as,

$$\int_{\partial\Omega_i} \langle f_c, n\rangle \, \mathrm{d}\partial\Omega_i \approx \sum_{j\in\mathcal{N}(i)} \mathrm{svol}(\Omega_{ij}) \frac{1}{2}((f_c \cdot n_{ij})(W_i) + (f_c \cdot n_{ij})(W_j)) - D_{ij}(W) \tag{3.11a}$$

$$D_{ij}(W) = \left|A_{ij}^{\mathrm{Roe}}\right| \left[\frac{1}{2}\Psi_{ij}(W_j - W_i) s_{ij}(W)(1-\Psi_{ij})(L_j(W) - L_i(W))\right], \tag{3.11b}$$

where $\mathrm{svol}(\Omega_{ij})$ denotes the surface area of the face ij, L_i stands for the Laplacian operator and the parameter $s_{ij}(W)$ is incorporated to deal with highly stretched cells. Finally, the linear operator A^{Roe} denotes the Roe matrix:

$$L_i(W) = \sum_{j\in\mathcal{N}(i)} (W_j - W_i), \tag{3.12a}$$

$$\Psi_{ij} = \min\{8 \cdot \max\{\Psi_i, \Psi_j\}, 1\}, \qquad \Psi_i = \left| \frac{\sum_{j\in\mathcal{N}(i)}(p_j - p_i)}{\sum_{j\in\mathcal{N}(i)}(p_j + p_i)} \right|, \tag{3.12b}$$

$$A_{ij}^{\text{Roe}} = \frac{\partial(f_c \cdot n_{ij})}{\partial W}[W_{\text{Roe}}]. \tag{3.12c}$$

Nevertheless, previous discretization scheme is only applied to the convective terms of the mean flow. The discretization for the inviscid fluxes of the turbulent flow equations follows the same approach as in equation (3.11) but is restricted to first order terms instead. The resulting simplified expression is presented in section 3.2.3.1. (see equation (3.35)).

The reader is referred to [5] for a detailed definition of each of the previous terms.

The structure of the Roe matrix is identical to the derivative of the convective flux evaluated on the face ij, but formulated in Roe averaged variables on the face. The construction of this matrix as well as the implemented entropy fix to avoid instabilities are topic of section 3.3.1.. However, let us provide in here the formulation for the Roe-averaged variables [18]:

$$\rho_{ij,\text{Roe}} = \sqrt{\rho_i \rho_j}, \tag{3.13a}$$

$$\left(u_{ij,\text{Roe}}\right)_k = \frac{(u_i)_k\sqrt{\rho_i} + (u_j)_k\sqrt{\rho_j}}{\sqrt{\rho_i} + \sqrt{\rho_j}}, \qquad k = 1,2,3, \tag{3.13b}$$

$$H_{ij,\text{Roe}} = \frac{H_i\sqrt{\rho_i} + H_j\sqrt{\rho_j}}{\sqrt{\rho_i} + \sqrt{\rho_j}}. \tag{3.13c}$$

3.1.3. Spatial Discretization of Viscous Terms

For each control volume, the discretization of the viscous terms, equation (3.5c), is performed by direct evaluation of the arithmetic average of the variables through each control volume face,

$$\omega_{ij} = \frac{1}{2}(\omega_j + \omega_i), \tag{3.14}$$

where ω represents a transported quantity. Despite its contrived appearance, average formulation provides a reliable approximation and allows for an efficient implementation of the viscous terms. Then, for an inner volume Ω_i, the evaluation of equation (3.5c) is expressed by,

$$\int_{\partial\Omega_i} \langle f_v, n\rangle \, \mathrm{d}\partial\Omega_i \approx \sum_{j\in\mathcal{N}(i)} \text{svol}(\Omega_{ij})(f_v \cdot n_{ij})(W_i, W_j, \nabla W_i, \nabla W_j). \tag{3.15}$$

Despite for equation (3.11), this scheme applies to both the mean flow and the turbulence model equations.

For the complete evaluation of equation (3.15) it is necessary to compute the gradients on the face for the velocity u and the transported variable $\tilde{\nu}$ appearing in the definition of viscous stress tensor, equations (2.6) and (2.17), as well as for the temperature T required for the formulation of the heat conduction, see equation (2.7). Green-Gauss

(GG) method is used to approximate the first order derivatives for the velocity and temperature,

$$\left(\frac{\partial \omega}{\partial x_k}\right)_{ij}^{\mathrm{GG}} = \frac{1}{2}\left[\left(\frac{\partial \omega}{\partial x_k}\right)_{i}^{\mathrm{GG}} + \left(\frac{\partial \omega}{\partial x_k}\right)_{j}^{\mathrm{GG}}\right], \tag{3.16a}$$

$$\left(\frac{\partial \omega}{\partial x_k}\right)_{i}^{\mathrm{GG}} = \frac{1}{\mathrm{vol}(\Omega_k)} \sum_{j \in \mathcal{N}(i)} \mathrm{svol}(\Omega_{ij}) \frac{n_{k,ij}}{2} (\omega_j + \omega_i), \tag{3.16b}$$

where again ω represents a generic variable such as the velocity and the temperature, and n_k describes the kth entry of the normal vector.

For the computation of the gradients of $\tilde{\nu}$, we use thin shear layer (TSL) approach instead. This method originates from the classical boundary layer assumptions, where viscous gradients acting in the normal direction dominate over the other directions, and thus can be neglected. Although this method in general implies a considerable error on the computations, it presents significant simplifications on the formulation with low associated computational resources. TSL formulation for a general variable ω is given by

$$\left(\frac{\partial \omega}{\partial x_k}\right)_{ij}^{\mathrm{TSL}} = n_{k,ij} \frac{\omega_j - \omega_i}{\Delta\left(p^{(j)}, p^{(i)}\right)}, \tag{3.17}$$

A key advantage for using TSL method in contrast to Green-Gauss, is that with this approach the resulting stencil of the discretization is much more compact, as the viscous fluxes do only depend on the direct neighbors of the control volume, $\mathcal{N}(i)$.

3.1.4. Spatial Discretization of Source Terms

As presented in section 2.2.1., the turbulent flow equations introduce the contribution of source terms into the governing equations. Its discretization is implemented in a straightforward manner using the midpoint rule approximation [19], where Q is assumed to be constant inside the control volume. Thus the following holds,

$$\int_{\Omega_i} Q_i \, \mathrm{d}\Omega_i \approx \mathrm{vol}(\Omega_i) Q(W_i, \nabla W_i). \tag{3.18}$$

Finally, to close this section, we recall from the definitions of the production and diffusion terms, equations (2.20a) and (2.20c), the discretization of the gradients of velocity and $\tilde{\nu}$ are required. These are computed using GG method, already presented in previous section.

3.1.5. Initial and boundary conditions

Due to the nature of the Reynolds Averaged Navier-Stokes equations, both, the initial and boundary conditions have to be imposed on the computational domain. This is a non trivial task, as these equations are very sensitive to these values, having an important impact on the solution process. In particular, all boundary conditions are applied weakly through the flux on the boundary. As can be observed in figure 3.1 for

a node centered dual mesh, the value of the flow unknowns are located directly over the boundary $\partial\Omega$. However, only half a control volume is defined there. Hence, we use a fictitious cell, that is, the boundary cell is assumed to be artificially extended to form a complete cell and thus compute the flux through that interface. This procedure is depicted in figure 3.3. The discretization of the boundary and initial conditions is not presented in this section as it is not the focus of the work, but the main aspects of its formulation are explained.

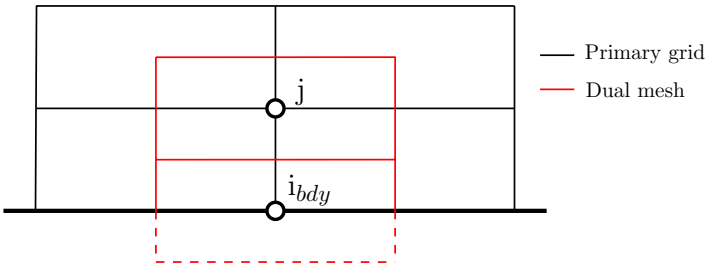

Figure 3.3: Representation of a 2D primary grid and the quadrilateral dual mesh for the boundary.

All problems considered for investigation in chapter 5 correspond to a solid surface body in a viscous flow. Ideally, to represent an accurate behavior of the physical model, we should consider an infinite domain to represent the surrounding flow. However, it is not possible to reproduce such conditions. Thus, the open domain must be truncated and bounded by an artificial boundary. The definition of such an exterior geometry is also of important relevance since it has to represent the unaltered flow conditions, i.e., free-stream, without introducing notable effects on the accuracy of the solution neither involving unnecessary computational resources. In such boundaries we formulate the so-called farfield boundary conditions, representing the values of the flow field at infinity, that is, the variable upstream of the body. Its implementation is given by,

$$W_{i,bnd} = W_\infty = (\rho_\infty, \rho_\infty u_{1,\infty}, \rho_\infty u_{2,\infty}, \rho_\infty u_{3,\infty}, \rho_\infty E_\infty, \tilde{\nu}_\infty)^T, \tag{3.19}$$

where following the recommendations in [13] for a fully turbulent simulation the value of $\tilde{\nu}_\infty$ is given by,

$$\tilde{\nu}_\infty = f_\infty \nu_{l,\infty} \qquad 3 \leq f_\infty \leq 5. \tag{3.20}$$

For all our computations we have used $f_\infty = 3$.

The next type of boundary conditions to consider is the so-called no-slip wall. This type of boundary condition ensures that the velocity and the normal derivative of the temperature on a solid surface is set to zero (adiabatic wall). Then, the following holds,

$$u|_{\partial\Omega} = 0, \qquad \left.\frac{\partial T}{\partial n}\right|_{\partial\Omega} = 0, \qquad \tilde{\nu}|_{\partial\Omega} = 0. \tag{3.21}$$

Finally, the symmetry boundary condition has to be considered when the flow is symmetrical with respect to a plane. Mathematically, it is similar to the slip wall boundary condition where only the normal flux is set to zero,

$$\left.\frac{\partial u}{\partial n}\right|_{\partial\Omega} = 0, \qquad \left.\frac{\partial T}{\partial n}\right|_{\partial\Omega} = 0, \qquad \left.\frac{\partial \tilde{\nu}}{\partial n}\right|_{\partial\Omega} = 0. \tag{3.22}$$

In that sense, the evaluation of the discretization at the boundary is performed such as the fluxes over $\partial\Omega$ directly satisfy the corresponding boundary condition in i_{bdy}.

The initial conditions are of important care, specially for a Newton's method such as the implicit Runge-Kutta method that will be presented in section 3.2.2.. There is no a straightforward solution for its implementation. Therefore, we initialize the flow field with the same values as the farfield variables. In that sense, in general the initial conditions are far from being a good approximation to the final steady state solution.

From a mathematical point of view, it can be demonstrated that the only necessary parameters to implement the farfield boundary conditions, and thus the initial conditions, are the Mach and Reynolds' numbers, the angle of attack, and the Sutherland's constant.

3.2. Solution methods

This section presents the algorithms used to drive the residual of the system of equations expressed in equation (3.9) towards zero. In the first part of this section we overview the multigrid method. Then, we describe the time integration, the smoother.

3.2.1. Agglomeration multigrid

The multigrid methodology is an essential element for the solution algorithm, which must be understood as a convergence acceleration technique. It is implemented by a Full Approximation Scheme (FAS) strategy [8, 20], with te possibility to perform several cycling strategies, e.g., V, W-cycle.

The fundamental idea of multigrid is to smooth the errors through the recursively computation of the solution and the residual on the multiple coarse grid levels. Then, the coarse grid corrections or defects are interpolated back to the finest mesh where will be finally smoothed [20].

The definition of the coarse grids is realized by an agglomeration strategy. This procedure consists on, for a given grid level, the next coarser grid is generated by fusing the control volumes with its neighbors. Such a procedure is depicted in figure 3.4. This procedure is repeated successively to generate different multigrid levels. For the discretization presented in section 3.1., it is not necessary to distinguish between the finest dual grid and the set of coarser grids.

Besides that, the smoother, explained in section 3.2.2., is able to damp the high-frequency components of the error, and therefore reduce the global error. As a consequence, the convergence rate is further increased.

The multigrid scheme requires the projection and interpolation of the defects from the solution and the residual between the different successive grid levels. These transfer operations are performed by the projection and interpolation operators. We refer to [5, Section 5.1.4] for their definition and formulation.

A further application is the so-called full-multigrid [20]. At the beginning of the simulation, the multigrid technique can be subsequently used on the coarsest grid levels

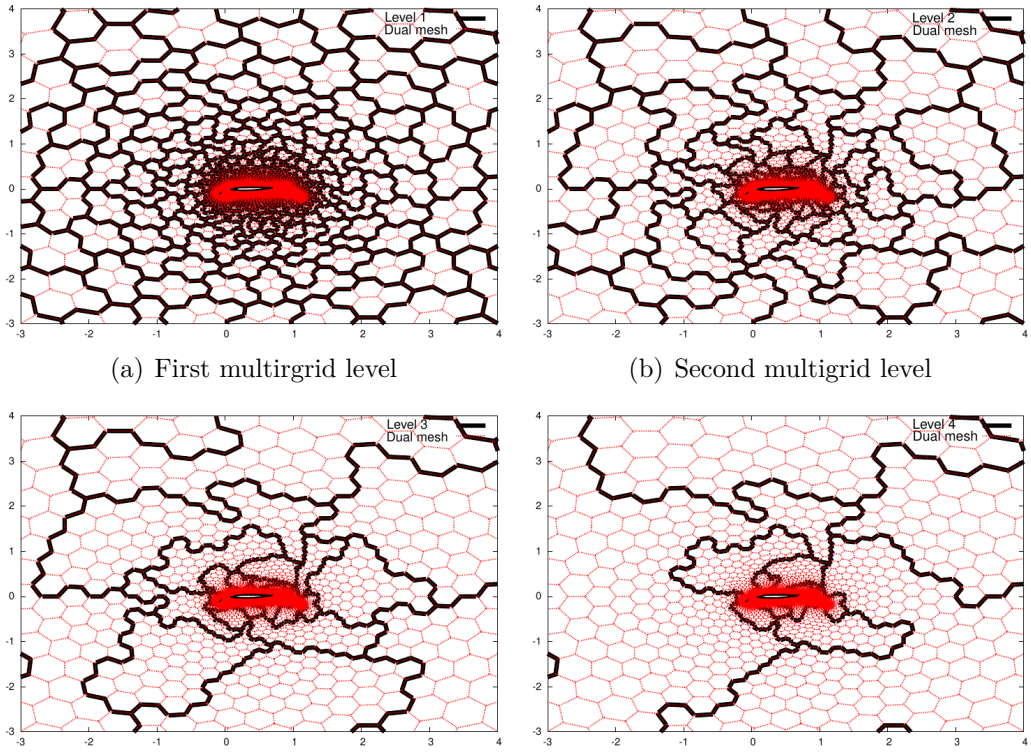

(a) First multirgrid level (b) Second multigrid level

(c) Thrid multigrid level (d) Fourth multigrid level

Figure 3.4: Coarsening strategy in isotropic section of a 2D mesh.

to compute a better starting solution for the finest grid. In doing so, the finest grid process starts from the computed approximated solution rather than from the initial conditions. Since the coarser grid operations are faster than the finest grid, the convergence rate of the algorithm is improved. A demonstration of this procedure is shown in section 5.4..

This technique along with the implicit smoother make up the driver of the solution algorithm.

3.2.2. Implicit Runge-Kutta smoother

Section 3.1.1. was enclosed with a first order ordinary differential equation, equation (3.9). As exposed there, it needs to be integrated in time to smooth the solution towards the steady state. This section is devoted to describe the implicit Runge-Kutta (RK) method employed as a smoother for that equation. The general formulation of this algorithm consists on a multi stage (s-stage) implicit Runge-Kutta given by the Butcher tableau [21],

Table 3.1: Butcher tableau

c	$\mathcal{A}$
	b^T

where,

$$\mathcal{A} = \begin{pmatrix} \alpha_{11} & 0 & \dots & 0 \\ \alpha_{21} & \ddots & \ddots & \vdots \\ \vdots & \ddots & \ddots & 0 \\ 0 & \ddots & \alpha_{s,s-1} & \alpha_{s,s} \end{pmatrix}, \quad b = \begin{pmatrix} 0 \\ \vdots \\ 0 \\ \alpha_{s+1,s} \end{pmatrix}, \quad c = \begin{pmatrix} 0 \\ \vdots \\ 0 \end{pmatrix}. \tag{3.23}$$

Denoting the discrete evolution with the superscript n and $n+1$ to represent the stages corresponding to time t and $t+\Delta t$ respectively with Δt standing for the time step, then the general expression for the implicit s-stage Runge-Kutta scheme has the following form,

$$\begin{aligned} k_1 &= -\mathbf{M}^{-1}\mathbf{R}(\mathbf{W}^n + \alpha_{11}\Delta t k_1) \\ k_2 &= -\mathbf{M}^{-1}\mathbf{R}(\mathbf{W}^n + \alpha_{21}\Delta t k_1 + \alpha_{22}\Delta t k_2) \\ &\vdots \\ k_s &= -\mathbf{M}^{-1}\mathbf{R}(\mathbf{W}^n + \alpha_{s.s-1}\Delta t k_{s-1} + \alpha_{s,s}\Delta t k_s) \\ \mathbf{W}^{(n+1)} &= \mathbf{W}^{(n)} + \alpha_{s+1,s}\Delta t k_s, \end{aligned} \tag{3.24}$$

Then a Newton's method truncated after one iteration is used to approximate the solution of the arisen non-linear system of equations, $k_1, \dots, k_s$. Hence, to find the root of the function we express,

$$g_j(k) = k + \mathbf{M}^{-1}\mathbf{R}(\mathbf{W}^n + \alpha_{j,j-1}\Delta t k_{j-1} + \alpha_{j,j}\Delta t k), \tag{3.25}$$

which derivative is given by,

$$\frac{dg_j(k)}{dk} = \mathbf{I} + \alpha_{j,j}\Delta t \mathbf{M}^{-1}\frac{d\mathbf{R}}{d\mathbf{W}}(\mathbf{W}^n + \alpha_{j,j-1}\Delta t k_{j-1} + \alpha_{j,j}\Delta t k). \tag{3.26}$$

Assuming initial guess $k^{(0)} = 0$ we approximate the roots for the stages $j = 1, \dots, s$ by,

$$k_j = -\left[\frac{dg_j\left(k^{(0)}\right)}{dk}\right]^{-1}\left(g_j\left(k^{(0)}\right)\right). \tag{3.27}$$

Using equation (3.24) together with equation (3.27) the implicit Runge-Kutta scheme can be represented by,

$$\begin{aligned} k_1 &= -\left[\frac{dg_j\left(k^{(0)}\right)}{dk}\right]^{-1}\mathbf{M}^{-1}\mathbf{R}(\mathbf{W}^n) \\ k_2 &= -\left[\frac{dg_j\left(k^{(0)}\right)}{dk}\right]^{-1}\mathbf{M}^{-1}\mathbf{R}(\mathbf{W}^n + \alpha_{21}\Delta t k_1) \\ &\vdots \\ k_s &= -\left[\frac{dg_j\left(k^{(0)}\right)}{dk}\right]^{-1}\mathbf{M}^{-1}\mathbf{R}(\mathbf{W}^n + \alpha_{s.s-1}\Delta t k_{s-1}) \\ \mathbf{W}^{(n+1)} &= \mathbf{W}^{(n)} + \alpha_{s+1,s}\Delta t k_s, \end{aligned} \tag{3.28}$$

Now, defining $\mathbf{W}^{(0)} = \mathbf{W}^n$ and the update as,

$$\mathbf{W}^{(j)} = \mathbf{W}^n - \alpha_{j+1,j}\Delta t \left[\frac{dg_j\left(k^{(0)}\right)}{dk}\right]^{-1} \mathbf{M}^{-1}\mathbf{R}\left(\mathbf{W}^{(j-1)}\right),$$

the implicit Runge-Kutta can be reformulated equivalently as,

$$\begin{aligned}
\mathbf{W}^{(0)} &= \mathbf{W}^n \\
\mathbf{W}^{(1)} &= \mathbf{W}^{(0)} - \alpha_{21}\mathbf{P}_1\left(\mathbf{W}^{(0)}\right)^{-1}\mathbf{R}\left(\mathbf{W}^{(0)}\right) \\
&\vdots \\
\mathbf{W}^{(s)} &= \mathbf{W}^{(0)} - \alpha_{s+1,s}\mathbf{P}_s\left(\mathbf{W}^{(s-1)}\right)^{-1}\mathbf{R}\left(\mathbf{W}^{(s-1)}\right) \\
\mathbf{W}^{(n+1)} &= \mathbf{W}^{(s)},
\end{aligned} \tag{3.29a}$$

with the linear operator for stage j given by,

$$\mathbf{P}_j\left(\mathbf{W}^{(j-1)}\right) = (\Delta T)^{-1}\mathbf{M} + \alpha_{j,j}\frac{\mathrm{d}\mathbf{R}}{\mathrm{d}\mathbf{W}}\left(\mathbf{W}^{(j-1)}\right). \tag{3.29b}$$

ΔT appearing in the equation above denotes the local time step. Since we only seek to approximate steady state solutions, instead of using the same time step for each of the control volumes, an acceleration technique is implemented, and the local time step is employed instead. This technique consists on using the maximum local time step Δt_i for each control volume independently from the rest, accelerating the convergence solution. By definition, the time step matrix on equation (3.29b) results in $\Delta T = \mathrm{diag}(\mathrm{diag}(\Delta t_i))$, where,

$$\begin{aligned}
\Delta t_i = &\mathrm{CFL}\cdot \mathrm{vol}(\Omega_i)\left[\sum_{j\in\mathcal{N}(i)}\frac{1}{2}(|V_{ij}| + a_{ij}\mathrm{svol}(\Omega_{ij})) + \right. \\
&\left.\frac{C_v\mu_{\mathrm{eff},ij}\mathrm{svol}(\Omega_{ij})}{\Delta\left(p^{(j)},p^{(i)}\right)\rho_i}\left(\max\left\{\frac{4}{3},\frac{\kappa_{\mathrm{eff},ij}(\gamma-1)}{\kappa_{\mathrm{eff},ij}}\right\}\right)\right]^{-1}, \quad C_v = 8.
\end{aligned} \tag{3.30}$$

The term CFL stands for the Courant-Friedrichs-Lewy (CFL) number. Finally, we emphasize that under some circumstances, such as considering a one stage scheme, $\mathrm{CFL} = \infty$ and $\alpha_{j,j} = \alpha_{21} = \alpha_{s+1,s} = 1$, the algorithm becomes:

$$\mathbf{W}^{n+1} = \mathbf{W}^n - \left(\frac{\mathrm{d}\mathbf{R}}{\mathrm{d}\mathbf{W}}(\mathbf{W}^n)\right)^{-1}\mathbf{R}(\mathbf{W}^n),$$

yielding to a Newton's method. In that sense, for our context the implicit Runge-Kutta scheme may be interpreted as a generalization of Newton's method.

3.2.3. Preconditioning strategy

The previous section ended with the algorithm for the time integration of the discretized equations. At this point, we have nearly presented all fundamental aspects required

for the solution procedure, the only remaining task is to compute the derivative of the residual with respect to the flow and turbulence variables $\frac{\mathrm{d}\mathbf{R}}{\mathrm{d}\mathbf{W}}$, also known as the Jacobian, which has a block structure,

$$\frac{\mathrm{d}\mathbf{R}}{\mathrm{d}\mathbf{W}} = \begin{pmatrix} \frac{\partial R_1}{\partial W_1} & \cdots & \frac{\partial R_1}{\partial W_N} \\ \vdots & \ddots & \vdots \\ \frac{\partial R_N}{\partial W_1} & \cdots & \frac{\partial R_N}{\partial W_N} \end{pmatrix}. \tag{3.31}$$

Although one can consider the exact formulation of $\frac{\mathrm{d}\mathbf{R}}{\mathrm{d}\mathbf{W}}$ for the construction of $\mathbf{P}_j$, its implementation results in a significant amount of time and memory storage, which in general, results in an inefficient algorithm. Indeed, the exact construction of $\frac{\mathrm{d}\mathbf{R}}{\mathrm{d}\mathbf{W}}$ may be avoided by considering a preconditioner $\mathbf{Prec}_j$ quite similar to the operator $\mathbf{P}_j$, i.e., $\mathbf{Prec}_j \approx \mathbf{P}_j$. Furthermore, the implementation of such preconditioner should lead to an efficient algorithm, i.e., low computational cost and easy to implement. The definition of $\mathbf{Prec}_j$ is based on the introduction of acceptable simplification assumptions to $\mathbf{P}_j$. In this section, we present these theoretical concepts, meanwhile the construction of the preconditioner is devoted to section 3.3..

We start the discussion of the definition of the preconditioner by considering a general hexahedral element in 3D. Due to the approximations used for the discretization of the residual, for every control volume we will need to take into account 25 entries, i.e., neighbors, neighbors of neighbors and itself. This results in large sparse matrices, hampering the solution algorithms, that is, making them more complex to solve with large computational time. Instead, a simplification is considered and only direct neighbors of i, i.e., $\mathcal{N}(i)$, are considered for the discretization of the residual. This first order simplification reduces the entries of the stencil operator. For the same control volume, the number of nonzero entries is reduced to only 7. Therefore, we approximate the full residual with a first order simplification, that is $\mathbf{R}^{1\mathrm{st}} \approx \mathbf{R}$. Then, analogously to equation (3.5) the simplified construction of the residual holds,

$$\frac{\mathrm{d}\mathbf{R}^{1\mathrm{st}}}{\mathrm{d}\mathbf{W}} = \frac{\mathrm{d}\mathbf{R}_c^{1\mathrm{st}}}{\mathrm{d}\mathbf{W}} - \frac{\mathrm{d}\mathbf{R}_v^{1\mathrm{st}}}{\mathrm{d}\mathbf{W}} - \frac{\mathrm{d}\mathbf{R}_Q^{1\mathrm{st}}}{\mathrm{d}\mathbf{W}} \approx \frac{\mathrm{d}\mathbf{R}}{\mathrm{d}\mathbf{W}}. \tag{3.32}$$

In that sense, we define,

$$\mathbf{Prec}_j = (\Delta T)^{-1}\mathbf{M} + \alpha_{jj}\frac{\mathrm{d}\mathbf{R}^{1\mathrm{st}}}{\mathrm{d}\mathbf{W}}\left(\mathbf{W}^{(j-1)}\right) \approx \mathbf{P}_j. \tag{3.33}$$

Differentiating the inviscid flux, equation (3.11), requires the complete derivation of $\left|A_{ij}^{\mathrm{Roe}}\right|$. The full derivative of the dissipative operator involves a tensor of third order [5], implying tremendous computations. We therefore introduce the second simplification and assume that $\left|A_{ij}^{\mathrm{Roe}}\right|$ is constant. Consequently we assume,

$$\frac{\partial\left|A_{ij}^{\mathrm{Roe}}\right|}{\partial W_k} = 0. \tag{3.34}$$

We will further simplify considerably the construction of the preconditioner by assuming constant effective viscosity μ_{eff} and effective conductivity κ_{eff} for the mean flow

equations, meanwhile we only consider constant laminar viscosity μ_l for the turbulent flow equations. For a compact representation of the previous statement, we will denote $\mu = const$ when referring to $\mu_{\text{eff}} = const$ and $\mu_{\text{l}} = const$, but special attention is required when dealing with mean or turbulent flow equations. This last assumption is not quite physically accurate but it is reasonable and realizes an efficient implementation of the preconditioner. As demonstrated in [5, Section 4.3] within this consideration the number of operations required for the computation of the derivative of the residual is significantly reduced.

In summary, the definition of the preconditioner is guided by the following three rules,

1) $\mathbf{R}$ is approximated only with first order discretization, $\mathbf{R}^{\text{1st}}$.

2) We assume the operator $\left|A_{ij}^{\text{Roe}}\right|$ is constant.

3) The effective viscosity μ_{eff} and effective conductivity κ_{eff} are considered constant for the mean flow, meanwhile μ_l is considered constant for the turbulent flow equations.

Finally, for the implementation of equation (3.33) in equation (3.29a), we assume that the preconditioner slightly changes over one Runge-Kutta iteration, and thus it is only evaluated on the first stage of the scheme, i.e., $\mathbf{Prec}_j = \mathbf{Prec}_1$. Freezing it results in an overall more efficient algorithm [5, Sections 6.3 and 6.4] and [6].

In the following, we present the resulting discretization of the residual for the definition of the preconditioner considering the aforementioned assumptions.

3.2.3.1. Inviscid Terms

We start with the discretization of the convective residual $R_{c,i}$. For the sake of simplicity, hereon we will neglect the ij surface notation for the normal vector, i.e., $n_{ij} = n = (n_1, n_2, n_3)^T$. Applying rule 1) to equation (3.11) the simplified first order convective residual holds,

$$R_{c,i}^{\text{1st}} = \int_{\partial\Omega_i} \langle f_c, n\rangle \, \mathrm{d}\partial\Omega_i \approx \sum_{j\in\mathcal{N}(i)} \text{svol}(\Omega_{ij}) \frac{1}{2}((f_c\cdot n)(W_i) + (f_c\cdot n)(W_j)) - \frac{1}{2}\left|A_{ij}^{\text{Roe}}\right|(W_j - W_i). \quad (3.35)$$

Previous expression can be rewritten in the following form,

$$\int_{\partial\Omega_i} \langle f_c, n\rangle \, \mathrm{d}\partial\Omega_i \approx \text{svol}(\Omega_{ij}) \mathcal{H}_c^{\text{1st}}(W(i,\mathcal{N}(i)), W(j,\mathcal{N}(j)), n), \quad (3.36)$$

where $\mathcal{H}_c^{\text{1st}}$ represents a numerical flux function. The above expression is employed for the discretization of the convective residual on the construction of the preconditioner as well as for the approximation of the turbulent convective residual, as it was explained in section 3.1.2..

The computation of $R_{c,i}^{1\text{st}}$ requires the differentiation of the numerical flux function $\mathcal{H}_c^{1\text{st}}$. As already stated in rule 2), the dissipation operator A_{ij}^{Roe} is assumed to be constant, and hence the following holds,

$$\frac{\partial}{\partial W_k}\sum_{j\in\mathcal{N}(i)}\frac{1}{2}((f_c\cdot n)(W_i)+(f_c\cdot n)(W_j))\approx\frac{1}{2}\begin{cases}0, & k=i,\\ \frac{\partial\langle f_c,n\rangle(W_k)}{\partial W_k}, & k\in\mathcal{N}(i),\\ 0, & k\neq i, k\notin\mathcal{N}(i),\end{cases}\tag{3.37a}$$

and

$$\frac{\partial}{\partial W_k}\sum_{j\in\mathcal{N}(i)}\frac{1}{2}\left|A_{ij}^{\text{Roe}}\right|(W_j-W_i)\approx\frac{1}{2}\begin{cases}\sum_{j\in\mathcal{N}(i)}\left|A_{ij}^{\text{Roe}}\right|, & k=i,\\ -\left|A_{ik}^{\text{Roe}}\right|, & k\in\mathcal{N}(i),\\ 0, & k\neq i, k\notin\mathcal{N}(i).\end{cases}\tag{3.37b}$$

Therefore, we obtain an approximate derivative for equation (3.36) by,

$$\frac{\partial\mathcal{H}_{c,i}^{1\text{st}}}{\partial W_k}\approx\frac{1}{2}\begin{cases}\sum_{j\in\mathcal{N}(i)}\left|A_{ij}^{\text{Roe}}\right|, & k=i,\\ \frac{\partial\langle f_c,n\rangle(W_k)}{\partial W_k}-\left|A_{ik}^{\text{Roe}}\right|, & k\in\mathcal{N}(i),\\ 0, & k\neq i, k\notin\mathcal{N}(i).\end{cases}\tag{3.38}$$

The obtained expression for $\frac{\partial R_{c,i}^{1\text{st}}}{\partial W}$ only depends on its direct neighbor information, significantly reducing its complexity of construction and the associated memory requirements.

3.2.3.2. Viscous terms

As explained in section 3.1.3., when using Green-Gauss method, the residual depends on the variables of i, $\mathcal{N}(i)$, and $\mathcal{N}(\mathcal{N}(i))$, which will produce large sparse matrices and thus becoming more troublesome to find a solution. For that reason, restricting to rule 1), instead of considering Green-Gauss method for the approximation of the required gradients appearing on the derivative of the viscous residual $R_{v,i}$, we use the TSL approach. Furthermore, rule 3) must be taken into account when computing the derivative of the viscous fluxes.

Analogously to the convective fluxes, we rewrite the viscous terms approximation as,

$$R_{v,i}^{1\text{st}}=\int_{\partial\Omega_i}\langle f_v,n\rangle\,\mathrm{d}\partial\Omega_i\approx\text{svol}(\Omega_{ij})\mathcal{H}_v^{1\text{st}}(W(i),W(j),n),\tag{3.39}$$

The resulting approximate derivative for equation (3.39) can be written as,

$$\frac{\mathcal{H}_{v,i}^{1\text{st}}}{\partial W_k}\approx\begin{cases}\sum_{j\in\mathcal{N}(i)}\left[\frac{\partial\langle f_v,n\rangle(W_i,W_j)}{\partial W_i}\right]^{\text{TSL},\mu=\text{const}}, & k=i,\\ \left[\frac{\partial\langle f_v,n\rangle(W_i,W_k)}{\partial W_k}\right]^{\text{TSL},\mu=\text{const}}, & k\in\mathcal{N}(i),\\ 0, & k\neq i, k\notin\mathcal{N}(i).\end{cases}\tag{3.40}$$

3.2.3.3. Source terms

Finally, regarding the derivative of the source terms $\frac{\partial Q}{\partial W}$ we state that for its formulation only rule 3) is considered, $\mu_l = const$ simplification.

3.2.4. Solution algorithm

In the previous section we introduced the approximations assumed for the construction of the preconditioner required for the Runge-Kutta algorithm. However, as observed in equation (3.29a), the inverse of $\mathbf{Prec}_j$ is required. Although several major simplification has been included for its construction, this operation would still result in an inefficient scheme. This can simply be prevented by considering the general expression of equation (3.29a) in the following form,

$$\mathbf{Prec}_j \Delta \mathbf{W}^{(j)} = -\alpha_{j+1,j} \mathbf{R}\Big(\mathbf{W}^{(j-1)}\Big), \tag{3.41}$$

with $\Delta \mathbf{W}^{(j)} = \mathbf{W}^{(j)} - \mathbf{W}^{(0)}$.

Equation (3.41) represents a linear system which needs to be approximately solved in order to find the value of $\Delta \mathbf{W}^{(j)}$. The selected solution algorithm has to be efficient, avoiding the computation of $\mathbf{Prec}^{-1}$. In the following we will present the solving methodology to efficiently approximate a solution of that linear system. Before that, it is worthwhile to first note that the resulting matrices from the discrete set of equations are non well suited, i.e., they are large sparse, not symmetric neither block diagonal dominant matrices. Furthermore, typically for high Reynolds number viscous flows, unstructured meshes with large anisotropic cells near the solid walls are employed, such as high aspect ratio cells. This introduces stiffness into the discrete set of equations [22]. With respect to these reasons, instead of solving for the original given problem, the solution procedure is based on what we define as a line procedure [5, 23].

For a given mesh, the cells that represent an anisotropy are coupled together forming a line. The line search algorithm that is used to identify the directions of strong coupling is detailed in [5, and references therein]. We will denote this group of cells forming a line by G_i,

$$G_i \subset G, \qquad G_j \cap G_i = \emptyset, \quad i \neq j, \qquad \cup_{j=1}^{n} G_j = G, \qquad G = \{1, \ldots, N_{\text{elem}}\}.$$

Along a line, the operator $\mathbf{Prec}_j$ results in a tri-diagonal matrix $\mathbf{Tri}_{G_i}$. Within this context, the preconditioner is used as a line implicit preconditioning technique,

$$\mathbf{Tri}_{G_i} = (\Delta T_{G_i})^{-1} \mathbf{M}_{G_i} + \frac{\mathrm{d}\mathbf{R}_{G_i}^{1\text{st}}}{\mathrm{d}\mathbf{W}_{G_i}} \Big(\mathbf{W}_{G_i}^{(j-1)}\Big).$$

For the approximation of the linear system defined by equation (3.41) we use an iterative method, the Block line Symmetric Gauss-Seidel method (SGS). This consists on

applying Gauss-Seidel method [24, 25] along each identified line. Therefore,

$$x_{G_i}^{k+1} = (1-\omega)x_{G_i}^{(k)} + \omega \mathbf{Tri}_{G_i}^{-1}\left(b_{G_i} - \sum_{j\in G_1,\dots,G_{i-1}, j\notin G_i} \mathbf{Prec}_{G_i,j} x_j^{(k+1)} - \sum_{j\in\{1,\dots,N\}\setminus\{G_1,\dots,G_i\}} \mathbf{Prec}_{G_i,j} x_j^{(k)}\right) \tag{3.42}$$

where ω is a relaxation parameter used to accelerate the convergence of the system, and $\mathbf{Prec}_{G_i,j}$ stands for the rest of entries of the $\mathbf{Prec}$ matrix not comprised along the line. Further, equation (3.42) may be rewritten as,

$$x_{G_i}^{k+1} = (1-\omega)x_{G_i}^{(k)} + \omega \mathbf{Tri}_{G_i}^{-1} b, \tag{3.43}$$

where instead of computing the inverse of $\mathbf{Tri}_{G_i}$, we solve for,

$$\mathbf{Tri}_{G_i} h = b,$$

using a Block Thomas algorithm [21, 26].

Finally, to carry out the symmetric Gauss-Seidel method, a forward sweep followed by a backward sweep are performed on equation (3.42).

3.3. Construction of the preconditioner

It is the goal of this section to present the construction of the derivative of the residual $\frac{\mathrm{d}\mathbf{R}^{1\mathrm{st}}}{\mathrm{d}\mathbf{W}}$ defined on previous section by equation (3.32). This section is an extension of the results in section 3.2.3., however, the computation of previous expression consolidate one of the objectives of this thesis, and therefore a full section is devoted to it.

3.3.1. Derivative of Inviscid Terms

Before going into the details of the computations of the derivative of the approximated inviscid fluxes, we first consider equation (3.38). As highlighted in section 3.1.2., $\frac{\partial\langle f_c,n\rangle(W_k)}{\partial W_k}$ and $\left|A_{ik}^{\mathrm{Roe}}\right|$ have the same structure, see equation (3.12c). Therefore, in the following we will focus on the construction of the Roe matrix. However, it is worth noting that $\frac{\partial\langle f_c(W_k),n\rangle}{\partial W_k}$ is constructed employing point variables meanwhile A_{ij}^{Roe} is constructed using Roe variables. For the sake of simplicity, the notation referring to point or Roe variables is neglected.

The derivatives of the convective flux $\langle f_c, n\rangle$ in normal direction n are given by,

$$\frac{\partial\langle f_c(W),n\rangle}{\partial W} = VI + a_1 {b_1}^T + a_2 {b_2}^T, \tag{3.44}$$

where,

$$
\begin{aligned}
a_1 &= \left(1, u_1, u_2, u_3, H, \tfrac{\tilde{\nu}}{\rho}\right)^T, \\
a_2 &= \left(0, n_1, n_2, n_3, V, 0\right)^T, \\
b_1 &= \left(-V, n_1, n_2, n_3, 0, 0\right)^T, \\
b_2 &= (\gamma-1)\left(\tfrac{\|u\|_2^2}{2}, -u_1, -u_2, -u_3, 1, 0\right)^T.
\end{aligned}
$$

The completeness derivation of the previous expression is detailed in appendix A. The compact matrix notation of equation (3.44) is written below,

$$
\frac{\partial \langle f_c(W), n\rangle}{\partial W} =
\begin{pmatrix}
0 & n_1 & n_2 & n_3 & 0 & 0 \\
\frac{n_1\zeta_2\|u\|_2^2}{2} - u_1 V & n_1\zeta_3 u_1 + V & n_2 u_1 - n_1\zeta_2 u_2 & n_3 u_1 - n_1\zeta_2 u_3 & n_1\zeta_2 & 0 \\
\frac{n_2\zeta_2\|u\|_2^2}{2} - u_2 V & n_1 u_2 - n_2\zeta_2 u_1 & n_2\zeta_3 u_2 + V & n_3 u_2 - n_2\zeta_2 u_3 & n_2\zeta_2 & 0 \\
\frac{n_3\zeta_2\|u\|_2^2}{2} - u_3 V & n_1 u_3 - n_3\zeta_2 u_1 & n_2 u_3 - n_3\zeta_2 u_2 & n_3\zeta_3 u_3 + V & n_3\zeta_2 & 0 \\
\left(\zeta_2\|u\|_2^2 - \gamma E\right)V & n_1\zeta_1 - \zeta_2 u_1 V & n_2\zeta_1 - \zeta_2 u_2 V & n_3\zeta_1 - \zeta_2 u_3 V & \gamma V & 0 \\
-\frac{\tilde{\nu}}{\rho}V & \frac{\tilde{\nu}}{\rho}n_1 & \frac{\tilde{\nu}}{\rho}n_2 & \frac{\tilde{\nu}}{\rho}n_3 & 0 & V
\end{pmatrix},
\tag{3.45a}
$$

with

$$
\Phi = \frac{1}{2}(\gamma-1)\|u\|_2^2, \qquad \zeta_1 = \gamma E - \Phi, \qquad \zeta_2 = \gamma - 1, \qquad \zeta_3 = 2 - \gamma. \tag{3.45b}
$$

In addition, the assembling of the Roe matrix is based on the eigendecomposition of equation (3.45a). Then, the following set of eigenvectors are obtained for the previous matrix,

$$
\begin{aligned}
g_1 &= n_1 y_1 + a y_2, & g_4 &= a_1 + a a_2, \\
g_2 &= n_2 y_1 + a y_3, & g_5 &= a_1 - a a_2, \\
g_3 &= n_3 y_1 + a y_4, & g_6 &= \left(0, 0, 0, 0, 0, 1\right)^T,
\end{aligned}
\tag{3.46}
$$

where a denotes the speed of sound for a thermally perfect gas $a = \sqrt{\gamma p/\rho}$, and,

$$
\begin{aligned}
y_1 &= \left(1, u_1, u_2, u_3, \tfrac{\|u\|_2^2}{2}, 0\right)^T, \\
y_2 &= \left(0, 0, n_3, -n_2, u_2 n_3 - u_3 n_2, 0\right)^T, \\
y_3 &= \left(0, -n_3, 0, n_1, u_3 n_1 - u_1 n_3, 0\right)^T, \\
y_4 &= \left(0, n_2, -n_1, 0, u_1 n_2 - u_2 n_1, 0\right)^T.
\end{aligned}
$$

Therefore, the matrix given by equation (3.45) has the following set of eigenpairs:

$$
\{(V, g_1), (V, g_2), (V, g_3), (V + a, g_4), (V - a, g_5), (V, g_6)\} \tag{3.47}
$$

Denoting by G the matrix of eigenvectors, i.e., $G = \big(g_1, g_2, g_3, g_4, g_5, g_6\big)$, it is possible to define the inverse of G by,

$$J \coloneqq G^{-1} = \begin{pmatrix} q_1 \\ q_2 \\ q_3 \\ q_4 \\ q_5 \\ q_6 \end{pmatrix}, \tag{3.48}$$

with the components of J given by,

$$\begin{aligned} q_1 &= n_1 p_1^T - \frac{1}{a} p_2^T, \qquad & q_4 &= \frac{1}{2a^2}\big(b_2^T + a b_1^T\big), \\ q_2 &= n_2 p_1^T - \frac{1}{a} p_3^T, \qquad & q_5 &= \frac{1}{2a^2}\big(b_2^T - a b_1^T\big), \\ q_3 &= n_3 p_1^T - \frac{1}{a} p_4^T, \qquad & q_6 &= \frac{\tilde{\nu}(\gamma-1)}{\rho a^2}\left(-\tfrac{\|u\|_2^2}{2}, u_1, u_2, u_3, -1, \tfrac{\rho a^2}{\tilde{\nu}(\gamma-1)}\right), \end{aligned} \tag{3.49}$$

with,

$$\begin{aligned} p_1 &= \frac{\tilde{\nu}(\gamma-1)}{a^2}\left(H - \|u\|_2^2, u_1, u_2, u_3, -1, 0\right)^T, \\ p_2 &= \left(u_2 n_3 - u_3 n_2, 0, -n_3, n_2, 0, 0\right)^T, \\ p_3 &= \left(u_3 n_1 - u_1 n_3, n_3, 0, -n_1, 0, 0\right)^T, \\ p_4 &= \left(u_1 n_2 - u_2 n_1, -n_2, n_1, 0, 0, 0\right)^T. \end{aligned}$$

In appendix A.1. the compact form defining the matrices G and J is provided.

For the implementation of the matrix valued operator $\left|A_{ij}^{\mathrm{Roe}}\right|$ the following holds,

$$\left|A_{ij}^{\mathrm{Roe}}\right| = \left|\frac{\partial \langle f_c(W), n\rangle}{\partial W}\right| = \sum_{j=1}^{6} |\alpha_j| g_j q_j, \tag{3.50}$$

where the scalars α_j are given by the eigenvalues:

$$\alpha_1 = \alpha_2 = \alpha_3 = \alpha_6 = V, \qquad \alpha_4 = V + a, \qquad \alpha_5 = V - a. \tag{3.51}$$

A common consideration on the construction of $\left|A_{ij}^{\mathrm{Roe}}\right|$ is to employ an entropy fix to prevent the arising of instabilities when one of the eigenvalues is ≈ 0, e.g., at stagnation points. The adopted entropy fix in the code follows [27], based onto replace the absolute eigenvalues by,

$$|\Lambda|_{\mathrm{ef}} = \mathrm{diag}\Big(|V|_{\mathrm{ef},1}, |V|_{\mathrm{ef},1}, |V|_{\mathrm{ef},1}, |V+a|_{\mathrm{ef},1}, |V-a|_{\mathrm{ef},1}, |V|_{\mathrm{ef},1}\Big), \tag{3.52}$$

with,

$$|V|_{\mathrm{ef},1} = |\lambda_i|_{\mathrm{ef},1} = \max\{|V|, \delta_{\mathrm{ef}}(|V|+a)\}, \qquad i = 1,2,3,6, \tag{3.53a}$$

$$|V+a|_{\mathrm{ef},2} = |\lambda_4|_{\mathrm{ef},2} = \max\{|V+a|, \delta_{\mathrm{ef}}(|V|+a)\}, \tag{3.53b}$$

$$|V-a|_{\mathrm{ef},3} = |\lambda_5|_{\mathrm{ef},3} = \max\{|V-a|, \delta_{\mathrm{ef}}(|V|+a)\}, \tag{3.53c}$$

with δ_{ef} representing the entropy fix value, 1/5 for the computations presented in this thesis.

Additionally, to extent the model to incompressible, low Mach number flows, $\left|A_{ij}^{\text{Roe}}\right|$ is rewritten and expressed with respect to local Mach number $M = M_{\text{Roe}} = \frac{V_{\text{Roe}}}{a_{\text{Roe}}}$. Then, equation (3.53) is reformulated in the following form:

$$|M|_{\text{ef},1} = \max\{|M|, \delta_{\text{ef}}(|M|+1)\}, \qquad i = 1,2,3,6 \tag{3.54a}$$

$$|M+1|_{\text{ef},2} = \max\{|M+1|, \delta_{\text{ef}}(|M|+1)\}, \tag{3.54b}$$

$$|M-1|_{\text{ef},3} = \max\{|M-1|, \delta_{\text{ef}}(|M|+1)\}, \tag{3.54c}$$

$$M_0^{(1)} = \frac{1}{2}\Big(|M+1|_{\text{ef},2} - |M-1|_{\text{ef},3}\Big), \tag{3.54d}$$

$$M_0^{(2)} = \frac{1}{2}\Big(-2|M|_{\text{ef},1} + |M+1|_{\text{ef},2} - |M-1|_{\text{ef},3}\Big). \tag{3.54e}$$

Finally, the artificial matrix dissipation is formulated as,

$$\left|A^{\text{Roe}}\right|_{\text{ef}} = G|\Lambda|_{\text{ef}}G^{-1} = \begin{pmatrix} \left|A^{\text{Roe}}\right|_{\text{ef}_{(1,1)}} & \cdots & \left|A^{\text{Roe}}\right|_{\text{ef}_{(1,6)}} \\ \vdots & \ddots & \vdots \\ \left|A^{\text{Roe}}\right|_{\text{ef}_{(6,1)}} & \cdots & \left|A^{\text{Roe}}\right|_{\text{ef}_{(6,6)}} \end{pmatrix}. \tag{3.55}$$

With the intention of making lighter the reading of this thesis, the full entries of previous matrix are not explicitly written in here. The definition of its components can be found in appendix A.2.. Nevertheless, we first note that due to the nature of vectors q (see equation (3.49)),

$$\left|A^{\text{Roe}}\right|_{\text{ef}_{(i,6)}} = 0, \qquad i = 1,2,3,4,5. \tag{3.56}$$

Second remark is that the last row of the matrix has the following representation,

$$\left|A^{\text{Roe}}\right|_{\text{ef}_{(6,i)}} = \frac{\tilde{\nu}}{\rho}|\lambda|_{\text{ef}_2}q_{4,i} + \frac{\tilde{\nu}}{\rho}|\lambda|_{\text{ef}_3}q_{5,i} + |\lambda|_{\text{ef}_1}q_{6,i}, \qquad i \in [1,6], \tag{3.57a}$$

and hence,

$$\begin{aligned} \left|A^{\text{Roe}}\right|_{\text{ef}_{(6,1)}} &= \frac{1}{\rho}\left[\frac{\tilde{\nu}}{a}(\gamma-1)\frac{\|u\|_2^2}{2}M_0^{(2)} - \tilde{\nu}VM_0^{(1)}\right], \\ \left|A^{\text{Roe}}\right|_{\text{ef}_{(6,i+1)}} &= \frac{1}{\rho}\left[\tilde{\nu}n_iM_0^{(1)} + \tilde{\nu}(1-\gamma)\frac{u_i}{a}M_0^{(2)}\right], \qquad i = 1,2,3, \\ \left|A^{\text{Roe}}\right|_{\text{ef}_{(6,5)}} &= \frac{1}{\rho}\left[\frac{1}{a}(\gamma-1)\tilde{\nu}M_0^{(2)}\right], \\ \left|A^{\text{Roe}}\right|_{\text{ef}_{(6,6)}} &= |V|_{\text{ef}_1}. \end{aligned} \tag{3.57b}$$

3.3.2. Derivative of Viscous Terms

For simplicity of presentation, the derivatives of the viscous fluxes with respect to the variables at points i and j are presented in a compact notation form. We use

the following notation: point i will be denoted by a 0 and j is represented with a 1. Nevertheless, for the notation of the face ij we use the same notation up to now. Let $l = 0, 1$, then we have,

$$\left[\frac{\partial(f_v\cdot n)\Big(W_{p^{(0)}}, W_{p^{(1)}}\Big)}{\partial W_{p^{(l)}}}\right]^{\mathrm{TSL},\mu=\mathrm{const}} =$$

$$\xi^{(l)}\begin{pmatrix} 0 & 0 & 0 & 0 & 0 & 0 \\ (-1)^l(N_1u_1^{(l)}+\frac{1}{3}N_{12,13}^{(l)}) & (-1)^{l+1}N_1 & \frac{(-1)^{l+1}}{3}N_{12} & \frac{(-1)^{l+1}}{3}N_{13} & 0 & 0 \\ (-1)^l(N_2u_2^{(l)}+\frac{1}{3}N_{12,23}^{(l)}) & \frac{(-1)^{l+1}}{3}N_{12} & (-1)^{l+1}N_2 & \frac{(-1)^{l+1}}{3}N_{23} & 0 & 0 \\ (-1)^l(N_3u_3^{(l)}+\frac{1}{3}N_{13,23}^{(l)}) & \frac{(-1)^{l+1}}{3}N_{13} & \frac{(-1)^{l+1}}{3}N_{23} & (-1)^{l+1}N_3 & 0 & 0 \\ E_1^{(l)}+E_2^{(l)}+E_3^{(l)} & \frac{1}{\xi^{(l)}}\frac{\partial(f_v\cdot n)^{(5)}}{\partial z_2^{(l)}} & \frac{1}{\xi^{(l)}}\frac{\partial(f_v\cdot n)^{(5)}}{\partial z_3^{(l)}} & \frac{1}{\xi^{(l)}}\frac{\partial(f_v\cdot n)^{(5)}}{\partial z_4^{(l)}} & \frac{\kappa_{\mathrm{eff},ij}(1-\gamma)}{\mu_{\mathrm{eff},ij}} & 0 \\ E_4^{(l)} & 0 & 0 & 0 & 0 & E_5^{(l)} \end{pmatrix}, \tag{3.58}$$

where

$$\begin{aligned}
\xi^{(l)} &= \frac{\mu_{\mathrm{eff},ij}}{\Delta\Big(p^{(1)},p^{(0)}\Big)}\frac{1}{\rho^{(l)}},\\
N_1 &= \frac{4}{3}n_1^2+n_2^2+n_3^2, \qquad N_2 = n_1^2+\frac{4}{3}n_2^2+n_3^2, \qquad N_3 = n_1^2+n_2^2+\frac{4}{3}n_3^2,\\
N_{12} &= n_1n_2, \qquad N_{13} = n_1n_3, \qquad N_{23} = n_2n_3,\\
E_1^{(l)} &= (-1)^{(l)}\left\{u_{1,ij}\left[N_1u_1^{(l)}+\frac{1}{3}N_{12}u_2^{(l)}+\frac{1}{3}N_{12}u_3^{(l)}\right]\right.\\
&\quad \left.+u_{2,ij}\left[\frac{1}{3}N_{12}u_1^{(l)}+N_2u_2^{(l)}+\frac{1}{3}N_{23}u_3^{(l)}\right]+u_{3,ij}\left[\frac{1}{3}N_{13}u_1^{(l)}+\frac{1}{3}N_{23}u_2^{(l)}+N_3u_3^{(l)}\right]\right\},\\
E_2^{(l)} &= -\frac{1}{2}\frac{\Delta}{\mu_{\mathrm{eff},ij}}\sum_{k=1}^{3}u_k^{(l)}\sum_{q=1}^{3}n_q\Big(\tau_{kq}\Big)_{ij}^{\mathrm{TSL}},\\
E_3^{(l)} &= \frac{\kappa_{\mathrm{eff},ij}}{\mu_{\mathrm{eff},ij}}\Big(T^{(l)}-\frac{1}{2}(\gamma-1)\|u^{(l)}\|_2^2\Big),\\
\frac{\partial(f_v\cdot n)^{(5)}}{\partial z_2^{(l)}} &= \frac{\mu_{\mathrm{eff},ij}}{\Delta\rho^{(l)}}\left\{\frac{\Delta}{\mu_{\mathrm{eff},ij}}\frac{1}{2}\sum_{k=1}^{3}n_k\tau_{k1,ij}+(-1)^{l+1}\left[N_1u_{1,ij}+\frac{1}{3}N_{12}u_{2,ij}+\frac{1}{3}N_{13}u_{3,ij}\right]\right.\\
&\quad \left.+(-1)^l\frac{\kappa_{\mathrm{eff},ij}}{\mu_{\mathrm{eff},ij}}(\gamma-1)u_1^{(l)}\right\},\\
\frac{\partial(f_v\cdot n)^{(5)}}{\partial z_2^{(l)}} &= \frac{\mu_{\mathrm{eff},ij}}{\Delta\rho^{(l)}}\left\{\frac{\Delta}{\mu_{\mathrm{eff},ij}}\frac{1}{2}\sum_{k=1}^{3}n_k\tau_{k2,ij}+(-1)^{l+1}\left[\frac{1}{3}N_{12}u_{1,ij}+N_2u_{2,ij}+\frac{1}{3}N_{23}u_{3,ij}\right]\right.\\
&\quad \left.+(-1)^l\frac{\kappa_{\mathrm{eff},ij}}{\mu_{\mathrm{eff},ij}}(\gamma-1)u_2^{(l)}\right\},\\
\frac{\partial(f_v\cdot n)^{(5)}}{\partial z_2^{(l)}} &= \frac{\mu_{\mathrm{eff},ij}}{\Delta\rho^{(l)}}\left\{\frac{\Delta}{\mu_{\mathrm{eff},ij}}\frac{1}{2}\sum_{k=1}^{3}n_k\tau_{k3,ij}+(-1)^{l+1}\left[\frac{1}{3}N_{13}u_{1,ij}+\frac{1}{3}N_{23}u_{2,ij}+N_3u_{3,ij}\right]\right.\\
&\quad \left.+(-1)^l\frac{\kappa_{\mathrm{eff},ij}}{\mu_{\mathrm{eff},ij}}(\gamma-1)u_3^{(l)}\right\},
\end{aligned}$$

$$
\begin{aligned}
E_4^{(l)} &= -\frac{1}{2}\frac{1}{\rho^{(l)}}\frac{1}{\sigma}\frac{\mu_l^{(l)}}{\mu_{\text{eff},ij}}\left(\tilde{\nu}^{(1)}-\tilde{\nu}^{(0)}\right),\\
E_5^{(l)} &= \begin{cases} \frac{1}{2}\left(\tilde{\nu}^{(1)}-\tilde{\nu}^{(0)}\right)+(-1)^{l+1}\left(\nu_{l,ij}+\tilde{\nu}_{ij}\right), & \tilde{\nu}\geq 0\\ (-1)^{l+1}\left(\tilde{\nu}^{(l)}f_{n,ij}+\nu_{l,ij}\right)+\left(\tilde{\nu}_j^2-\tilde{\nu}_i^2\right)\frac{3\left(\chi^{(l)}\right)^2 c_{n1}}{\left(c_{n1}-\chi_{ij}^3\right)^2}\frac{\rho^{(l)}}{\mu_l^{(l)}}, & \tilde{\nu}<0 \end{cases},\\
\Delta &= \Delta\left(p^{(1)},p^{(0)}\right).
\end{aligned}
$$

All the details related to the derivation of equation (3.58) can be found in appendix B.

3.3.3. Derivative of Source Terms

For the derivative of the source terms, equation (3.5d), we note that a full derivative of all terms appearing in equations (2.20) and (2.21) is required. In the following we list all these computations to end up with the expression for $\frac{\partial Q}{\partial W}$.

We first start by,

$$
\frac{\partial\chi}{\partial W}=\frac{\partial\left(\frac{\rho\tilde{\nu}}{\mu_l}\right)}{\partial W}=\frac{\mu_l\frac{\partial(\rho\tilde{\nu})}{\partial W}-\rho\tilde{\nu}\frac{\partial\mu_l}{\partial W}}{\mu_l^2}=\frac{1}{\mu_l}\left(\frac{\partial(\rho\tilde{\nu})}{\partial W}-\chi\frac{\partial\mu_l}{\partial W}\right). \tag{3.59}
$$

Nevertheless, since we consider constant laminar viscosity $\mu_l = const$, previous expression can be simplified to,

$$
\frac{\partial\chi}{\partial W}=\frac{1}{\mu_l}\left(\frac{\partial\rho\tilde{\nu}}{\partial W}\right). \tag{3.60}
$$

Hence, the next derivatives are obtained,

$$
\frac{\partial f_{v1}}{\partial W}=\frac{1}{\left(\chi^3+c_{v1}^3\right)^2}\left[\left(\chi^3+c_{v1}^3\right)3\chi^2\frac{\partial\chi}{\partial W}-3\chi^5\frac{\partial\chi}{\partial W}\right]=\frac{3c_{v1}^3\chi^2}{\left(\chi^3+c_{v1}^3\right)^2}\frac{\partial\chi}{\partial W}, \tag{3.61a}
$$

$$
\begin{aligned}
\frac{\partial f_{v2}}{\partial W} &= -\frac{1}{(1+\chi f_{v1})^2}\left[(1+\chi f_{v1})\frac{\partial\chi}{\partial W}\right]-\chi\left(f_{v1}\frac{\partial\chi}{\partial W}+\chi\frac{\partial f_{v1}}{\partial W}\right)\\
&= \frac{1}{(1+\chi f_{v1})^2}\left(\chi^2\frac{\partial f_{v1}}{\partial W}-\frac{\partial\chi}{\partial W}\right),
\end{aligned} \tag{3.61b}
$$

$$
\frac{\partial f_{t2}}{\partial W}=-2c_{t3}c_{t4}\exp\left(-c_{t4}\chi^2\right)\chi\frac{\partial\chi}{\partial W}=-2c_{t4}f_{t2}\chi\frac{\partial\chi}{\partial W}. \tag{3.61c}
$$

By definition, the vorticity for a 3D flow field is formulated as,

$$
\begin{aligned}
\|\text{curl } u\|_2 = \Bigg\{ &\left[\left(\frac{\partial u_3}{\partial x_2}\right)^{\text{GG}}-\left(\frac{\partial u_2}{\partial x_3}\right)^{\text{GG}}\right]^2+\left[\left(\frac{\partial u_1}{\partial x_3}\right)^{\text{GG}}-\left(\frac{\partial u_3}{\partial x_1}\right)^{\text{GG}}\right]^2\\
&+\left[\left(\frac{\partial u_2}{\partial x_1}\right)^{\text{GG}}-\left(\frac{\partial u_1}{\partial x_2}\right)^{\text{GG}}\right]^2\Bigg\}^{1/2}.
\end{aligned} \tag{3.62}
$$

As mentioned in section 3.1.4., Green-Gauss gradients method is used to compute the gradients of the velocity appearing on the previous equation.

Further, the derivative of the vorticity is straightforward,

$$\begin{aligned}\frac{\partial \|\text{curl } u\|_2}{\partial W} = \frac{1}{\|\text{curl } u\|_2}\Bigg\{ &\left[\left(\frac{\partial u_3}{\partial x_2}\right)^{\text{GG}} - \left(\frac{\partial u_2}{\partial x_3}\right)^{\text{GG}}\right]\frac{\partial}{\partial W}\left[\left(\frac{\partial u_3}{\partial x_2}\right)^{\text{GG}} - \left(\frac{\partial u_2}{\partial x_3}\right)^{\text{GG}}\right] \\ &+\left[\left(\frac{\partial u_1}{\partial x_3}\right)^{\text{GG}} - \left(\frac{\partial u_3}{\partial x_1}\right)^{\text{GG}}\right]\frac{\partial}{\partial W}\left[\left(\frac{\partial u_1}{\partial x_3}\right)^{\text{GG}} - \left(\frac{\partial u_3}{\partial x_1}\right)^{\text{GG}}\right] \\ &+\left[\left(\frac{\partial u_2}{\partial x_1}\right)^{\text{GG}} - \left(\frac{\partial u_1}{\partial x_2}\right)^{\text{GG}}\right]\frac{\partial}{\partial W}\left[\left(\frac{\partial u_2}{\partial x_1}\right)^{\text{GG}} - \left(\frac{\partial u_1}{\partial x_2}\right)^{\text{GG}}\right]\Bigg\}.\end{aligned} \tag{3.63}$$

Special consideration has to be placed when the flow filed is irrotational, i.e., there are no velocity gradients. In this scenario, the vorticity will be equal to zero and the derivative of the vorticity will be singular. In these situations, from a physical point of view, $\frac{\partial \|\text{curl } u\|_2}{\partial W}$ is obviously equal to zero.

Now, the remaining task is to compute the derivative of the velocity gradients with respect to W appearing in equation (3.63). Denoting by z the flow field and turbulent variables $(z_1, z_2, z_3, z_4, z_5, z_6) := (\rho, \rho u_1, \rho u_2, \rho u_3, \rho E, \tilde{\nu})$, then we obtain from equation (3.16) for $i = 1,2,3$, $m = 2,3,4$,

$$\frac{\partial}{\partial z_1^{(l)}}\left(\frac{\partial u_i^{(k)}}{\partial x_j}\right)^{\text{GG}} = \frac{1}{\text{vol}(\Omega_k)}\begin{cases}\sum_{n\in\mathcal{N}(k)} -\text{svol}(\Omega_{kn})\frac{(n_{kn})_j}{2}\frac{u_i^{(l)}}{\rho^{(k)}}, & l = k \\ -\text{svol}(\Omega_{kl})\frac{(n_{kl})_j}{2}\frac{u_i^{(k)}}{\rho^{(l)}}, & l \in \mathcal{N}(k) \\ 0, & l \neq k, l \notin \mathcal{N}(k)\end{cases}, \tag{3.64a}$$

$$\frac{\partial}{\partial z_m^{(l)}}\left(\frac{\partial u_i^{(k)}}{\partial x_j}\right)^{\text{GG}} = \frac{1}{\text{vol}(\Omega_k)}\begin{cases}\sum_{n\in\mathcal{N}(k)} \text{svol}(\Omega_{kn})\frac{(n_{kn})_j}{2}\frac{1}{\rho^{(k)}}, & l = k \\ \text{svol}(\Omega_{kl})\frac{(n_{kl})_j}{2}\frac{1}{\rho^{(l)}}, & l \in \mathcal{N}(k) \\ 0, & l \neq k, l \notin \mathcal{N}(k)\end{cases}, \tag{3.64b}$$

and,

$$\frac{\partial}{\partial z_5^{(l)}}\left(\frac{\partial u_i^{(k)}}{\partial x_j}\right)^{\text{GG}} = \frac{\partial}{\partial z_6^{(l)}}\left(\frac{\partial u_i^{(k)}}{\partial x_j}\right)^{\text{GG}} = 0. \tag{3.64c}$$

For the computation of the derivative of the modified vorticity $\tilde{S}$, we first note that,

$$\frac{\partial \bar{S}}{\partial W} = \frac{1}{\kappa^2 d^2}\left(f_{v2}\frac{\partial \tilde{\nu}}{\partial W} + \tilde{\nu}\frac{\partial f_{v2}}{\partial W}\right). \tag{3.65}$$

Hence, in the case $\tilde{S} \geq -c_{v2}S$:

$$\frac{\partial \tilde{S}}{\partial W} = \frac{\partial \|\text{curl } u\|_2}{\partial W} + \frac{\partial \bar{S}}{\partial W}. \tag{3.66}$$

For the other case, when $\tilde{S} < -c_{v2}S$, we define,

$$\bar{S}^{\text{nom}} = S\Big(c_{v2}^2 S + c_{v3}\bar{S}\Big), \tag{3.67a}$$

$$\bar{S}^{\text{denom}} = S(c_{v3} - 2c_{v2})S - \bar{S}, \tag{3.67b}$$

in order to express:

$$\frac{\partial \tilde{S}}{\partial W} = \frac{\partial \|\text{curl } u\|_2}{\partial W} + \frac{\bar{S}^{\text{denom}} \frac{\partial \bar{S}^{\text{nom}}}{\partial W} - \bar{S}^{\text{nom}} \frac{\partial \bar{S}^{\text{denom}}}{\partial W}}{\Big(\bar{S}^{\text{denom}}\Big)^2}, \tag{3.68a}$$

$$\frac{\partial \bar{S}^{\text{nom}}}{\partial W} = 2c_{v2}^2 S \frac{\partial S}{\partial W} + c_{v3}\left(S\frac{\partial \bar{S}}{\partial W} + \bar{S}\frac{\partial S}{\partial W}\right), \tag{3.68b}$$

$$\frac{\partial \bar{S}^{\text{denom}}}{\partial W} = (c_{v3} - 2c_{v2})\frac{\partial S}{\partial W} - \frac{\partial \bar{S}}{\partial W}. \tag{3.68c}$$

The remaining required derivatives for the terms r, g and f_w are computed as,

$$\frac{\partial r}{\partial W} = \begin{cases} \frac{1}{\kappa^2 d^2 \tilde{S}^2}\Big(\tilde{S}\frac{\partial \tilde{\nu}}{\partial W} - \tilde{\nu}\frac{\partial \tilde{S}}{\partial W}\Big), & \frac{1}{\kappa^2 d^2 \tilde{S}^2} \leq 10 \\ 0, & else \end{cases}, \tag{3.69}$$

$$\frac{\partial g}{\partial W} = \frac{\partial r}{\partial W}\Big(1 + c_{w2}\Big(6r^5 - 1\Big)\Big), \tag{3.70}$$

$$\frac{\partial f_w}{\partial W} = \left(\frac{1 + c_{w3}^6}{g^6 + c_{w3}^6}\right)^{1/6}\frac{\partial g}{\partial W} + \left(\frac{1 + c_{w3}^6}{g^6 + c_{w3}^6}\right)^{-5/6}\frac{g}{6}\left(-\frac{6\Big(1 + c_{w3}^6\Big)g^5\frac{\partial g}{\partial W}}{\Big(g^6 + c_{w3}^6\Big)^2}\right). \tag{3.71}$$

Finally, the derivatives of the production and destruction can be computed by,

$$\frac{\partial Pr}{\partial W} = \begin{cases} c_{b1}\Big[-\tilde{S}\tilde{\nu}\frac{\partial f_{t2}}{\partial W} + (1 - f_{t2})\tilde{\nu}\frac{\partial \tilde{S}}{\partial W} + (1 - f_{t2})\tilde{S}\frac{\partial \tilde{\nu}}{\partial W}\Big], & \tilde{\nu} \geq 0 \\ c_{b1}(1 - c_{t3})\Big(\tilde{\nu}\frac{\partial S}{\partial W} + S\frac{\partial \tilde{\nu}}{\partial W}\Big), & else \end{cases}, \tag{3.72a}$$

$$\frac{\partial De}{\partial W} = \begin{cases} \Big(\frac{\tilde{\nu}}{d}\Big)^2\Big(c_{w1}\frac{\partial f_w}{\partial W} - \frac{c_{b1}}{\kappa^2}\frac{\partial f_{t2}}{\partial W}\Big) + \Big(c_{w1}f_w - \frac{c_{b1}}{\kappa^2}f_{t2}\Big)\frac{2\tilde{\nu}}{d^2}\frac{\partial \tilde{\nu}}{\partial W}, & \tilde{\nu} \geq 0 \\ -\frac{c_{w1}}{d^2}2\tilde{\nu}\frac{\partial \tilde{\nu}}{\partial W}, & else \end{cases} \tag{3.72b}$$

The derivative of the diffusion part Di holds,

$$\frac{\partial Di}{\partial W} = \frac{2c_b}{\sigma}\sum_{k=1}^{3}\left(\frac{\partial \tilde{\nu}}{\partial x_k}\right)^{\text{GG}}\frac{\partial}{\partial W}\left(\frac{\partial \tilde{\nu}}{\partial x_k}\right)^{\text{GG}}, \tag{3.72c}$$

with the derivatives with respect to the $\tilde{\nu}$ given by,

$$\frac{\partial}{\partial z_6^{(l)}}\left(\frac{\partial \tilde{\nu}^{(k)}}{\partial x_j}\right)^{\text{GG}} = \frac{1}{\text{vol}(\Omega_k)}\begin{cases} \sum_{n\in\mathcal{N}(k)}\text{svol}(\Omega_{ij})\frac{(n_{kn})_j}{2}, & l = k \\ \text{svol}(\Omega_{ij})\frac{(n_{kl})_j}{2}, & l \in \mathcal{N}(k) \\ 0, & l \neq k, l \notin \mathcal{N}(k) \end{cases}, \tag{3.73a}$$

since the derivatives with respect to the conservative variables satisfy,

$$\frac{\partial}{\partial z_i^{(l)}}\left(\frac{\partial \tilde{\nu}^{(k)}}{\partial x_j}\right)^{\text{GG}} = 0, \qquad i = 1, 2, 3, 4, 5. \tag{3.73b}$$

Because of GG method is used to discretize the gradients of $\tilde{\nu}$ in the derivative of D_i, the source terms are no longer local and thus depend on the direct neighbors.

This gives closure to the construction of the simplified Jacobian $\frac{\mathrm{d}\mathbf{R}^{1\mathrm{st}}}{\mathrm{d}\mathbf{W}}$. As noted, even when considering the assumptions introduced on section 3.2.3. and a stencil of immediate neighbors is achieved, the computation of such operator entails considerable complex derivatives and accordingly certain level of effort is required.

Chapter 4

TREATMENT OF TURBULENT FLOW EQUATIONS

This chapter covers the purpose of the investigations of this thesis, providing a discussion for the different solving strategies for the RANS equations. This includes the *loosely coupled*, the *fully coupled* and the intermediate step *weakly coupled* solvers, being the latter the mainstay of this thesis. To completely understand the key points characterizing each approach, one has to consider the nature of the problem, that is, the governing equations as well as the numerical methods implemented in the solution process. That is the reason why this chapter has been left for last.

At the beginning of the chapter we introduce the concept of the cross terms. Then, we present the loosely coupled approach and next we discuss the fully coupled. Although the weakly coupled technique is a intermediate step between the former approaches, for convenience we left its discussion for the end of the chapter.

4.1. Global solution strategy

In chapter 2 we have presented the mean flow equations along with the one equation of the Spalart-Allmaras turbulence model. Therefore, at the end of that chapter we ended up with the conservative variables vector $W_m = (\rho, \rho u_1, \rho u_2, \rho u_3, \rho E)^T$ and the additional artificial variable $W_t = (\tilde{\nu})$. Although, we have concluded that the vector of variables W comprises both, the mean flow and the turbulent flow variables, actually there are two types of approaches when it comes to the treatment of the turbulence equations problem. In the first one, which is the adopted for this thesis, is the so-called fully coupled or "*strongly coupled*" [3] approach, where all the variables are solved simultaneously, i.e., the additional transport-type equation is coupled to the mean flow equations. The second method is the so-called loosely coupled approach where the turbulent and the mean flow are solved separately. This later procedure is also known in the literature as "*decoupled*", "*time-lagged*" or "*uncoupled*" [2, 4, 28, 29, 30], although we rather prefer the loosely coupled terminology.

Before providing a definition of each strategy, we first define the cross terms of the Jacobian. In equation (3.29b) we introduced the term $\frac{\mathrm{d}\mathbf{R}}{\mathrm{d}\mathbf{W}}$, which construction was topic of section 3.3.. Each entry block of $\frac{\mathrm{d}\mathbf{R}}{\mathrm{d}\mathbf{W}}$ may be assembled as,

$$\frac{\partial R_i}{\partial W_i} = \left(\begin{array}{c|c} \frac{\partial R_\mathrm{m}}{\partial W_\mathrm{m}} & \frac{\partial R_\mathrm{m}}{\partial W_\mathrm{t}} \\ \hline \frac{\partial R_\mathrm{t}}{\partial W_\mathrm{m}} & \frac{\partial R_\mathrm{t}}{\partial W_\mathrm{t}} \end{array}\right) \tag{4.1}$$

where $\frac{\partial R_\mathrm{m}}{\partial W_\mathrm{m}}$ is a 5×5 matrix, meanwhile $\frac{\partial R_\mathrm{t}}{\partial W_\mathrm{t}}$ is of size 1×1. Hence, we define the cross terms as the derivative of the mean flow residual with respect to the turbulent flow

variables $\frac{\partial R_\mathrm{m}}{\partial W_\mathrm{t}}$ along with the derivative of the turbulent residual with respect to the mean flow variables $\frac{\partial R_\mathrm{t}}{\partial W_\mathrm{m}}$.

In the following three sections we further discuss the three solution techniques focusing on the key aspects of each of them together with its advantages and shortcomings.

4.2. Loosely coupled approach

To provide a deeper understanding of the cross terms and to explain the fundamentals of the loosely coupled method, we first consider the derivative of the mean flow residual with respect to the turbulent variables, i.e., $\frac{\partial R_\mathrm{m}}{\partial W_\mathrm{t}}$. As can be seen in the respective sections, more in concise equations (3.45), (3.56), (3.58) and (3.72), all these cross terms are exactly zero. This is a direct consequence of the S-A turbulence model, which neglects the turbulent kinetic energy contribution from the mean flow equations. Moreover, when comparing the magnitude of $\frac{\partial R_\mathrm{t}}{\partial W_\mathrm{m}}$ with the other terms in equation (4.1), one can argue that the derivatives of turbulent residual with respect to the mean flow variables are almost negligible. In the following we provide a detailed explanation for each of the three contributions, i.e., convective, viscous and source terms.

In particular for the inviscid components, they are mainly driven by the factor $\frac{\tilde{\nu}}{\rho}$, see equations (3.45a) and (3.57a). For a steady state solution, the value of transport variable $\tilde{\nu}$ is approximately zero, and even reaching zero machine value far away from the turbulent region. From this observation, a rough estimation can be made, and the factor $\frac{\tilde{\nu}}{\rho}$ can be approximated to zero, even though in the most turbulent regions of the flow field. Some examples demonstrating that fact are illustrated in figure 4.1.

For the viscous contribution, indeed its only component is given by E_4 in equation (3.58). This cross term is driven by the difference of the turbulent variable $\tilde{\nu}$ between adjacent control volume and usually it is of several orders of magnitude smaller than the rest of terms appearing in the Jacobian. Analogously to the inviscid contribution, it may be approximated to zero.

Finally for the source terms, again its contribution has a minor consideration. For instance, the most relevant contribution on these terms arises from the derivative of the vorticity. Far from the boundary layers and downstream wakes, where the flow can be nearly assumed to be almost irrotational, generally these terms can be approximated to zero, as already discussed in section 3.3.3..

Hence, one can argue that the cross terms are ≈ 0 and thus consider that the mean and turbulent flow equations are loosely coupled, significantly simplifying the expression for the Jacobian. Therefore due its relative simplicity of implementation, it is preferable to solve the set of equations in a loosely coupled manner. This approach has been followed by many researchers in the literature, e.g., [31, 32, 33, 34].

One of the first and direct benefits of this methodology is that naturally less number of operations are required, that is, there is no need to compute the cross terms. For example, returning to the definition of the vorticity, equation (3.62), note that $\|\mathrm{curl}\ u\|_2$ is solely depending on the velocity variables (mean flow). As a consequence, the derivative of the vorticity with respect to the turbulent variable W_t is exactly zero.

The major characteristic feature of the loosely coupled technique is the discretization

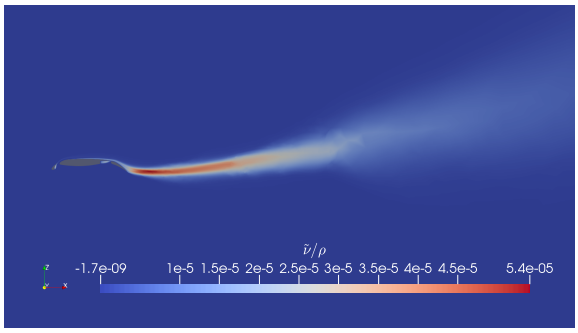

(a) MDA30P30N airfoil at $Re = 9 \cdot 10^6$, $M_\infty = 0.2$, $\alpha = 16°$

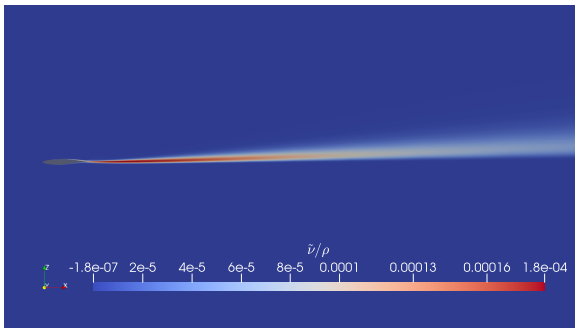

(b) RAE 2822 airfoil at $Re = 6.5 \cdot 10^6$, $M_\infty = 0.73$, $\alpha = 2.79°$

Figure 4.1: Steady state distribution of $\tilde{\nu}/\rho$.

of the governing equations. Within this approach, due to the assumption that all cross terms can be neglected, instead of having a single system of equations, as presented in equation (3.6), the discretization yields to a system of two ordinary differential equations,

$$\frac{d}{dt}\begin{pmatrix}\mathbf{W}_\mathrm{m}\\ \mathbf{W}_\mathrm{t}\end{pmatrix} = \begin{pmatrix}-\mathbf{M}_\mathrm{m}^{-1}\mathbf{R}_\mathrm{m}(\mathbf{W}_\mathrm{m},\mathbf{W}_\mathrm{t})\\ -\mathbf{M}_\mathrm{t}^{-1}\mathbf{R}_\mathrm{t}(\mathbf{W}_\mathrm{m},\mathbf{W}_\mathrm{t})\end{pmatrix}. \tag{4.2}$$

Although the computational grid for the turbulent and the mean equations is exactly the same, we have added the subscript m and t to the block diagonal mass matrix $\mathbf{M}$ to make clear that it has different dimensions.

At this end, the RANS equations along with the turbulence model instead of defining a system of equations we rather have equation (4.2). The procedure for solving the latter is called sequential solution [19, 29]. Each of the equation (4.2) is resolved for its dominant variable, that is, we assume that the mean flow equations only depend on $\mathbf{W}_\mathrm{m}$, and $\mathbf{W}_\mathrm{t}$ is temporary treated as a known constant. The turbulent equations are then solved for $\mathbf{W}_\mathrm{t}$ with an updated mean flow variables, treating $\mathbf{W}_\mathrm{m}$ as a known constant parameter. Hence, the following holds,

$$\frac{d}{dt}\mathbf{W}_\mathrm{m} = -\mathbf{M}_\mathrm{m}^{-1}\mathbf{R}_\mathrm{m}(\mathbf{W}_\mathrm{m};\mathbf{W}_\mathrm{t}), \tag{4.3a}$$

$$\frac{d}{dt}\mathbf{W}_\mathrm{t} = -\mathbf{M}_\mathrm{t}^{-1}\mathbf{R}_\mathrm{t}(\mathbf{W}_\mathrm{t};\mathbf{W}_\mathrm{m}). \tag{4.3b}$$

Then, equations (4.3a) and (4.3b) are solved sequentially employing the methods described in section 3.2..

In our context, we only seek to approximate steady state solutions, which allows to further exploit the scheme defined by equation (4.3). On each computation cycle, i.e., $t+\Delta t$, instead of carrying out one iteration on each of them, the scheme can be adapted to perform more iterations on the turbulence equations than in the mean flow. This is a common method to make the scheme more robust [19]. Furthermore, different CFL numbers can be used for the mean and the turbulent flow equations. In that sense, the loosely coupled approach has less restrictions when implementing the solution methods.

4.3. Fully coupled approach

This approach corresponds to the one used for derivation of the different sections throughout this thesis. It is based on the principle that the six variables define a single system of equations in which are all simultaneously solved.

For the discussion of this procedure we first start by stating that naturally, the turbulent flow equations have a strong dependence on the mean flow, as well as on the other way around, the mean flow equations are related to the turbulent equations by means of $\tilde{K}$, although some turbulence models, such as the one used in this thesis, simply neglect this term.

On the one hand, as pointed out by [1, 2], the loosely coupled approach presents deficiencies when solving for high turbulent regions, e.g. shear flows. It is possibly because the interaction between the two sets of equations is omitted. For viscous flows near solid surfaces and wakes, where large velocity gradients are created, the vorticity values are non-negligible. Hence, its derivative plays a relative important role on the computations. Unlike the loosely coupled approach, the fully coupled takes this derivative into account, see equation (3.63). On the other hand, when the RANS and turbulence equations are solved in a fully coupled manner, the mathematical formulation is consistent in opposite to the loosely coupled approach, as the cross terms are considered. In addition, the equations are solved all at once, preserving the integrity of the whole system. This allows to recover the full Newton's method equation (3.29a), and thus after each iteration, the result is expected to be consistent, in contrast to the loosely coupled technique. As a global result, less overall cycles are expected.

The major drawback from this approach is that 6×6 tri-diagonal block matrices systems need to be solved. Usually, the computation of such a system is more time demanding than the 5×5 along with the 1×1, and accordingly larger CPU times are expected.

We start the review in the literature by pointing that there is no clear answer to whether the two sets of equations should be solved fully or loosely coupled. According to [1], for an asymmetric bump test case, an implicit two-equation turbulence model fully coupled method presented better results regarding robustness and efficiency with respect to the loosely coupled approach. [2] also asserted that far superior effects on the final convergence as well as on the convergence rate are attained for a two-equation model fully coupled solver. For the solution procedures they employed multigrid methods together with different acceleration techniques and an implicit time-marching formulation. For the test cases, they considered a turbine cascade flow and the transonic flow around the RAE airfoil. Both of them considered the contribution of the turbulent kinetic energy into the mean flow equations.

On the one hand, this behaviour in accordance with [35], who stated that coupled methods are exploded only when the turbulent kinetic energy contribution is considered on the mean flow equations. On the other hand, [36] presented more robust and more accurate results for the coupled solver with the one equation Spalart-Allmaras turbulence model. Also, in somehow contradiction to [35], [3, 28] demonstrated that even when considering the turbulent kinetic energy, the fully coupled technique does not exhibit notable benefits. Moreover, they concluded that no difference is observed in the accuracy of the results neither in the convergence rate for the fully coupled and

loosely coupled methods. This is on the line with [4], who also pointed out that when considering the turbulent kinetic energy, the obtained results for the fully coupled are almost identical as for the loosely coupled manner.

A serious drawback of this approach is that some turbulence models such as the $k-\omega$ and $k-\varepsilon$ are not straightforward to implement when considering the turbulent kinetic energy. They require an special treatment of the boundary conditions which may represent a challenge when implementing the solver.

As may be deducted from previous expositions, there is a lack in the literature concerning comparative studies of the coupling strategies for the RANS equations. Moreover, there is no concise answer whether the turbulent transport equations should be coupled to the RANS equations or not. As stated, in some circumstances there is no much gain, and even no benefit at all, to solve the system of equations fully coupled. Considering the benefits from the loosely coupled approach and the uncertainties of the fully coupled, these are probably the main reasons why the loosely coupled is possibly the preferred solution technique.

4.4. Weakly coupled approach

In the loosely coupled approach, the turbulent and the mean flow equations are solved separately and hence the cross terms are simply not defined. For the fully coupled solver, both systems of equations are coupled together to define a unique system of equations which is solved at once. For this approach, it is mandatory to compute the cross terms. In addition, we present a third method, the so-called weakly coupled. This technique is based on an intermediate step between both presented methods. We consider a single system of equations as for the fully coupled, but we do not consider the cross terms, that is, they are simply set to zero as in the loosely coupled. This method, at least for the knowledge of the author, has not been seen previously in the literature.

The only difference between this approach and the loosely coupled strategy is the solution algorithm, i.e., how is the system of equations solved. Thus, within this procedure we can assess the "coupling" strategy procedure between the equations. Whence its name of weakly coupled.

Finally, we note that in the current framework ((block) CSR matrices), and using the Negative S-A turbulence model along with the fully coupled or weakly coupled approaches, the memory requirement to store the Jacobian $\frac{\mathrm{d}\mathbf{R}}{\mathrm{d}\mathbf{W}}$ is about 1.38 times more than for the loosely coupled. For a two equation turbulent mode, this ratio is about 1.69. Although in modern day computers specially on high environment clusters this plays a minor effect, it may be of major issue for consideration when carried out to complex 3D geometries, where high density meshes are required.

Chapter 5

NUMERICAL APPLICATION

This chapter is centered upon the verification and analysis of the performance of both implemented solvers, i.e., the weakly coupled (WC) and the fully coupled (FC). This investigation is carried out by studying several well known fully turbulent benchmark test cases. Furthermore, an assessment is performed by comparison of the obtained results with those obtained using a loosely coupled (LC) solver under the same framework. Besides that, for the validation, the computational results are compared against experimental data. It is the goal of this section to summarize and present these results.

Each of the following examples has been chosen because of its special interest. They present remarkable characteristics that stand out of from the others, such as the presence of a shock wave, massive flow separation and recirculation regions, demonstrating that the developed methods can be applied to a variety of different flows.

The CFL number is required for the computation of the local time step, see equation (3.30). We start the computations with a given CFL number, $\mathrm{CFL}_{\mathrm{init}}$. For stability of the solution, it is set to constant for the first 10 cycles, and then it is increased with a ratio of γ^{n-10}. However, in order to enforce a stable computation, a maximum CFL number $\mathrm{CFL}_{\mathrm{max}}$ is necessary. While in a fully or weakly coupled approach only one system of equations is solved and therefore only one CFL number is required, the treatment of the equations in a loosely coupled fashion allows for different CFL conditions for the mean and the turbulent flow equations. Thus, we can write the following,

$$\mathrm{CFL}_{\mathrm{mean}}(n) = \min\{\mathrm{CFL}_{\mathrm{mean,init}} \cdot f_{\mathrm{mean}}(n), \mathrm{CFL}_{\mathrm{mean,max}}\}, \tag{5.1a}$$

$$\mathrm{CFL}_{\mathrm{turb}}(n) = \min\Big\{\mathrm{CFL}_{\mathrm{turb,init}} \cdot f_{\mathrm{turb}}(n), \mathrm{CFL}_{\mathrm{turb,max}}\Big\}, \tag{5.1b}$$

$$f_{\mathrm{mean,turb}}(n) = \begin{cases} 1, & n < 10, \\ \gamma_{\mathrm{mean,turb}}^{n-10}, & n \geq 10 \end{cases}. \tag{5.1c}$$

For the weakly coupled and fully coupled computations the "mean" value parameters are used. We note that unless otherwise specified, we apply the full multigrid technique only for the 3D scenarios. Finally, to express that a computation ended with a non physical outcome we use the term "nan", referring to "not a number".

5.1. Criterion for convergence

The goal is to reach a steady state solution, i.e., the conservative variables and $\tilde{\nu}$ are not time-dependent. In particular, to study the convergence history and measure the residual, we rely on the two most important variables. The first one is density. It is present in all five components that define the vector of conservative variables for the mean flow. The second relevant variable of interest is the turbulent transport variable

$\tilde{\nu}$. Thus, to quantify their residual we define,

$$\text{density residual}(n) = \sqrt{\sum_{j=1}^{N_{\text{elem}}} \frac{\left(\mathbf{R}_{\rho,j}(\mathbf{W}^n)\right)^2}{\left(\text{vol}(\Omega_j)\right)^2}} \Big/ \sqrt{\sum_{j=1}^{N_{\text{elem}}} \frac{\left(\mathbf{R}_{\rho,j}(\mathbf{W}_\infty)\right)^2}{\left(\text{vol}(\Omega_j)\right)^2}}, \tag{5.2a}$$

$$\text{turbulent residual}(n) = \sqrt{\sum_{j=1}^{N_{\text{elem}}} \frac{\left(\mathbf{R}_{\tilde{\nu},j}(\mathbf{W}^n)\right)^2}{\left(\text{vol}(\Omega_j)\right)^2}} \Big/ \sqrt{\sum_{j=1}^{N_{\text{elem}}} \frac{\left(\mathbf{R}_{\tilde{\nu},j}(\mathbf{W}_\infty)\right)^2}{\left(\text{vol}(\Omega_j)\right)^2}}. \tag{5.2b}$$

Previous expressions represent the l_2 volume weighted norm for density and $\tilde{\nu}$ variables normalized with the reference values, i.e., initial conditions values. For the convergence criterion, we conclude that the obtained solution is accurate enough when the normalized density residual has been reduced 14 orders of magnitude with respect to the initial guess, i.e., equation (5.2a) is $< 10^{-14}$. Due to the difficulty of choosing a suitable initial condition value for the turbulent variable, in general it is not straightforward to reduce the normalized turbulent residual to zero machine.

Further parameters are required for the evaluation and validation of the obtained solution. We have restricted ourselves to the study of fully turbulent aerodynamic problems in open domains. A common aerodynamic practice is the assessment of the non-dimensional lift and drag coefficients, C_L and C_D respectively. The integration of the pressure and viscous stresses over the surface of an object yields to the computation of the total aerodynamic force acting on the body,

$$F = \int_{S_{\text{ref}}} \left(-\langle f_c(W), n\rangle + \langle f_v(W), n\rangle\right) \mathrm{d}S_{\text{ref}}, \tag{5.3}$$

where S_{ref} is the reference area of the body. The lift corresponds to the force component acting normal to the freestream direction, meanwhile, the drag is the parallel decomposition of F. Using polar coordinates and denoting α for the angle of attack (AoA),

$$\begin{aligned} g(\alpha) &= (0, \cos\alpha, 0, \sin\alpha, 0, 0)^T, \\ h(\alpha) &= (0, -\sin\alpha, 0, \cos\alpha, 0, 0)^T, \end{aligned}$$

thereby,

$$\begin{aligned} D &= \langle F,\ g(\alpha)\rangle, \\ L &= \langle F,\ h(\alpha)\rangle. \end{aligned}$$

Finally, the lift and drag coefficients are defined as,

$$C_D = \frac{D}{q_\infty S_{\text{ref}}} = C_{D,p} + C_{D,v}, \tag{5.4a}$$

$$C_L = \frac{L}{q_\infty S_{\text{ref}}} = C_{L,p} + C_{L,v}, \tag{5.4b}$$

where the subscript p denotes the effects due to pressure and the subscript v the viscous contribution, with $q_\infty = \frac{1}{2}\rho_\infty u_\infty^2$ the freestream dynamic pressure. Additionally,

we define the non-dimensional pressure C_p and skin friction C_f coefficients. The former one provides information about the pressure distribution along the surface, and thus direct evaluation of the conservative variable ρE, see equation (2.5). The latter, reports wall stress information and therefore the impact of the velocity gradients (see equation (2.6)). By definition, the following holds,

$$C_p = \frac{p - p_\infty}{q_\infty}, \quad p = \Big\langle \langle f_c(W(x)), n(x) \rangle, (0, n(x), 0)^T \Big\rangle, \quad x \in \partial\Omega, \tag{5.5a}$$

$$C_f = \frac{\tau_{\text{wall}}}{q_\infty}, \quad \tau_{\text{wall}} = \Big\langle \langle f_v(W(x)), n(x) \rangle, (0, t(x), 0)^T \Big\rangle, \quad x \in \partial\Omega, \tag{5.5b}$$

where $t(x)$ denotes the tangential vector. For the 2D cases, must be noted that the drag and lift coefficient values are per unit span.

5.2. Stability analysis

A very powerful methodology for the assessment of the behavior of the solution algorithm is the stability analysis. In our approach, we study and evaluate the stability of the preconditioner $\mathbf{Prec}_j$ from the Runge-Kutta algorithm. To do it so, we follow step by step the procedures described in [5, Section 7.2]. This method consists on a direct linear stability analysis, where the corresponding eigenvalues of the system are obtained for a qualitative characterization of the algorithm.

The analysis method is based on the linearized RANS and turbulence system of equations around the equilibrium point, i.e., the base flow corresponds to the steady state solution $\mathbf{W}^*$. By definition, this solution satisfies $\mathbf{R}(\mathbf{W}^*) = 0$. Then, an infinitesimal disturbance $\|\mathbf{W}\| < \varepsilon$ is introduced into $\mathbf{W}^*$ in order to evaluate its response behavior i.e., whether it is amplified or damped. Therefore we approximate,

$$\begin{aligned} \frac{d\mathbf{W}(t)}{dt} &= \frac{d(\mathbf{W}^* + \mathbf{W}(t))}{dt} = -\mathbf{M}^{-1}\mathbf{R}(\mathbf{W}^* + \mathbf{W}) \\ &\approx -\mathbf{M}^{-1}\left(\mathbf{R}(\mathbf{W}^*) + \frac{d\mathbf{R}}{d\mathbf{W}}(\mathbf{W}^*)\mathbf{W}\right) \\ &= -\mathbf{M}^{-1}\mathbf{A}\mathbf{W}(t), \qquad \mathbf{A} = \frac{d\mathbf{R}}{d\mathbf{W}}(\mathbf{W}^*). \end{aligned} \tag{5.6}$$

Then, the linearized counterpart is replaced into the RK algorithm yielding to,

$$\begin{aligned} \mathbf{W}^{(0)} &= \mathbf{W}^n \\ \mathbf{W}^{(1)} &= \mathbf{W}^{(0)} - \alpha_{21}\mathbf{Prec}_1^{-1}\mathbf{A}\mathbf{W}^{(0)} \\ &\vdots \\ \mathbf{W}^{(s)} &= \mathbf{W}^{(0)} - \alpha_{s+1,s}\mathbf{Prec}_1^{-1}\mathbf{A}\mathbf{W}^{(s-1)} \\ \mathbf{W}^{(n+1)} &= \mathbf{W}^{(s)}, \end{aligned} \tag{5.7}$$

which can be expressed by the polynomial expression,

$$\begin{aligned} \mathbf{W}^{n+1} &= q_s\Big(\mathbf{Prec}^{-1}\mathbf{A}\Big)\mathbf{W}^n, \\ q_s(z) &= 1 + \textstyle\sum_{j=1}^{s}(-1)^j z^j \prod_{i=s-j+1}^{s} \alpha_{i+1,i}. \end{aligned} \tag{5.8}$$

Considering the approximated linear model described by equation (5.8), the stability theory addresses that the necessary and sufficient condition for convergence is that the spectral radius of $q_s\left(\mathbf{Prec}^{-1}\mathbf{A}\right)$ is smaller than one:

$$\rho\Big(q_s\Big(\mathbf{Prec}^{-1}\mathbf{A}\Big)\Big) = \max_{i=1,\ldots,N_{\text{elem}}} |\lambda_i| < 1,\ \lambda_i = \text{eigenvalue}\Big(q_s\Big(\mathbf{Prec}^{-1}\mathbf{A}\Big)_{N_{\text{elem}}\times N_{\text{elem}}}\Big).$$

For the approximation of the eigenvalues we use a GMRES method [37] using Arnoldi's decomposition [38] truncated after a finite number of steps.

In particular we will consider the stability of the preconditioner for the fully coupled and the weakly coupled solvers, and the mean and turbulent preconditioners from the loosely coupled technique. Naturally, to perform such an analysis it is mandatory to obtain a converged solution.

5.3. CASE 9, RAE 2822

For this first example we consider the classical well known Royal Aircraft Establishment (RAE) 2822 airfoil [39] shown in figure 5.1. This two dimensional example is a relatively simple case which is extensively used for turbulence modeling validation [14]. It is characterized by a shock wave on the upper surface around the 53% of the chord length of the airfoil with induced separation behind the sock. Also weak separation occurs at the trailing edge. This can be observed in the C_f distribution in figure 5.2(b).

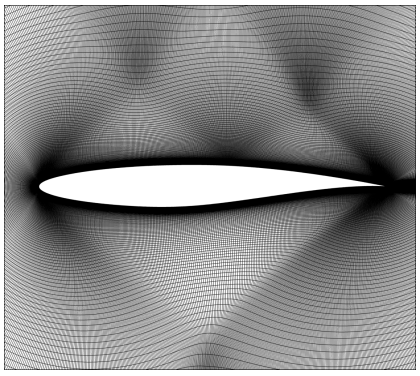

Figure 5.1: RAE 2822: Close-up view of the RAE 2822 mesh

As discussed in section 3.1.5., the flow field can be completely imposed by the Mach and Reynolds' numbers along with the angle of attack and the Sutherland's constant, which, for this latter parameter, we will consider 110.4 K for all our computations. Therefore, the RAE 2822 problem freestream physical conditions are given by:

- Reynolds number: $Re = 6.5 \cdot 10^6$.
- Inflow Mach number: $M_\infty = 0.73$.
- Angle of attack: $\alpha = 2.79°$.

The computations are performed in three different grid refinement levels: Coarse, Medium and Fine which dimensions are 320×64, 640×128 and 1280×256 respectively. The details are given in table 5.1.

Table 5.1: RAE 2822: Meshes data

Level	No. of points	No. of quadrilaterals
Coarse (C)	20832	20480
Medium (M)	82624	81920
Fine (F)	329088	327680

Through out previous chapters, different solution algorithms have been introduced, e.g., the implicit RK and the Block line Symmetric Gauss-Seidel method. To evaluate the robustness and efficiency of the solution methods for the developed solvers, several computations have been performed adjusting these parameters. In particular we investigate the robustness and number of cycles regarding the following parameters: time step γ, the number of stages of the implicit Runge-Kutta method and the number of Symmetric Gauss-Seidel sweeps. This study assessment is carried out for all the four studied benchmark test cases and for the three different solvers.

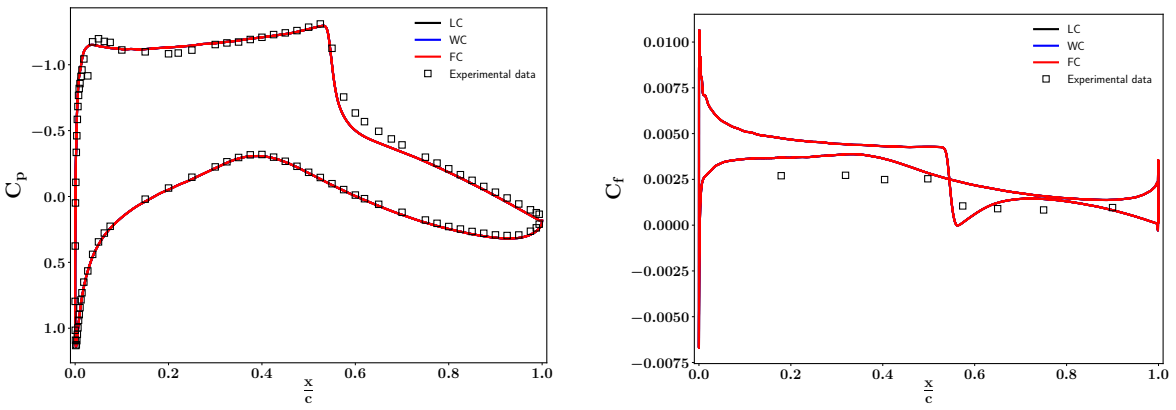

(a) C_p distribution

(b) C_f distribution

Figure 5.2: RAE 2822: Pressure and skin friction coefficients distributions for the 1280×256 mesh.

As discussed in chapter 4, for the weakly coupled and fully coupled methods the same number of nonlinear multigrid cycles for the turbulent flow equations is carried per one nonlinear multigrid cycle for the mean flow, i.e., a ratio of $1:1$. However, it has been demonstrated [5] that when solving the equations in a loosely coupled fashion, increasing this ratio results in an effective strategy, both robustness and convergence rate of the solution are increased. Hence relations greater than $1:1$ steps between the mean flow and turbulent flow equations are applied for the solution strategy of the loosely coupled approach. Nevertheless, for the purposes of this investigation, we additionally study the loosely coupled technique with a ratio of $1:1$. In table 5.2 the summary for the different solver variants for the current example is presented.

Table 5.2: RAE 2822: Solver configuration

Level	C	M								F			
Variant	V1	V1	V2	V3	V4	V5	V6	V7	V8	V1	V2	V3	V4
No. of RK stages	3	3	3	3	3	5	5	5	3	3	3	3	3
γ (mean, turb)	1.5, 5	1.5, 5	1.2, 1.2	1.5, 5	1.2, 1.2	1.5, 5	1.2, 1.2	1.2, 1.2	1.5, 5	5, 5	1.2, 1.2	5, 5	1.2, 1.2
No. of Gauss-Seidel sweeps	5	5	5	7	7	5	5	7	5	5	5	5	5
No. of turb. steps per mean flow	3	3	3	3	3	3	3	3	1	3	3	1	1
No. of multigrid levels	4	4	4	4	4	4	4	4	4	4	4	4	4
CFL_{init} (mean, turb)	10, 10	10, 10	10, 10	10, 10	10, 10	10, 10	10, 10	10, 10	10, 10	10, 10	10, 10	10, 10	10, 10
CFL_{max} (mean, turb)	1e3, 1e3	1e3, 1e3	1e3, 1e3	1e3, 1e3	1e3, 1e3	1e3, 1e3	1e3, 1e3	1e3, 1e3	1e3, 1e3	1e3, 1e3	1e3, 1e3	1e3, 1e3	1e3, 1e3
Multigrid cycle (mean, turb)	4w, 4w	4w, 4w	4w, 4w	4w, 4w	4w, 4w	4w, 4w	4w, 4w	4w, 4w	4w, 4w	4w, 4w	4w, 4w	4w, 4w	4w, 4w
No. of domains	4	8	8	8	8	8	8	8	8	24	24	24	24

The convergence histories of the density residual and the turbulent residual for the medium mesh are shown in figure 5.3. The C_p and C_f distributions for the finest grid (F-V2) are shown in figure 5.2 along with the experimental data. As can be observed the results are in far agreement.

The corresponding numerical results for the different computations are presented in table 5.3. A major result is that the weakly coupled and fully coupled techniques have a beneficial impact on the total number of multigrid cycles, demonstrating that less iterations are required. Besides that, the CPU time per iteration for both solvers is greater than for the loosely coupled with a ratio $1:1$. These observations are in agreement with the expectations discussed in previous chapter. The obtained results indicate that the increase of the number of SGS sweeps has a negligible and even counterproductive effect on the number of iterations. In addition, the increase on the number of stages of the Runge-Kutta algorithm has a slightly detrimental impact on the overall cycles. Unfortunately, for the finest grid 1280×256 a smaller time step is required for both, the weakly coupled and fully coupled solvers.

Being aware of these last results, we further investigate the F-V1 case for the weakly coupled and loosely coupled manners. To do it so we perform the spectral analysis described in section 5.2. for both approaches. For the base flow $\mathbf{W}^*$ we have used the converged solution from the loosely coupled solver. The results from this analysis, presented in figure 5.4, reveal additionally and more in depth information about the solution algorithms, in particular for the Newton's method. As observed in that figure, the largest eigenvalue is ≤ 1 meaning that the solution algorithm for both approaches is stable. Thus, the consequence of the divergence behavior issues from the initial conditions. As mentioned in section 3.1.5. usually the initial conditions are far from being a good approximation for the root of the system of equations. For a Newton's methods it is well known that convergence and robustness are reached only when the initial conditions are close to the root. Since the initial conditions used for the simulations are non well suited, the divergence on the solution for these solvers is not an unexpected result at all.

5.4. MDA30P30N

As a second 2D case, we consider the McDonnell-Douglas 30P30N (MDA30P30N) high-lift configuration, shown in figure 5.5. This test case is described in [40] with the following physical parameters,

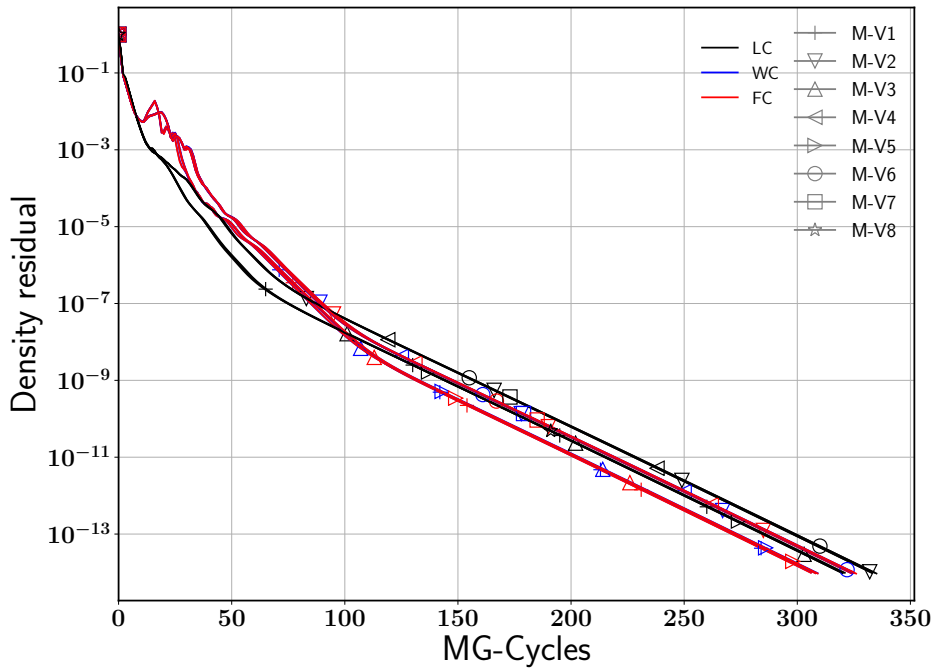

(a) Density residual

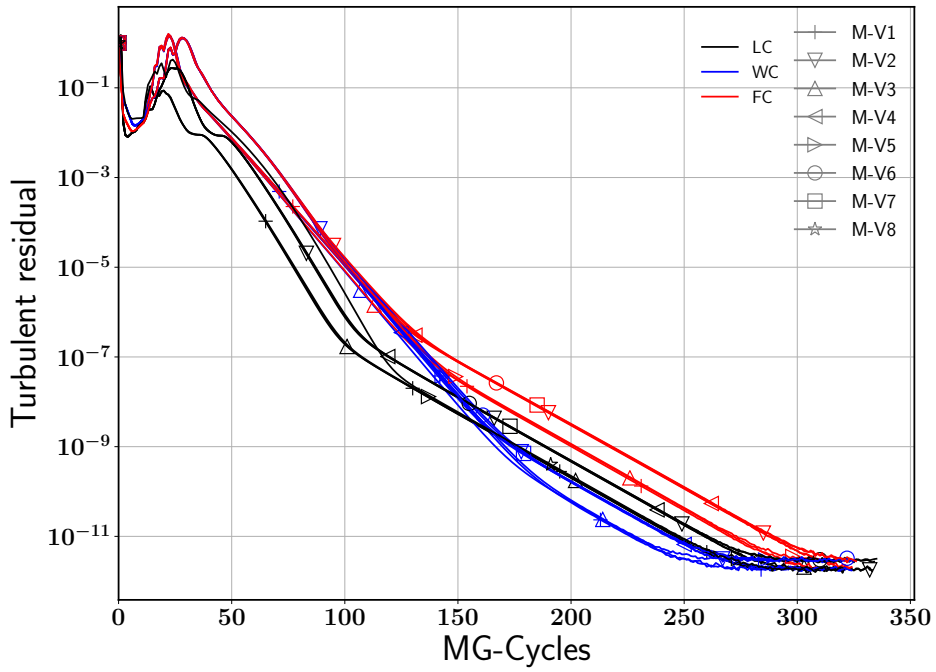

(b) Turbulent residual

Figure 5.3: RAE 2822: Convergence history for the 640×128 mesh.

Table 5.3: RAE 2822: Computational results

Level-Variant	Solver	Steps	Residual	$C_{D,p}$	$C_{D,v}$	$C_{L,p}$	$C_{L,v}$	Turb. Residual	Time (s)
C-V1	LC	182	$9.827595 \cdot 10^{-15}$	$1.122920 \cdot 10^{-2}$	$5.861403 \cdot 10^{-3}$	$7.800406 \cdot 10^{-1}$	$-4.687653 \cdot 10^{-7}$	$7.857933 \cdot 10^{-13}$	284.503
	WC	200	$9.520291 \cdot 10^{-15}$	$1.122920 \cdot 10^{-2}$	$5.861403 \cdot 10^{-3}$	$7.800406 \cdot 10^{-1}$	$-4.687653 \cdot 10^{-7}$	$7.635123 \cdot 10^{-13}$	254.861
	FC	200	$9.809225 \cdot 10^{-15}$	$1.122920 \cdot 10^{-2}$	$5.861403 \cdot 10^{-3}$	$7.800406 \cdot 10^{-1}$	$-4.687653 \cdot 10^{-7}$	$8.229872 \cdot 10^{-13}$	345.674
M-V1	LC	320	$9.595835 \cdot 10^{-15}$	$1.157256 \cdot 10^{-2}$	$5.726488 \cdot 10^{-3}$	$7.935695 \cdot 10^{-1}$	$2.694585 \cdot 10^{-6}$	$1.745443 \cdot 10^{-12}$	1569.271
	WC	306	$9.976892 \cdot 10^{-15}$	$1.157256 \cdot 10^{-2}$	$5.726488 \cdot 10^{-3}$	$7.935695 \cdot 10^{-1}$	$2.694585 \cdot 10^{-6}$	$1.812690 \cdot 10^{-12}$	1172.719
	FC	306	$9.818968 \cdot 10^{-15}$	$1.157256 \cdot 10^{-2}$	$5.726488 \cdot 10^{-3}$	$7.935695 \cdot 10^{-1}$	$2.694585 \cdot 10^{-6}$	$2.112500 \cdot 10^{-12}$	1406.486
M-V2	LC	333	$9.744666 \cdot 10^{-15}$	$1.157256 \cdot 10^{-2}$	$5.726488 \cdot 10^{-3}$	$7.935695 \cdot 10^{-1}$	$2.694585 \cdot 10^{-6}$	$1.790807 \cdot 10^{-12}$	1633.076
	WC	324	$9.517800 \cdot 10^{-15}$	$1.157256 \cdot 10^{-2}$	$5.726488 \cdot 10^{-3}$	$7.935695 \cdot 10^{-1}$	$2.694585 \cdot 10^{-6}$	$1.877586 \cdot 10^{-12}$	1247.291
	FC	324	$9.492841 \cdot 10^{-15}$	$1.157256 \cdot 10^{-2}$	$5.726488 \cdot 10^{-3}$	$7.935695 \cdot 10^{-1}$	$2.694585 \cdot 10^{-6}$	$2.042258 \cdot 10^{-12}$	1499.630
M-V3	LC	320	$9.626233 \cdot 10^{-15}$	$1.157256 \cdot 10^{-2}$	$5.726488 \cdot 10^{-3}$	$7.935695 \cdot 10^{-1}$	$2.694585 \cdot 10^{-6}$	$1.785832 \cdot 10^{-12}$	1727.149
	WC	308	$9.693291 \cdot 10^{-15}$	$1.157256 \cdot 10^{-2}$	$5.726488 \cdot 10^{-3}$	$7.935695 \cdot 10^{-1}$	$2.694585 \cdot 10^{-6}$	$1.755515 \cdot 10^{-12}$	1317.609
	FC	308	$9.545934 \cdot 10^{-15}$	$1.157256 \cdot 10^{-2}$	$5.726488 \cdot 10^{-3}$	$7.935695 \cdot 10^{-1}$	$2.694585 \cdot 10^{-6}$	$2.076089 \cdot 10^{-12}$	1592.863
M-V4	LC	333	$9.836897 \cdot 10^{-15}$	$1.157256 \cdot 10^{-2}$	$5.726488 \cdot 10^{-3}$	$7.935695 \cdot 10^{-1}$	$2.694585 \cdot 10^{-6}$	$1.669055 \cdot 10^{-12}$	1791.880
	WC	324	$9.818310 \cdot 10^{-15}$	$1.157256 \cdot 10^{-2}$	$5.726488 \cdot 10^{-3}$	$7.935695 \cdot 10^{-1}$	$2.694585 \cdot 10^{-6}$	$1.736849 \cdot 10^{-12}$	1352.963
	FC	324	$9.822708 \cdot 10^{-15}$	$1.157256 \cdot 10^{-2}$	$5.726488 \cdot 10^{-3}$	$7.935695 \cdot 10^{-1}$	$2.694585 \cdot 10^{-6}$	$2.060772 \cdot 10^{-12}$	1642.644
M-V5	LC	321	$9.799580 \cdot 10^{-15}$	$1.157256 \cdot 10^{-2}$	$5.726488 \cdot 10^{-3}$	$7.935695 \cdot 10^{-1}$	$2.694585 \cdot 10^{-6}$	$3.034383 \cdot 10^{-12}$	2066.672
	WC	309	$9.590057 \cdot 10^{-15}$	$1.157256 \cdot 10^{-2}$	$5.726488 \cdot 10^{-3}$	$7.935695 \cdot 10^{-1}$	$2.694585 \cdot 10^{-6}$	$2.858135 \cdot 10^{-12}$	1648.902
	FC	309	$9.412834 \cdot 10^{-15}$	$1.157256 \cdot 10^{-2}$	$5.726488 \cdot 10^{-3}$	$7.935695 \cdot 10^{-1}$	$2.694585 \cdot 10^{-6}$	$3.113596 \cdot 10^{-12}$	1914.955
M-V6	LC	334	$9.969339 \cdot 10^{-15}$	$1.157256 \cdot 10^{-2}$	$5.726488 \cdot 10^{-3}$	$7.935695 \cdot 10^{-1}$	$2.694585 \cdot 10^{-6}$	$2.732900 \cdot 10^{-12}$	2159.596
	WC	325	$9.694207 \cdot 10^{-15}$	$1.157256 \cdot 10^{-2}$	$5.726488 \cdot 10^{-3}$	$7.935695 \cdot 10^{-1}$	$2.694585 \cdot 10^{-6}$	$2.843748 \cdot 10^{-12}$	1714.826
	FC	325	$9.720583 \cdot 10^{-15}$	$1.157256 \cdot 10^{-2}$	$5.726488 \cdot 10^{-3}$	$7.935695 \cdot 10^{-1}$	$2.694585 \cdot 10^{-6}$	$2.950094 \cdot 10^{-12}$	1994.650
M-V7	LC	335	$9.409136 \cdot 10^{-15}$	$1.157256 \cdot 10^{-2}$	$5.726488 \cdot 10^{-3}$	$7.935695 \cdot 10^{-1}$	$2.694585 \cdot 10^{-6}$	$3.167920 \cdot 10^{-12}$	2415.968
	WC	325	$9.996932 \cdot 10^{-15}$	$1.157256 \cdot 10^{-2}$	$5.726488 \cdot 10^{-3}$	$7.935695 \cdot 10^{-1}$	$2.694585 \cdot 10^{-6}$	$2.937511 \cdot 10^{-12}$	1960.200
	FC	326	$9.342179 \cdot 10^{-15}$	$1.157256 \cdot 10^{-2}$	$5.726488 \cdot 10^{-3}$	$7.935695 \cdot 10^{-1}$	$2.694585 \cdot 10^{-6}$	$2.790416 \cdot 10^{-12}$	2261.010
M-V8	LC	320	$9.983000 \cdot 10^{-15}$	$1.157256 \cdot 10^{-2}$	$5.726488 \cdot 10^{-3}$	$7.935695 \cdot 10^{-1}$	$2.694585 \cdot 10^{-6}$	$1.999982 \cdot 10^{-12}$	1000.082
F-V1	LC	633	$9.766894 \cdot 10^{-15}$	$1.172304 \cdot 10^{-2}$	$5.703238 \cdot 10^{-3}$	$7.982617 \cdot 10^{-1}$	$2.584813 \cdot 10^{-6}$	$6.717642 \cdot 10^{-12}$	5424.712
	WC	nan	nan	nan	nan	nan	nan	nan	nan
	FC	nan	nan	nan	nan	nan	nan	nan	nan
F-V2	LC	651	$9.982645 \cdot 10^{-15}$	$1.172304 \cdot 10^{-2}$	$5.703238 \cdot 10^{-3}$	$7.982617 \cdot 10^{-1}$	$2.584813 \cdot 10^{-6}$	$6.954834 \cdot 10^{-12}$	5601.149
	WC	639	$9.810563 \cdot 10^{-15}$	$1.172304 \cdot 10^{-2}$	$5.703238 \cdot 10^{-3}$	$7.982617 \cdot 10^{-1}$	$2.584813 \cdot 10^{-6}$	$6.839093 \cdot 10^{-12}$	4576.011
	FC	639	$9.777050 \cdot 10^{-15}$	$1.172304 \cdot 10^{-2}$	$5.703238 \cdot 10^{-3}$	$7.982617 \cdot 10^{-1}$	$2.584813 \cdot 10^{-6}$	$7.027770 \cdot 10^{-12}$	5375.364
F-V3	LC	621	$9.919259 \cdot 10^{-15}$	$1.172304 \cdot 10^{-2}$	$5.703238 \cdot 10^{-3}$	$7.982617 \cdot 10^{-1}$	$2.584813 \cdot 10^{-6}$	$6.978413 \cdot 10^{-12}$	3504.829
F-V4	LC	648	$9.844957 \cdot 10^{-15}$	$1.172304 \cdot 10^{-2}$	$5.703238 \cdot 10^{-3}$	$7.982617 \cdot 10^{-1}$	$2.584813 \cdot 10^{-6}$	$7.059961 \cdot 10^{-12}$	5289.653

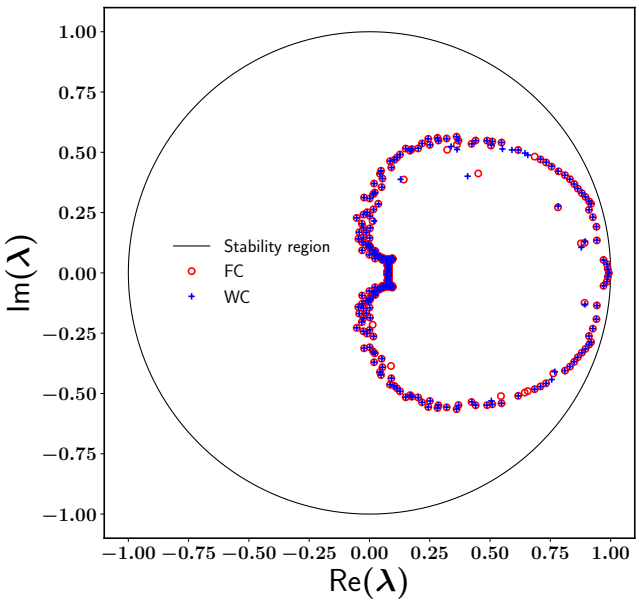

Figure 5.4: RAE 2822: Approximate spectrum

- Reynolds number: $Re = 9.0 \cdot 10^6$.
- Inflow Mach number: $M_\infty = 0.2$.
- Angle of attack: $\alpha = 16.0°$.

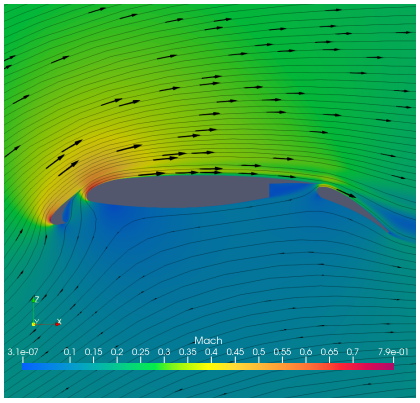

Figure 5.5: MDA30P30N: Mach number with streamlines visualization

At that configuration, this multi-element airfoil is characterized by significant recirculation regions, considerable vorticity gradients and steep density gradients as depicted in figure 5.5. As for the CASE 9, the study is performed in three different unstructured meshes. They are constituted by both quadrilaterals and triangle face shape elements. An overview of their characteristics is presented in table 5.4. Here, as well as for the previous test case, we also study the influence of the different parameters of the solution methods. The solver variations are summarized in table 5.5. Nevertheless, we note here that the MDA30P30N is much more sensitive to the parameter tweaking, and a steady state solution was not reached for all the computations.

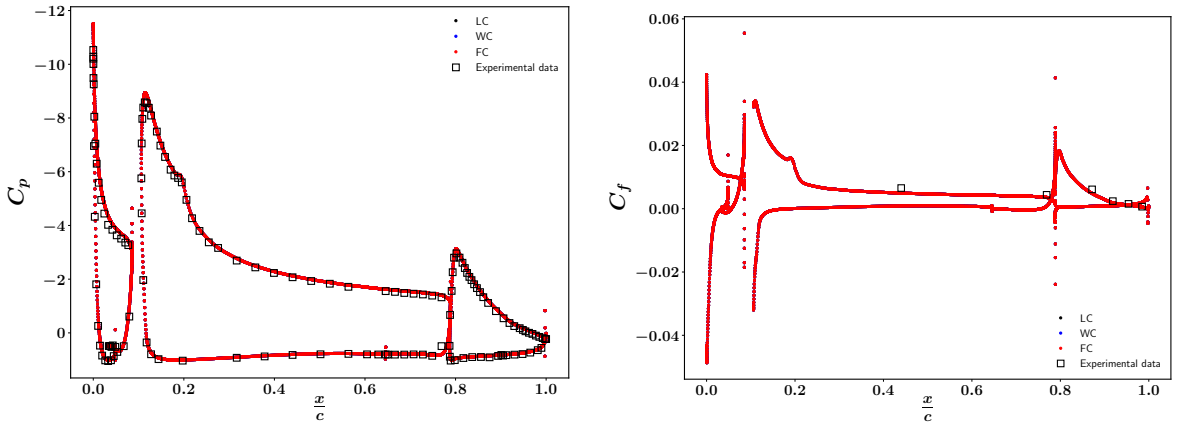

(a) C_p distribution (b) C_f distribution

Figure 5.6: MDA30P30N: Pressure and skin friction coefficients distributions for the finest mesh.

The results for the different simulations are summarized in table 5.6. A plot of the C_p and C_f distributions for the Fine mesh are shown in figure 5.6. The convergence

Table 5.4: MDA30P30N: Meshes data

Level	No. of points	No. of elements
Coarse (C)	119510	118867
Medium (M)	240955	240086
Fine (F)	485832	484673

Table 5.5: MDA30P30N: Solver configuration

Level	Coarse (C)	Medium (M)								Fine (F)	
Algorithm	V1	V1	V2	V3	V4	V5	V6	V7	V8	V1	V2
No. of RK stages	3	3	3	3	3	5	5	5	3	3	3
γ (mean, turb)	1.5, 1.5	1.5, 1.5	1.2, 1.2	1.5, 1.5	1.2, 1.2	1.5, 1.5	1.2, 1.2	1.2, 1.2	1.5, 1.5	2.5, 2.5	2.5, 2.5
No. of Gauss-Seidel sweeps	5	5	5	7	7	5	5	7	5	5	5
No. of turb. steps per mean flow	5	5	5	5	5	5	5	5	1	3	1
No. of multigrid levels	4	4	4	4	4	4	4	4	4	4	4
CFL_{init} (mean, turb)	10, 10	10, 10	10, 10	10, 10	10, 10	10, 10	10, 10	10, 10	10, 10	10, 10	10, 10
CFL_{max} (mean, turb)	1e3, 1e3	1e3, 1e3	1e3, 1e3	1e3, 1e3	1e3, 1e3	1e3, 1e3	1e3, 1e3	1e3, 1e3	1e3, 1e3	1e3, 1e3	1e3, 1e3
Multigrid cycle (mean, turb)	4w, 3v	4w, 3v	4w, 3v	4w, 3v	4w, 3v	4w, 3v	4w, 3v	4w, 3v	4w, 3v	4w, 3v	4w, 3v
No. of domains	4	8	8	8	8	8	8	8	8	24	24

histories of the density residual and the turbulent residual are shown in figure 5.7 for the medium mesh computations. The first thing to notice from these results is that for several solver configurations, the weakly coupled and fully coupled approaches present a divergent behavior. Being aware of these results, we have performed the eigenvalues stability analysis for these solvers at that particular cases. As for the CASE 9 we have used the converged solution from the loosely coupled solver as the base flow. The results of this analysis are shown in figure 5.8.

The results from the stability analysis prove that all the eigenvalues are ≤ 1. This outcome is analogous to the previous RAE 2822 test case and therefore the same interpretation about the initial conditions can be concluded. To prove the dependency on the initial conditions we consider the computation M-V6 case but now employing a full multigrid approach instead. As explained in section 3.2.1., this technique can be used to find a good initial guess for the finest mesh rather than starting from the initial conditions. The convergence histories of the residuals are shown in figure 5.9, demonstrating that the weakly coupled and fully coupled are able to reach a steady state solution when good initial conditions are used. The minus numbering in the MG-Cycles graph refer to the full multigrid approach, where 50 iterations are performed on each grid level.

An important remark is that, unlike for the CASE 9 example, now the increase in the number of SGS sweeps has a severe positive impact on the solution algorithm. For instance, a steady state solution, which was not reached for the fully coupled solver with the computation M-V1, is now achieved for the M-V3. In addition, the number of cycles is considerable reduced for the weakly coupled. As a counterpart, the increment in the number of stages of the RK algorithm has no notorious effect. In contrast to the SGS sweeps increment, it does not allow to stabilize the computations for the fully coupled, as indicated by the results from the computation M-V5. Even more has a detrimental effect, as may be observed comparing the results from the M-V2 and M-V6 computations.

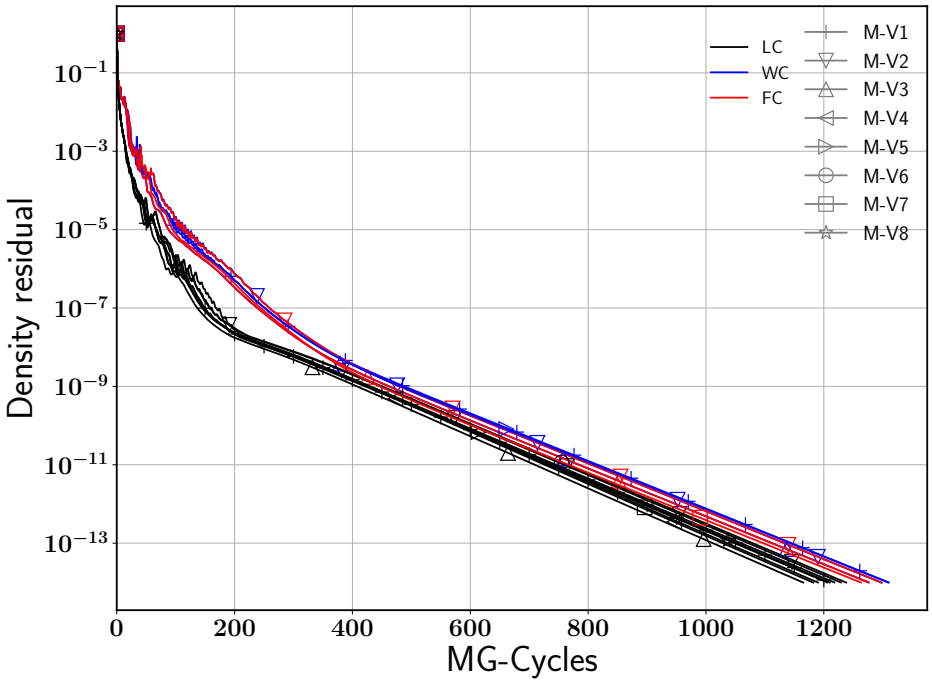

(a) Density residual

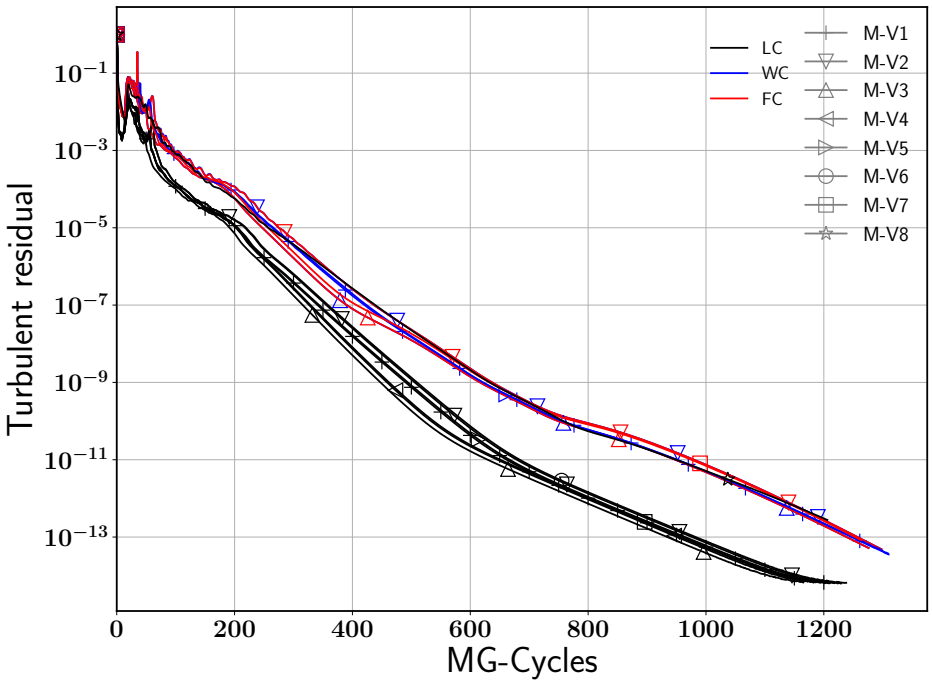

(b) Turbulent residual

Figure 5.7: MDA30P30N: Convergence history for the medium mesh.

Table 5.6: MDA30P30N: Computational results

Level-Variant	Solver	Steps	Residual	$C_{D,p}$	$C_{D,v}$	$C_{L,p}$	$C_{L,v}$	Turb. Residual	Time (s)
C-V1	LC	1214	$9.893141 \cdot 10^{-15}$	$4.161897 \cdot 10^{-2}$	$9.501822 \cdot 10^{-3}$	$4.118556 \cdot 10^{0}$	$1.333415 \cdot 10^{-3}$	$1.108616 \cdot 10^{-14}$	10804.154
	WC	1223	$9.933422 \cdot 10^{-15}$	$4.161897 \cdot 10^{-2}$	$9.501822 \cdot 10^{-3}$	$4.118556 \cdot 10^{0}$	$1.333415 \cdot 10^{-3}$	$1.174071 \cdot 10^{-13}$	10161.231
	FC	1226	$9.945566 \cdot 10^{-15}$	$4.161897 \cdot 10^{-2}$	$9.501822 \cdot 10^{-3}$	$4.118556 \cdot 10^{0}$	$1.333415 \cdot 10^{-3}$	$1.110265 \cdot 10^{-13}$	12831.104
M-V1	LC	1210	$9.924300 \cdot 10^{-15}$	$4.130793 \cdot 10^{-2}$	$9.525583 \cdot 10^{-3}$	$4.136807 \cdot 10^{0}$	$1.318726 \cdot 10^{-3}$	$6.392164 \cdot 10^{-15}$	12897.541
	WC	1310	$9.933248 \cdot 10^{-15}$	$4.130793 \cdot 10^{-2}$	$9.525583 \cdot 10^{-3}$	$4.136807 \cdot 10^{0}$	$1.318726 \cdot 10^{-3}$	$3.553269 \cdot 10^{-14}$	13253.658
	FC	nan	nan	nan	nan	nan	nan	nan	nan
M-V2	LC	1229	$9.933456 \cdot 10^{-15}$	$4.130793 \cdot 10^{-2}$	$9.525583 \cdot 10^{-3}$	$4.136807 \cdot 10^{0}$	$1.318726 \cdot 10^{-3}$	$6.269823 \cdot 10^{-15}$	13006.627
	WC	1298	$9.833016 \cdot 10^{-15}$	$4.130793 \cdot 10^{-2}$	$9.525583 \cdot 10^{-3}$	$4.136807 \cdot 10^{0}$	$1.318726 \cdot 10^{-3}$	$4.844339 \cdot 10^{-14}$	13151.966
	FC	1298	$9.788630 \cdot 10^{-15}$	$4.130793 \cdot 10^{-2}$	$9.525583 \cdot 10^{-3}$	$4.136807 \cdot 10^{0}$	$1.318726 \cdot 10^{-3}$	$4.774273 \cdot 10^{-14}$	15841.447
M-V3	LC	1165	$9.911379 \cdot 10^{-15}$	$4.130793 \cdot 10^{-2}$	$9.525583 \cdot 10^{-3}$	$4.136807 \cdot 10^{0}$	$1.318726 \cdot 10^{-3}$	$6.675957 \cdot 10^{-15}$	13838.797
	WC	1276	$9.992680 \cdot 10^{-15}$	$4.130793 \cdot 10^{-2}$	$9.525583 \cdot 10^{-3}$	$4.136807 \cdot 10^{0}$	$1.318726 \cdot 10^{-3}$	$5.238764 \cdot 10^{-14}$	14821.515
	FC	1276	$9.918291 \cdot 10^{-15}$	$4.130793 \cdot 10^{-2}$	$9.525583 \cdot 10^{-3}$	$4.136807 \cdot 10^{0}$	$1.318726 \cdot 10^{-3}$	$5.198634 \cdot 10^{-14}$	17898.853
M-V4	LC	1182	$9.880794 \cdot 10^{-15}$	$4.130793 \cdot 10^{-2}$	$9.525583 \cdot 10^{-3}$	$4.136807 \cdot 10^{0}$	$1.318726 \cdot 10^{-3}$	$6.656257 \cdot 10^{-15}$	14373.842
	WC	nan	nan	nan	nan	nan	nan	nan	nan
	FC	nan	nan	nan	nan	nan	nan	nan	nan
M-V5	LC	1218	$9.943651 \cdot 10^{-15}$	$4.130793 \cdot 10^{-2}$	$9.525583 \cdot 10^{-3}$	$4.136807 \cdot 10^{0}$	$1.318726 \cdot 10^{-3}$	$6.471062 \cdot 10^{-15}$	17634.223
	WC	1309	$9.970243 \cdot 10^{-15}$	$4.130793 \cdot 10^{-2}$	$9.525583 \cdot 10^{-3}$	$4.136807 \cdot 10^{0}$	$1.318726 \cdot 10^{-3}$	$3.773334 \cdot 10^{-14}$	18776.683
	FC	nan	nan	nan	nan	nan	nan	nan	nan
M-V6	LC	1238	$9.869760 \cdot 10^{-15}$	$4.130793 \cdot 10^{-2}$	$9.525583 \cdot 10^{-3}$	$4.136807 \cdot 10^{0}$	$1.318726 \cdot 10^{-3}$	$6.554429 \cdot 10^{-15}$	18180.395
	WC	nan	nan	nan	nan	nan	nan	nan	nan
	FC	nan	nan	nan	nan	nan	nan	nan	nan
M-V7	LC	1190	$9.910828 \cdot 10^{-15}$	$4.130793 \cdot 10^{-2}$	$9.525583 \cdot 10^{-3}$	$4.136807 \cdot 10^{0}$	$1.318726 \cdot 10^{-3}$	$6.855221 \cdot 10^{-15}$	19871.326
	WC	nan	nan	nan	nan	nan	nan	nan	nan
	FC	1263	$9.940273 \cdot 10^{-15}$	$4.130793 \cdot 10^{-2}$	$9.525583 \cdot 10^{-3}$	$4.136807 \cdot 10^{0}$	$1.318726 \cdot 10^{-3}$	$8.368857 \cdot 10^{-14}$	23581.473
M-V8	LC	1206	$9.929757 \cdot 10^{-15}$	$4.130793 \cdot 10^{-2}$	$9.525583 \cdot 10^{-3}$	$4.136807 \cdot 10^{0}$	$1.318726 \cdot 10^{-3}$	$2.763386 \cdot 10^{-13}$	8577.351
F-V1	LC	1299	$9.976555 \cdot 10^{-15}$	$4.109779 \cdot 10^{-2}$	$9.511532 \cdot 10^{-3}$	$4.138132 \cdot 10^{0}$	$1.282623 \cdot 10^{-3}$	$1.095060 \cdot 10^{-14}$	27286.527
	WC	1326	$9.937291 \cdot 10^{-15}$	$4.109779 \cdot 10^{-2}$	$9.511532 \cdot 10^{-3}$	$4.138132 \cdot 10^{0}$	$1.282623 \cdot 10^{-3}$	$3.820212 \cdot 10^{-14}$	30518.892
	FC	1327	$9.904678 \cdot 10^{-15}$	$4.109779 \cdot 10^{-2}$	$9.511532 \cdot 10^{-3}$	$4.138132 \cdot 10^{0}$	$1.282623 \cdot 10^{-3}$	$3.848231 \cdot 10^{-14}$	40680.226
F-V2	LC	nan	nan	nan	nan	nan	nan	nan	nan

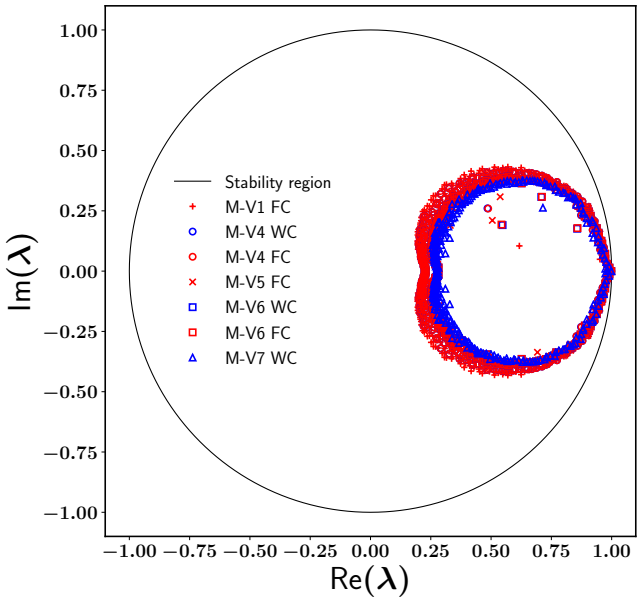

Figure 5.8: MDA30P30N: Approximate spectrum.

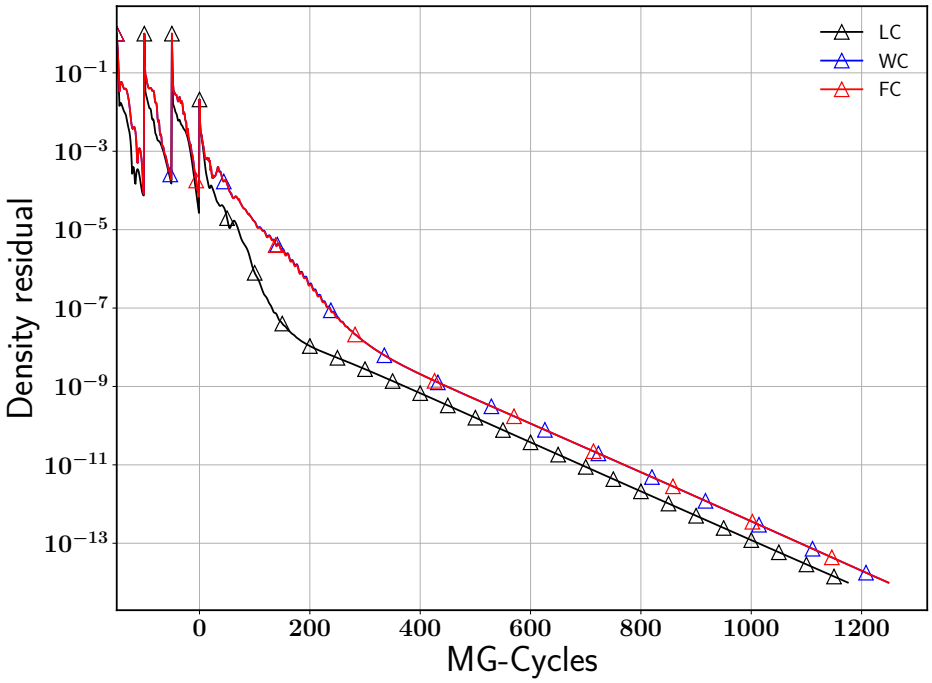

(a) Density residual

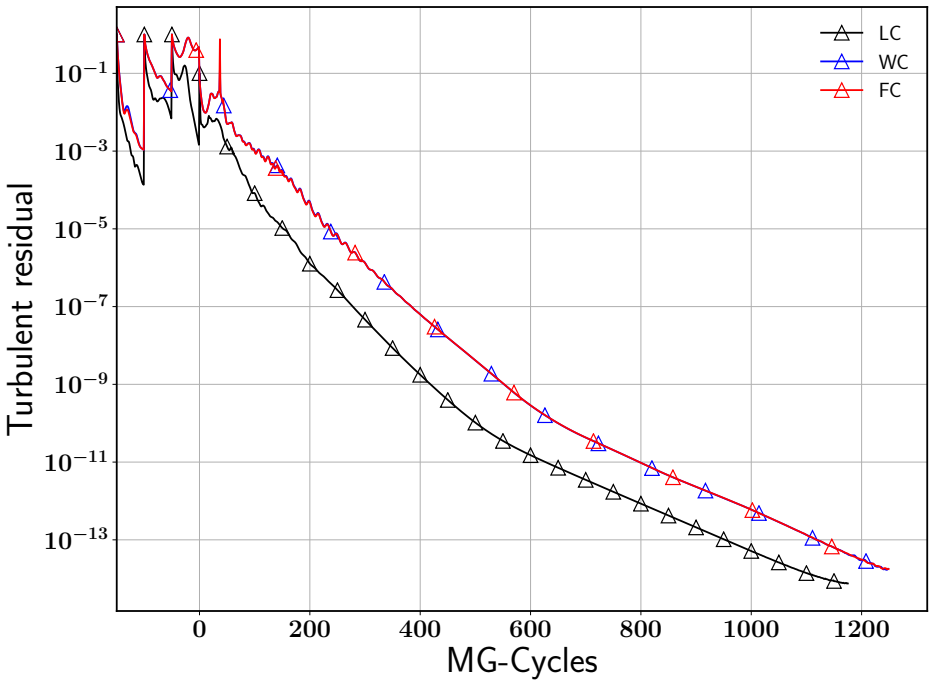

(b) Turbulent residual

Figure 5.9: MDA30P30N: Convergence history for the M-V6 using full multigrid.

Another important corollary is, the loosely coupled approach with a ratio of $1:1$ was not successful for the finest grid F-V2 whereas the weakly coupled and the fully coupled achieved a convergent solution for the computation F-V1.

5.5. DPW5 CRM

For this test case we consider the NASA Common Research Model geometry, figure 5.10(a), and configuration employed as one of the test cases on the fifth AIAA Drag Prediction Model [41]. The goal of this first 3D benchmark test case is to compute the total drag at cruise conditions where a target lift coefficient of $C_L = 0.5 \pm 0.001$ is desired. The original study is carried out on five different mesh refinement levels, L1,..., L5, and for two types of cell shapes meshes, hexaedral and hybrid. However we will restrict our study to the first four hexhaedral meshes, summarized in table 5.7 and with a detailed description provided in [41].

The cruise flight is given by the following conditions:

- Reynolds number: $Re = 5.0 \cdot 10^6$.
- Inflow Mach number: $M_\infty = 0.85$.
- Target lift coefficient: $C_L = 0.500$ with an uncertainty of ± 0.001.

Table 5.7: DPW5 CRM: Meshes data

Level	No. of Hexahedrons	No. of points
L1	638976	660177
L2	2156544	2204089
L3	5111808	5196193
L4	17252352	17441905

The solver variants and the corresponding numerical results are provided in tables 5.8 and 5.9 respectively.

Table 5.8: DPW5 CRM: Solver configuration

Level	L1	L2								L3	L4		
Algorithm	V1	V1	V2	V3	V4	V5	V6	V7	V8	V1	V1	V2	V3
No. of RK stages	3	3	3	3	3	5	5	5	3	3	3	3	3
γ (mean, turb)	1.1, 1.1	2, 2	1.2, 1.2	2, 2	1.2, 1.2	2, 2	1.2, 1.2	1.2, 1.2	2, 2	1.1, 1.1	1.05, 1.05	1.05, 1.05	1.05, 1.05
No. of Gauss-Seidel sweeps	3	3	3	5	5	3	3	5	3	3	3	5	5
No. of turb. steps per mean flow	3	3	3	3	3	3	3	3	1	3	3	3	3
No. of multigrid levels	4	4	4	4	4	4	4	4	4	4	4	4	3
CFL_{init} (mean, turb)	3, 3	3, 3	3, 3	3, 3	3, 3	3, 3	3, 3	3, 3	3, 3	3, 3	2, 3	2, 3	2, 3
CFL_{max} (mean, turb)	1e3, 1e3	1e3, 1e3	1e3, 1e3	1e3, 1e3	1e3, 1e3	1e3, 1e3	1e3, 1e3	1e3, 1e3	1e3, 1e3	1e3, 1e3	250, 250	250, 250	250, 250
Multigrid cycle (mean, turb)	4w, 3v	4w, 3v	4w, 3v	4w, 3v	4w, 3v	4w, 3v	4w, 3v	4w, 3v	4w, 3v	4w, 3v	3v, 2v	3v, 2v	3v, 2v
No. of domains	24	48	48	48	48	48	48	48	48	72	192	192	192

Regarding the Symmetric Gauss-Seidel sweeps and Runge-Kutta stages, when performing more iterations on the former parameter a reduction of the overall cycles is observed. Nevertheless, unlike for the MDA30P30N, increasing the SGS sweeps is not

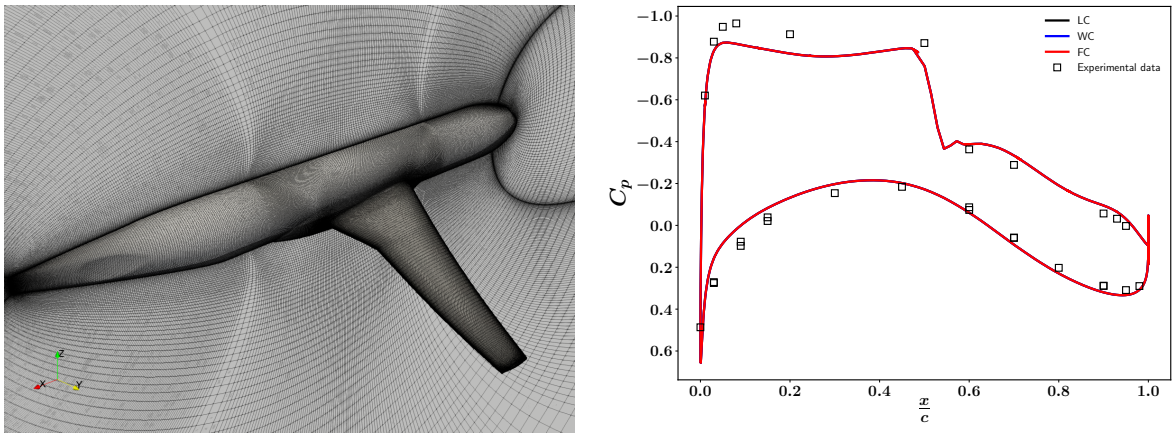

(a) Hexahedral L4 mesh

(b) C_p distribution for L4-V1

Figure 5.10: DPW5 CRM: Hexahedral L4 mesh and the computed C_p distribution at the 50.2% wing span.

enough to stabilize the solution for the weakly and fully coupled, as indicated by the L2-V3 computation. As expected, the increment in the stages of the RK algorithm does not help to stabilize the solution algorithm for these solvers.

The C_p distribution for the L4-V1 computation is shown in figure 5.10(b). The convergence histories of the density and turbulent residuals are shown in figure 5.11.

It is of interest to study the weakly coupled and fully coupled solvers for the divergent computations. As has already been done for previous cases, we study the stability behavior of the algorithm. Unfortunately, this technique was not successful and did not reveal any deeper understanding. Thus instead, we simply used the converged solution from the loosely coupled approach as a restart for the weakly coupled and fully coupled solvers. For all three cases (L2-V1, L2-V3 and L2-V5), the computations were able to perform 1000 additional cycles, proving that the solution algorithm for these solvers is stable. It confirms that the divergence issues rely on the Newton's method initial conditions.

Finally, the three solver strategies presented almost the same number of MG-Cycles for the computations on the L1, L2 and L3 meshes, whereas for the L4 mesh, more iterations are required for the weakly coupled and fully coupled strategies.

5.6. NASA Trap Wing

Based on the results from previous examples, we investigate a further test case. For this last example we consider the NASA Trap wing, shown in figure 5.12(a), used as an investigation model for the first AIAA High Lift Prediction Workshop [42]. On the one hand it is characterized because it is a pure 3D scenario. On the other hand, it stands for high lift configuration. Once again, we have used three levels of mesh refinement, roughly summarized in table 5.10. The physical conditions describing the flow field are:

- Reynolds number: $Re = 4.3 \cdot 10^6$.

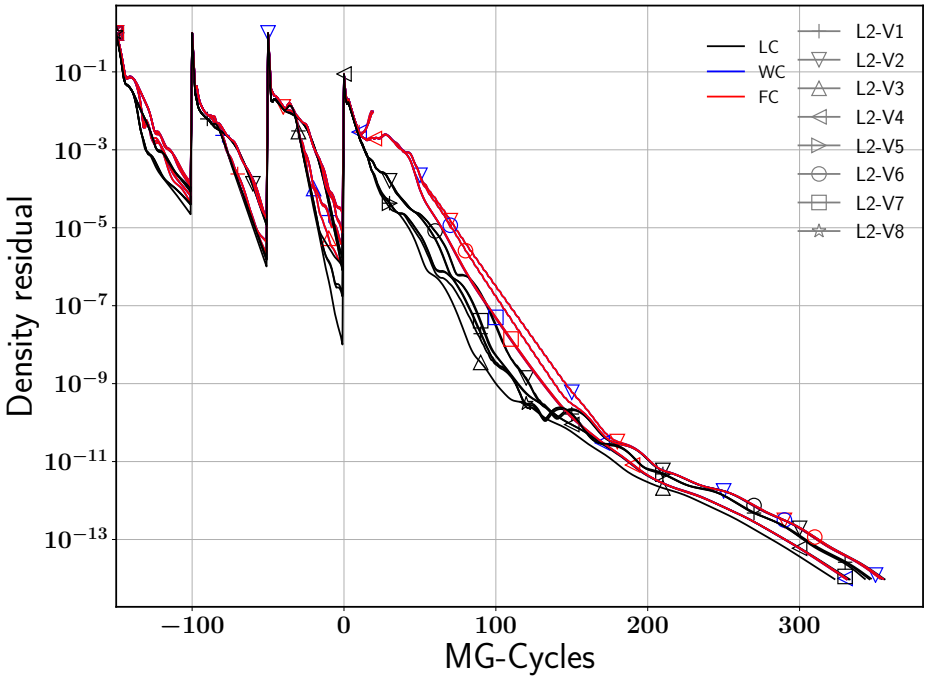

(a) Density residual

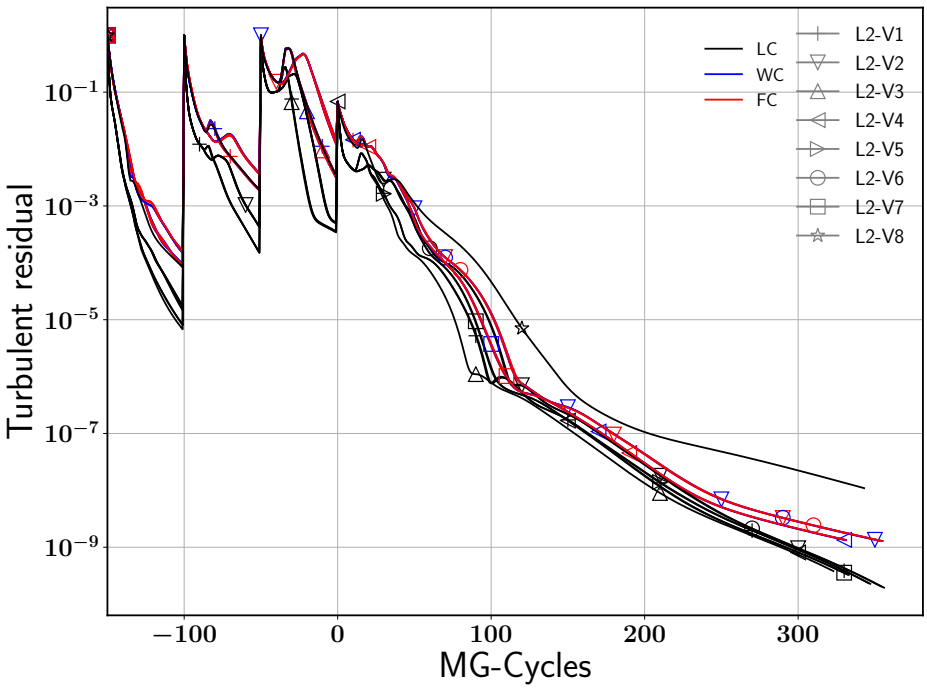

(b) Turbulent residual

Figure 5.11: DPW5 CRM: Convergence history for the L2 mesh.

Table 5.9: DPW5 CRM: Computational results

Level-Variant	Solver	Steps	Residual	$C_{D,p}$	$C_{D,v}$	$C_{L,p}$	$C_{L,v}$	Turb. Residual	Time (s)
L1-V1	LC	284	$9.635088 \cdot 10^{-15}$	$1.448039 \cdot 10^{-2}$	$1.086491 \cdot 10^{-2}$	$5.002824 \cdot 10^{-1}$	$-2.344776 \cdot 10^{-4}$	$7.530002 \cdot 10^{-11}$	9380.694
	WC	285	$9.524338 \cdot 10^{-15}$	$1.448039 \cdot 10^{-2}$	$1.086491 \cdot 10^{-2}$	$5.002824 \cdot 10^{-1}$	$-2.344776 \cdot 10^{-4}$	$1.240750 \cdot 10^{-8}$	10488.124
	FC	284	$9.620395 \cdot 10^{-15}$	$1.448039 \cdot 10^{-2}$	$1.086491 \cdot 10^{-2}$	$5.002824 \cdot 10^{-1}$	$-2.344776 \cdot 10^{-4}$	$1.265403 \cdot 10^{-8}$	13895.451
L2-V1	LC	346	$9.547239 \cdot 10^{-15}$	$1.366086 \cdot 10^{-2}$	$1.121407 \cdot 10^{-2}$	$5.005192 \cdot 10^{-1}$	$-2.271181 \cdot 10^{-4}$	$2.325271 \cdot 10^{-10}$	19842.074
	WC	nan	nan	nan	nan	nan	nan	nan	nan
	FC	nan	nan	nan	nan	nan	nan	nan	nan
L2-V2	LC	354	$9.809311 \cdot 10^{-15}$	$1.366086 \cdot 10^{-2}$	$1.121407 \cdot 10^{-2}$	$5.005192 \cdot 10^{-1}$	$-2.271181 \cdot 10^{-4}$	$2.047666 \cdot 10^{-10}$	20229.376
	WC	353	$9.972580 \cdot 10^{-15}$	$1.366086 \cdot 10^{-2}$	$1.121407 \cdot 10^{-2}$	$5.005192 \cdot 10^{-1}$	$-2.271181 \cdot 10^{-4}$	$1.300408 \cdot 10^{-9}$	22590.877
	FC	353	$9.950357 \cdot 10^{-15}$	$1.366086 \cdot 10^{-2}$	$1.121407 \cdot 10^{-2}$	$5.005192 \cdot 10^{-1}$	$-2.271181 \cdot 10^{-4}$	$1.306061 \cdot 10^{-9}$	29900.188
L2-V3	LC	323	$9.673310 \cdot 10^{-15}$	$1.366086 \cdot 10^{-2}$	$1.121407 \cdot 10^{-2}$	$5.005192 \cdot 10^{-1}$	$-2.271181 \cdot 10^{-4}$	$3.809132 \cdot 10^{-10}$	20263.591
	WC	nan	nan	nan	nan	nan	nan	nan	nan
	FC	nan	nan	nan	nan	nan	nan	nan	nan
L2-V4	LC	332	$9.525207 \cdot 10^{-15}$	$1.366086 \cdot 10^{-2}$	$1.121407 \cdot 10^{-2}$	$5.005192 \cdot 10^{-1}$	$-2.271181 \cdot 10^{-4}$	$3.319368 \cdot 10^{-10}$	20873.741
	WC	331	$9.448675 \cdot 10^{-15}$	$1.366086 \cdot 10^{-2}$	$1.121407 \cdot 10^{-2}$	$5.005192 \cdot 10^{-1}$	$-2.271181 \cdot 10^{-4}$	$1.327595 \cdot 10^{-9}$	23220.758
	FC	331	$9.407964 \cdot 10^{-15}$	$1.366086 \cdot 10^{-2}$	$1.121407 \cdot 10^{-2}$	$5.005192 \cdot 10^{-1}$	$-2.271181 \cdot 10^{-4}$	$1.336166 \cdot 10^{-9}$	30354.100
L2-V5	LC	347	$9.944391 \cdot 10^{-15}$	$1.366086 \cdot 10^{-2}$	$1.121407 \cdot 10^{-2}$	$5.005192 \cdot 10^{-1}$	$-2.271181 \cdot 10^{-4}$	$2.276593 \cdot 10^{-10}$	32015.845
	WC	nan	nan	nan	nan	nan	nan	nan	nan
	FC	nan	nan	nan	nan	nan	nan	nan	nan
L2-V6	LC	356	$9.558789 \cdot 10^{-15}$	$1.366086 \cdot 10^{-2}$	$1.121407 \cdot 10^{-2}$	$5.005192 \cdot 10^{-1}$	$-2.271181 \cdot 10^{-4}$	$1.943700 \cdot 10^{-10}$	32847.929
	WC	355	$9.707911 \cdot 10^{-15}$	$1.366086 \cdot 10^{-2}$	$1.121407 \cdot 10^{-2}$	$5.005192 \cdot 10^{-1}$	$-2.271181 \cdot 10^{-4}$	$1.283027 \cdot 10^{-9}$	36391.288
	FC	355	$9.689375 \cdot 10^{-15}$	$1.366086 \cdot 10^{-2}$	$1.121407 \cdot 10^{-2}$	$5.005192 \cdot 10^{-1}$	$-2.271181 \cdot 10^{-4}$	$1.287588 \cdot 10^{-9}$	49032.944
L2-V7	LC	333	$9.465250 \cdot 10^{-15}$	$1.366086 \cdot 10^{-2}$	$1.121407 \cdot 10^{-2}$	$5.005192 \cdot 10^{-1}$	$-2.271181 \cdot 10^{-4}$	$3.260687 \cdot 10^{-10}$	33933.170
	WC	331	$9.980472 \cdot 10^{-15}$	$1.366086 \cdot 10^{-2}$	$1.121407 \cdot 10^{-2}$	$5.005192 \cdot 10^{-1}$	$-2.271181 \cdot 10^{-4}$	$1.342291 \cdot 10^{-9}$	37958.700
	FC	331	$9.950993 \cdot 10^{-15}$	$1.366086 \cdot 10^{-2}$	$1.121407 \cdot 10^{-2}$	$5.005192 \cdot 10^{-1}$	$-2.271181 \cdot 10^{-4}$	$1.350620 \cdot 10^{-9}$	49754.553
L2-V8	LC	343	$9.721478 \cdot 10^{-15}$	$1.366086 \cdot 10^{-2}$	$1.121407 \cdot 10^{-2}$	$5.005192 \cdot 10^{-1}$	$-2.271181 \cdot 10^{-4}$	$1.093675 \cdot 10^{-8}$	14762.363
L3-V1	LC	432	$9.764342 \cdot 10^{-15}$	$1.349729 \cdot 10^{-2}$	$1.134353 \cdot 10^{-2}$	$5.006635 \cdot 10^{-1}$	$-2.269487 \cdot 10^{-4}$	$2.233854 \cdot 10^{-10}$	39640.271
	WC	432	$9.620121 \cdot 10^{-15}$	$1.349729 \cdot 10^{-2}$	$1.134353 \cdot 10^{-2}$	$5.006635 \cdot 10^{-1}$	$-2.269487 \cdot 10^{-4}$	$3.636473 \cdot 10^{-10}$	44385.632
	FC	432	$9.618753 \cdot 10^{-15}$	$1.349729 \cdot 10^{-2}$	$1.134353 \cdot 10^{-2}$	$5.006635 \cdot 10^{-1}$	$-2.269487 \cdot 10^{-4}$	$3.643944 \cdot 10^{-10}$	61648.919
L4-V1	LC	1533	$9.720890 \cdot 10^{-15}$	$1.337881 \cdot 10^{-2}$	$1.144732 \cdot 10^{-2}$	$5.005532 \cdot 10^{-1}$	$-2.275395 \cdot 10^{-4}$	$1.036436 \cdot 10^{-13}$	92330.700
	WC	1675	$9.838752 \cdot 10^{-15}$	$1.337881 \cdot 10^{-2}$	$1.144732 \cdot 10^{-2}$	$5.005532 \cdot 10^{-1}$	$-2.275395 \cdot 10^{-4}$	$8.682150 \cdot 10^{-11}$	107782.779
	FC	1674	$9.788288 \cdot 10^{-15}$	$1.337881 \cdot 10^{-2}$	$1.144732 \cdot 10^{-2}$	$5.005532 \cdot 10^{-1}$	$-2.275395 \cdot 10^{-4}$	$8.763508 \cdot 10^{-11}$	153234.620
L4-V2	LC	nan	nan	nan	nan	nan	nan	nan	nan
	WC	nan	nan	nan	nan	nan	nan	nan	nan
	FC	1043	$9.876340 \cdot 10^{-15}$	$1.337881 \cdot 10^{-2}$	$1.144732 \cdot 10^{-2}$	$5.005532 \cdot 10^{-1}$	$-2.275395 \cdot 10^{-4}$	$5.914540 \cdot 10^{-10}$	105255.627
L4-V3	LC	977	$9.793066 \cdot 10^{-15}$	$1.337881 \cdot 10^{-2}$	$1.144732 \cdot 10^{-2}$	$5.005532 \cdot 10^{-1}$	$-2.275395 \cdot 10^{-4}$	$6.748525 \cdot 10^{-12}$	67259.072
	WC	1069	$9.936983 \cdot 10^{-15}$	$1.337881 \cdot 10^{-2}$	$1.144732 \cdot 10^{-2}$	$5.005532 \cdot 10^{-1}$	$-2.275395 \cdot 10^{-4}$	$6.961520 \cdot 10^{-10}$	78474.594
	FC	1065	$9.922493 \cdot 10^{-15}$	$1.337881 \cdot 10^{-2}$	$1.144732 \cdot 10^{-2}$	$5.005532 \cdot 10^{-1}$	$-2.275395 \cdot 10^{-4}$	$7.052946 \cdot 10^{-10}$	106057.361

- Inflow Mach number: $M_\infty = 0.2$.
- Angle of attack: $\alpha = 37°$.

The selected angle of attack is beyond the stall [42] and therefore this geometry presents outstanding phenomena, such as fully separated 3D flow with several regions of reattachment. The flow field visualization at 50% of the wing span is given in figure 5.12(b). Besides that, the inflow Mach number can be considered to lay on the incompressible limit, the numerical solution to handle with all these conditions is not an easy task, making a very attractive study case. Nevertheless, it is not an straightforward example, thus full multigrid approach for the start-up phase is employed for all the computations.

Table 5.10: NASA Trap wing: Meshes data

Level	No. of points	No. of elements
Coarse (C)	3727008	10169092
Medium (M)	11047965	38017477
Fine (F)	32445391	127443165

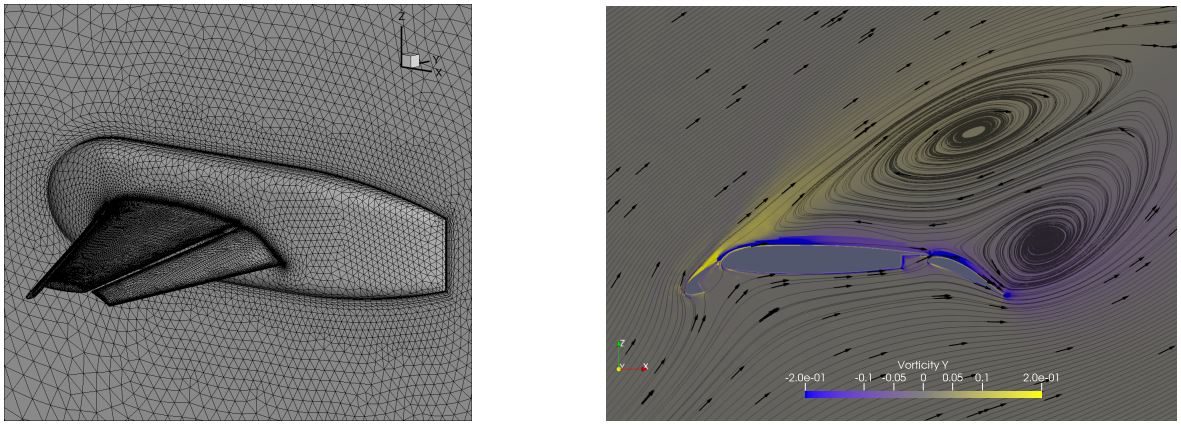

(a) NASA Trap wing geometry and mesh

(b) Y-vorticity component with streamlines visualization

Figure 5.12: NASA Trap wing: NASA Trap wing view and flow field visualization.

Table 5.11: NASA Trap wing: Solver configuration

Level	Coarse (C)								Medium (M)	Fine (F)
Algorithm	V1	V2	V3	V4	V5	V6	V7	V8	V1	V1
No. of RK stages	3	3	3	3	5	5	5	3	3	3
γ (mean, turb)	2, 2	1.1, 1.1	2, 2	1.1, 1.1	2, 2	1.1, 1.1	1.1, 1.1	2, 2	1.1, 1.1	1.1, 1.1
No. of Gauss-Seidel sweeps	5	5	7	7	5	5	7	5	5	5
No. of turb. steps per mean flow	3	3	3	3	3	3	3	1	3	3
No. of multigrid levels	3	3	3	3	3	3	3	3	3	3
$\mathrm{CFL}_{\mathrm{init}}$ (mean, turb)	3, 3	3, 3	3, 3	3, 3	3, 3	3, 3	3, 3	3, 3	3, 3	3, 3
$\mathrm{CFL}_{\mathrm{max}}$ (mean, turb)	200, 200	200, 200	200, 200	200, 200	200, 200	200, 200	200, 200	200, 200	200, 200	200, 200
Multigrid cycle (mean, turb)	3v, 3v	3v, 3v	3v, 3v	3v, 3v	3v, 3v	3v, 3v	3v, 3v	3v, 3v	3v, 3v	3v, 3v
No. of domains	72	72	72	72	72	72	72	72	192	384

Table 5.12: NASA Trap wing: Computational results

Level-Variant	Solver	Steps	Residual	$C_{D,p}$	$C_{D,v}$	$C_{L,p}$	$C_{L,v}$	Turb. Residual	Time (s)
C-V1	LC	2517	$9.965248 \cdot 10^{-15}$	$8.297993 \cdot 10^{-1}$	$8.394513 \cdot 10^{-3}$	$2.079539 \cdot 10^{0}$	$-2.213441 \cdot 10^{-3}$	$1.944808 \cdot 10^{-15}$	91664.995
	WC	nan	nan	nan	nan	nan	nan	nan	nan
	FC	nan	nan	nan	nan	nan	nan	nan	nan
C-V2	LC	2554	$9.995560 \cdot 10^{-15}$	$8.297993 \cdot 10^{-1}$	$8.394513 \cdot 10^{-3}$	$2.079539 \cdot 10^{0}$	$-2.213441 \cdot 10^{-3}$	$1.977065 \cdot 10^{-15}$	92994.130
	WC	nan	nan	nan	nan	nan	nan	nan	nan
	FC	nan	nan	nan	nan	nan	nan	nan	nan
C-V3	LC	nan	nan	nan	nan	nan	nan	nan	nan
	WC	nan	nan	nan	nan	nan	nan	nan	nan
	FC	nan	nan	nan	nan	nan	nan	nan	nan
C-V4	LC	nan	nan	nan	nan	nan	nan	nan	nan
	WC	nan	nan	nan	nan	nan	nan	nan	nan
	FC	nan	nan	nan	nan	nan	nan	nan	nan
C-V5	LC	nan	nan	nan	nan	nan	nan	nan	nan
	WC	nan	nan	nan	nan	nan	nan	nan	nan
	FC	nan	nan	nan	nan	nan	nan	nan	nan
C-V6	LC	nan	nan	nan	nan	nan	nan	nan	nan
	WC	nan	nan	nan	nan	nan	nan	nan	nan
	FC	nan	nan	nan	nan	nan	nan	nan	nan
C-V7	LC	nan	nan	nan	nan	nan	nan	nan	nan
	WC	nan	nan	nan	nan	nan	nan	nan	nan
	FC	nan	nan	nan	nan	nan	nan	nan	nan
C-V8	LC	nan	nan	nan	nan	nan	nan	nan	nan
M-V1	LC	3755	$9.978661 \cdot 10^{-15}$	$8.168753 \cdot 10^{-1}$	$9.035962 \cdot 10^{-3}$	$1.946281 \cdot 10^{0}$	$-3.143233 \cdot 10^{-3}$	$1.709689 \cdot 10^{-12}$	191973.57
	WC	nan	nan	nan	nan	nan	nan	nan	nan
	FC	nan	nan	nan	nan	nan	nan	nan	nan
F-V1	LC	3784	$9.985237 \cdot 10^{-15}$	$8.260343 \cdot 10^{-1}$	$9.073044 \cdot 10^{-3}$	$1.899156 \cdot 10^{0}$	$-3.343863 \cdot 10^{-3}$	$1.689623 \cdot 10^{-12}$	394978.55
	WC	nan	nan	nan	nan	nan	nan	nan	nan
	FC	nan	nan	nan	nan	nan	nan	nan	nan

As reported in table 5.12 most of the computations were not successful and ended with a "not a number". In particular, none of the computations for the weakly coupled or the fully coupled techniques converged to a steady state. As a further stabilization attempt we increased the number of SGS sweeps up to 35. Unfortunately, within this implementation it was possible to reach a converged solution. Finally, trying to increase the depth of the multigrid cycle has also failed. Therefore, we are not in a position to further discuss about the solving strategies.

To assess the stability, we followed the same approach as for the DPW5 CRM. The weakly coupled and fully coupled simulations have been restarted using the converged solution from the loosely coupled. These computations are very time and computational resources demanding, so it was not possible to extensively study each of them, only for the C-V1, C-V3 and C-V5. Though, as expected, the restarted computations were able to run 1000 additional multigrid cycles. Hence demonstrating once again that the implemented solution algorithms are able to provide convergence when well-posed initial conditions are given.

It can be observed that for this simulation it is very hard to obtain converged results. Indeed, comparing C-V3 with C-V1 and C-V4 with C-V2, which only difference is the number of Symmetric Gauss-Seidel sweeps, there is no theoretical understanding to answer the reason why C-V3 and C-V4 present a divergence behaviour. One expects that with more SGS sweeps the computed solution after each iteration is smoother and thus a more consistent algorithm, but obviously it is not the case. Aside from this, the loosely coupled approach with a $1:1$ ratio, computation C-V8, has not reached a steady state. These evidences clearly indicate how difficult is to set up the proper conditions for a CFD computation.

Chapter 6

CONCLUSIONS

For the present work, a complete fully coupled and the so-called weakly coupled methods for the Reynolds Averaged Navier-Stokes equations in conjunction with the one equation Negative Spalart-Allmaras turbulence model have been developed. We presented and detailed the mathematical derivation of these approaches as well as the numerical methods implemented for their discretization.

The assessment of the these solvers was based on the numerical investigation of both strategies when applied to four well known fully turbulent compressible flow benchmark test cases, including two and three dimensional geometries. In particular, the properties of the schemes were studied focusing on the accuracy, the number of cycles and convergence rate. The results have been compared with experimental data and those obtained with a loosely coupled solver under the same framework. For most of the test cases machine accuracy was reached and reasonable agreement with the experimental data is achieved, ensuring the effectiveness of the developed methods.

6.1. Summary and discussion of the results

As observed, although the coupling strategy and the linear operator $\mathbf{Prec}_j$ for the weakly and fully coupled manners are different than for the loosely coupled, there is no impact on the computed values, they are all identical, e.g. the location of the shock waves, the separation points and the lift, drag, pressure and skin friction coefficients values.

It has been shown for the CASE 9, when numerically coupling the turbulence equation to the mean flow, the number of required MG-Cycles for convergence has been considerably reduced with respect to the loosely coupled solver. Interestingly it was found that the weakly coupled and fully coupled techniques present almost the same identical behavior for all the computations, i.e., same number of cycles and convergence rate. Such an observation provides insights into the mathematical relationship between the RANS and the S-A turbulence model equations. Upon previous reflections one can therefore argue that the solver efficiency improvement is due to the coupling strategy, and accordingly, the evaluation of the cross derivatives of the Jacobian has no impact on the solution algorithm. The present results are in line with the discussion provided in section 4.2., where we highlighted that the cross terms can be approximated to zero.

For the DPW5 CRM case, the results evidence that the three solvers present almost the same number of MG-Cycles and convergence rate. This outcome reveals that the coupling strategy has no influence on the solution algorithm. Besides that, the suggested strategy, weakly coupled, presents better performances, than the fully coupled. Thus, analogously to the RAE 2822 test case the same interpretation about the cross terms of the Jacobian can be concluded.

Regarding the multi-element airfoil and the NASA Trap-Wing examples, none of the previous behaviors is observed. For all the computations, the loosely coupled technique

simply required less number of cycles and presented a better convergence rate. Further, for those examples, the results for the weakly and the fully coupled solvers fundamentally disagreed. It has been shown that for some computations the effort required to build the full Jacobian is worthwhile, as it improves the convergence of the coupling method.

It was seen that several computations for the weakly coupled and fully coupled approaches have a divergent behavior and suddenly ended with a non physical outcome. Each of these "nans" appeared on the start-up phase, that is, on the first iterations on the finest dual grid level. In this scenario, the computed solution is far from the root of the system of equations. Under this circumstance, increasing the number of stages on the implicit Runge-Kutta algorithm deteriorates the convergence of the system, and in some cases the solution is even sent far from the root. In contrast, carrying out more sweeps to solve the inner system of equations, in general smoothers the approximated solution and thereby the number of MG-cycles is decreased. For some cases, increasing the number of Symmetric Gauss-Seidel sweeps allows to stabilize the computations. Moreover, thorough the stability analysis, it could be corroborated that the largest eigenvalue from the weakly and fully coupled strategies is smaller than one. These points when combined together lead to the conclusion that the developed methods are indeed stable, and the consequence for the divergence issues from the ill-conditioned initial conditions instead.

When numerically solving the RANS equations with a turbulence model, several mathematical approximations and assumptions are made. Therefore, the characterization of the original set of equations is changed to certain level. Furthermore, the implemented solution algorithms present limitations. For instance, from a theoretical point of view, Newton's method is a very efficient and powerful technique, whereas in practice it is not straightforward to implement and does not always work. It presents several restrictions such as the initial guess may lay close to the root and the derivative shall not be equal to zero [26, 43]. Usually, when analyzing the nature of the governing equations, there is a lack of understanding on how to easily circumvented these problems. Therefore, it is a difficult task to develop robust and efficient solvers.

Not much has been said about the required computational time for the coupled strategies. As indicated, the CPU time for these solvers is larger than for the loosely coupled approach with a ratio $1:1$. Nevertheless, the development of such routines rely on private software and we must admit that they are not implemented in the most optimal way, as they have been developed to ensure good robustness instead. So, time efficiency has not been addressed for the present work despite its crucial relevance for practical and scientific purposes. Therefore, it is of major importance for future work to optimize the code for potentially eliminate the additional implementation cost and thus improve the efficiency of these algorithms.

It is important to emphasize, from the author's experience, the major difficulty to find a well-posed combination of parameter settings to successfully run a CFD simulation. As an example of this parameter sensitive situation, one can consider the computations for the L4 mesh on the DPW5CRM for the loosely coupled. As shown, when increasing the number of SGS sweeps to 5 a divergent behaviour is observed. However, when the number of SGS sweeps is increased to 5 along with a reduction of the number of multigrid levels to 3, the solution reaches a steady state.

We note that indeed the reported results are in agreement and disagreement from those found in the literature. After the application of the developed methods to four different cases, we have provided a more in depth understanding about the coupling strategies. Despite some of the investigations found in the literature which have been presented in chapter 4, we conclude that, for some circumstances, the coupled strategy has an significant effect on the solution convergence. It has been demonstrated to perform poorly or better than the loosely coupled technique. Nevertheless, the superiority or inferiority in the convergence rate is highly sensitive to the study case as well as on the solver parameters. So far, these are encouraging results to continue with the investigation.

Throughout the discussion of all major aspects for the assessment of the developed solvers, and according to the obtained results we finally arrive at a key conclusion:

> **The loosely coupled approach presented better robustness properties and computational time in comparison with the fully coupled approach**.

Nonetheless, all the results and conclusions shall be viewed with respect to the turbulence model, the solver parameters, the considered test cases and mesh sizes.

6.2. Future work

While the Negative Spalart-Allmaras turbulence model presented promising results, an interesting line for further investigation is to consider another turbulence model, such as the two equation $k-\omega$ or the $k-\varepsilon$, when both, the turbulent kinetic energy is ignored and included on the mean flow equations. For example, as suggested in [35], considerable benefits are attained when the mean flow equations introduce this term. Accounting for the coupling strategy, a level of interaction between both sets of equations is expected to be gained, since not every entry of $\frac{\partial R_{\mathrm{m}}}{\partial W_{\mathrm{t}}}$ is equal zero, probably obtaining more consistent results, and thus reducing the overall cycles.

As previously discussed, the initialization of the flow variables is not well-posed. In particular, they are not appropriate for the coupled solvers, with remarkable consideration for the turbulent variable $\tilde{\nu}$. The initial guess is far from being a good approximation, such that its normalized residual increases considerably after a few iterations, see figures 5.3(b) and 5.7(b). The magnitude of these peaks is considerably larger for the weakly and fully coupled than for the loosely coupled. Conversely, this increase in the normalized turbulent residual is not observed when the full multigrid technique is employed instead, see figure 5.11(b). Therefore, it is of importance for future investigation to consider the proper initial conditions to overcome the start up problem to expect a convergent behavior. However, as already discussed, there is no general criterion to guarantee the convergence of the Newton's method, i.e., the initial conditions shall be "sufficiently" close to the root. In that sense, for this type of investigation much more experience is needed in practice.

While the assessment of the developed solvers covered the numerical investigation of three parameters: the time step, the number os SGS sweeps and RK stages, the solution algorithms are subject to a large variety of parameters. Although it is quite difficult to find a suitable combination for all of them at the same time, it is worthwhile to

consider further work with regards to the rest of parameters, such as the relaxation parameter from the Symmetric Gauss-Seidel. Also, from the discretization perspective point of view, further investigation can be conducted to study the influence of choice of gradients, in particular to use the same method for discretization on the residual $\mathbf{R}$ as well as on the Jacobian $\frac{\mathrm{d}\mathbf{R}}{\mathrm{d}\mathbf{W}}$, possibly increasing the consistency of the Newton's method.

BIBLIOGRAPHY

[1] G. Barakos and D. Drikakis. Implicit implementation of two-equation turbulence models in compressible navier-stokes methods. *Proceedings of the 1996 7th UMIST Colloquium on Computational Fluid Dynamics, Manchester, UK, 2-3 May 1996*, 0363(January 2016), 1996. 3, 38

[2] Feng Liu and Xiaoqing Zheng. A Strongly Coupled Time-Marching Method for Solving the Navier–Stokes and. *Journal of Computational Physics*, 300:289–300, 1996. 3, 35, 38

[3] Seungsoo Lee and Dong Whan Choi. On coupling the Reynolds-averaged Navier-Stokes equations with two-equation turbulence model equations. *International Journal for Numerical Methods in Fluids*, 50(2):165–197, 2006. 3, 35, 38

[4] Robert F. Kunz and Budugur Lakshminarayana. Stability of explicit navier-stokes procedures using k-ϵ and k - ϵ/algebraic reynolds stress turbulence models. *Journal of Computational Physics*, 103(1):141–159, 1992. 3, 35, 39

[5] Stefan Langer. Preconditioned Newton methods to approximate solutions of the Reynolds averaged Navier-Stokes equations. *DLR Deutsches Zentrum fur Luft- und Raumfahrt e.V. - Forschungsberichte*, 2018-Janua(19):1–285, 2018. 4, 10, 13, 15, 18, 22, 23, 25, 43, 45, 71, 75

[6] Stefan Langer. Agglomeration multigrid methods with implicit Runge-Kutta smoothers applied to aerodynamic simulations on unstructured grids. *Journal of Computational Physics*, 277:72–100, 2014. 4, 23

[7] Brian W. Kernighan and Dennis M. Ritchie. *The C programming language*. Prentice Hall, New Jersey :, 2nd ed edition, 1988. 4

[8] Jiri Blazek. *Computational Fluid Dynamics: Principles and Applications*. 2005. 5, 6, 7, 13, 18

[9] Klaus A. Hoffmann and Steve T. Chiang. *Computational fluid dynamics Volume I*. Engineering Education System, Wichita, KS :, 4th ed. edition, 2000. 5

[10] Klaus A. Hoffmann and Steve T. Chiang. *Computational fluid dynamics Volume III*. Engineering Education System, Wichita, Kan., 4. ed., 1. print edition, 2000. 5, 6

[11] David C Wilcox. *Turbulence Modelling for CFD 3rd Edftion*. 2006. 8

[12] S. B. Pope. *Turbulent flows*. Cambridge University Press, repr. with corr. edition, 2000. 8

[13] Steven R Allmaras, Forrester T Johnson, and Philippe R. Spalart. Modifications and clarifications for the implementation of the Spalart-Allmaras turbulence model. *Seventh International Conference on Computational Fluid Dynamics*, (ICCFD7-1902):1–11, 2012. 8, 17

[14] Langley research center: Turbulence modeling resource. https://turbmodels.larc.nasa.gov/spalart.html. Accessed: February 7, 2020. 8, 44

[15] P. R. Spalart and S. R. Allmaras. One-equation turbulence model for aerodynamic flows. *Recherche aerospatiale*, (1):5–21, 1994. 9

[16] Eli Turkel. Improving the accuracy of central difference schemes. *Lecture Notes in Physics*, 10 1988. 14

[17] R.C Swanson and Eli Turkel. On central-difference and upwind schemes. *Journal of Computational Physics*, 101(2):292 – 306, 1992. 14

[18] P. L. Roe. Approximate Riemann Solvers, Parameter Vectors, and Difference Schemes. *Journal of Computational Physics*, 43:357–372, 1981. 14, 15

[19] Joel H. Ferziger, Milovan Peric, and Robert L. Street. *Computational Methods for Fluid Dynamics*. Cham: Springer, 4th edition, 2019. 16, 37

[20] Ulrich Trottenberg, C. W. Oosterlee, and Anton Schüller. *Multigrid*. Academic Press, San Diego [Calif.] [etc.] :, 2001. 18

[21] Endre Suli and David F. Mayers. *An Introduction to Numerical Analysis*. 2003. 19, 26

[22] Stefan Langer. Application of point implicit Runge-Kutta methods to inviscid and laminar flow problems using AUSM and AUSM(+) upwinding. *International Journal of Computational Fluid Dynamics*, 25(5):255, 2011. 25, 75

[23] Stefan Langer. Point and Line Implicit Methods to Improve the Efficiency and Robustness of the DLR TAU Code. *New Results in Numerical*, page 419, 2013. 25

[24] O. Axelsson. *Iterative solution methods*. Cambridge University Press, 1994. 26

[25] C. T. Kelley. *Iterative methods for linear and nonlinear equations*. Society for Industrial and Applied Mathematics, Philadelphia :, 1995. 26

[26] Steven C. Chapra and Raymond P. Canale. *Numerical methods for engineers*. McGraw-Hill, New York :, seventh edition edition, 2015. 26, 62

[27] Dimitri J. Mavriplis. Unstructured-mesh discretizations and solvers for computational aerodynamics. *AIAA Journal*, 46(6):1281–1298, 2008. 28

[28] C. Content, P. Y. Outtier, and P. Cinnella. Coupled/Uncoupled solutions of RANS equations using a Jacobian-free Newton-Krylov method. *21st AIAA Computational Fluid Dynamics Conference*, pages 1–13, 2013. 35, 38

[29] Francesco Grasso and Charles G. Speziale. Supersonic flow computations by two-equation turbulence modeling. *9th Computational Fluid Dynamics Conference, 1989*, 1989. 35, 37

[30] Lee Thong See, Liao Wei, editor="Armfield Steve W. Tong, Low Hong", Patrick Morgan, and Karkenahalli Srinivas. Turbulence modeling using artificial compressibility with implicit lu-sgs method. pages 799–800, 2003. 35

[31] C. Rossow and Roy Swanson. *Efficient Flow Computation Including Turbulent Transport*, volume 112, pages 91–99. 10 2010. 36

[32] R. C. Swanson, E. Turkel, and C. C. Rossow. Convergence acceleration of Runge-Kutta schemes for solving the Navier-Stokes equations. *Journal of Computational Physics*, 224(1):365–388, 2007. 36

[33] R. C. Swanson and C.-C. Rossow. An Initial Investigation of the Effects of Turbulence Models on the Convergence of the RK/Implicit Scheme. (August), 2008. 36

[34] M. Wasserman, Y. Mor-Yossef, I. Yavneh, and J. B. Greenberg. A robust implicit multigrid method for RANS equations with two-equation turbulence models. *Journal of Computational Physics*, 229(16):5820–5842, 2010. 36

[35] Sankaran Venkateswaran and Lutz Merkle. Analysis of preconditioning methods for the euler and navier-stokes equations. 1999. 38, 63

[36] C. Wervaecke, H. Beaugendre, and B. Nkonga. A fully coupled RANS Spalart-Allmaras SUPG formulation for turbulent compressible flows on stretched-unstructured grids. *Computer Methods in Applied Mechanics and Engineering*, 233-236:109–122, 2012. 38

[37] Alfio Quarteroni, Fausto Saleri, and Riccardo Sacco. *Numerical mathematics*. Springer, Barcelona [etc.] :, 2nd ed edition, 2007. 44

[38] Y. Saad. *Iterative methods for sparse linear systems*. SIAM, Philadelphia :, 2nd ed. edition, 2003. 44

[39] P.H. Cook, M.C.P. Firmin, M.A. McDonald, and Royal Aircraft Establishment. *Aerofoil RAE 2822: Pressure Distributions, and Boundary Layer and Wake Measurements*. Technical memorandum / Royal Aircraft Establishment. RAE, 1977. 44

[40] Steven M. Klausmeyer and John C. Lin. Comparative Results from a CFD Challenge Over a 2D Three-Element High-Lift Airfoil. *NASA Technical Memorandum 112858*, pages 1–49, 1997. 46

[41] David W. Levy, Tom Zickuhr, John Vassberg, Shreekant Agrawal, Richard A. Wahls, Shahyar Pirzadeh, and Michael J. Hemsch. Summary of data from the first AIAA CFD drag prediction workshop. *40th AIAA Aerospace Sciences Meeting and Exhibit*, pages 1–31, 2002. 54

[42] C. L. Rumsey, J. P. Slotnick, M. Long, R. A. Stuever, and T. R. Wayman. Summary of the first AIAA CFD high-lift prediction workshop. *Journal of Aircraft*, 48(6):2068–2079, 2011. 55, 57

[43] Richard L. Burden, J. Douglas. Faires, Brooks/Cole Publishing Company., and Cengage Learning (Firm). *Numerical analysis*. Brooks/Cole, Cengage Learning, [Pacific Grove (California), etc.] :, 2011. 62

APPENDICES

Appendix A

DERIVATIVE OF THE CONVECTIVE TERMS

The mean and turbulent flow inviscid fluxes equations (2.3) and (2.17) may be rewritten altogether as,

$$\langle f_c, n\rangle = V\begin{pmatrix}\rho\\ \rho u_1\\ \rho u_2\\ \rho u_3\\ \rho E\\ \tilde{\nu}\end{pmatrix} + p\begin{pmatrix}0\\ n_1\\ n_2\\ n_3\\ 0\\ 0\end{pmatrix} + Vp\begin{pmatrix}0\\ 0\\ 0\\ 0\\ 1\\ 0\end{pmatrix} = VW + p\begin{pmatrix}0\\ n_1\\ n_2\\ n_3\\ V\\ 0\end{pmatrix}. \tag{A.1}$$

The derivative of $\langle f_c, n\rangle$ yields to,

$$\frac{\partial\langle f_c, n\rangle}{\partial W} = V\mathbf{I} + W\frac{\partial V}{\partial W} + \begin{pmatrix}0\\ n_1\\ n_2\\ n_3\\ V\\ 0\end{pmatrix}\frac{\partial p}{\partial W} + p\begin{pmatrix}0\\ 0\\ 0\\ 0\\ \frac{\partial V}{\partial W}\\ 0\end{pmatrix}, \tag{A.2}$$

with

$$\frac{\partial V}{\partial W} = \frac{1}{\rho}\left(-V, n_1, n_2, n_3, 0, 0\right), \tag{A.3a}$$

$$\frac{\partial p}{\partial W} = (\gamma-1)\left(\frac{\|u\|_2^2}{2}, -u_1, -u_2, -u_3, 1, 0\right). \tag{A.3b}$$

equation (A.2) can be simplified to,

$$\frac{\partial\langle f_c, n\rangle}{\partial W} = V\mathbf{I} + \begin{pmatrix}1\\ u_1\\ u_2\\ u_3\\ H\\ \frac{\tilde{\nu}}{\rho}\end{pmatrix}\left(-V, n_1, n_2, n_3, 0, 0\right) + \begin{pmatrix}0\\ n_1\\ n_2\\ n_3\\ V\\ 0\end{pmatrix}\frac{\partial p}{\partial W}. \tag{A.4}$$

For the computation of the previous expression we note that on the one hand, can be proved that the derivative of the convective terms for the mean flow equations with respect to the mean conservative variables $\frac{\partial\langle f_c^{\mathrm{m}}, n\rangle}{\partial W_{\mathrm{m}}}$ is equal to the loosely coupled approach. For an exhaustive derivation the reader is referred to [5]. On the other hand, the derivative of mean convective fluxes with respect to the turbulent variable $\frac{\partial\langle f_c^{\mathrm{m}}, n\rangle}{\partial W_{\mathrm{t}}}$ is given by,

$$\frac{\partial(\rho V)}{\partial\tilde{\nu}} = \frac{\partial(\rho u_1 V + p n_1)}{\partial\tilde{\nu}} = \frac{\partial(\rho u_2 V + p n_2)}{\partial\tilde{\nu}} = \frac{\partial(\rho u_3 V + p n_3)}{\partial\tilde{\nu}} = \frac{\partial(\rho H V)}{\partial\tilde{\nu}} = 0.$$

Additionally, the derivative the inviscid terms for the turbulent flow equations, with respect to W is given by,

$$\frac{\partial(V\tilde{\nu})}{\partial W} = \frac{1}{\rho}\left(-V\tilde{\nu}, \tilde{\nu}n_1, \tilde{\nu}n_2, \tilde{\nu}n_3, 0, \rho V\right).$$

Thus, the resulting full matrix notation of equation (A.4) is represented as,

$$\frac{\partial\langle f_c, n\rangle}{\partial W} = \begin{pmatrix} 0 & n_1 & n_2 & n_3 & 0 & 0 \\ \frac{n_1\zeta_2\|u\|_2^2}{2} - u_1V & n_1\zeta_3u_1 + V & n_2u_1 - n_1\zeta_2u_2 & n_3u_1 - n_1\zeta_2u_3 & n_1\zeta_2 & 0 \\ \frac{n_2\zeta_2\|u\|_2^2}{2} - u_2V & n_1u_2 - n_2\zeta_2u_1 & n_2\zeta_3u_2 + V & n_3u_2 - n_2\zeta_2u_3 & n_2\zeta_2 & 0 \\ \frac{n_3\zeta_2\|u\|_2^2}{2} - u_3V & n_1u_3 - n_3\zeta_2u_1 & n_2u_3 - n_3\zeta_2u_2 & n_3\zeta_3u_3 + V & n_3\zeta_2 & 0 \\ \left(\zeta_2\|u\|_2^2 - \gamma E\right)V & n_1\zeta_1 - \zeta_2u_1V & n_2\zeta_1 - \zeta_2u_2V & n_3\zeta_1 - \zeta_2u_3V & \gamma V & 0 \\ -\frac{\tilde{\nu}}{\rho}V & \frac{\tilde{\nu}}{\rho}n_1 & \frac{\tilde{\nu}}{\rho}n_2 & \frac{\tilde{\nu}}{\rho}n_3 & 0 & V \end{pmatrix}, \tag{A.5a}$$

with

$$\Phi = \frac{1}{2}(\gamma-1)\|u\|_2^2, \qquad \zeta_1 = \gamma E - \Phi, \qquad \zeta_2 = \gamma - 1, \qquad \zeta_3 = 2 - \gamma. \tag{A.5b}$$

A.1. Eigendecomposition

The eigenvectors of $\frac{\partial\langle f_c, n\rangle}{\partial W}$, G, presented in equation (3.46) are given by,

$$g_1 = \begin{pmatrix} n_1 \\ n_1u_1 \\ n_1u_2 + an_3 \\ n_1u_3 - an_2 \\ n_1\frac{\|u\|_2^2}{2} + a(u_2n_3 - u_3n_2) \\ 0 \end{pmatrix}, \qquad g_2 = \begin{pmatrix} n_2 \\ n_2u_1 - an_3 \\ n_2u_2 \\ n_2u_3 + an_1 \\ n_2\frac{\|u\|_2^2}{2} + a(u_3n_1 - u_1n_3) \\ 0 \end{pmatrix},$$

$$g_3 = \begin{pmatrix} n_3 \\ n_3u_1 + an_2 \\ n_3u_2 - an_1 \\ n_3u_3 \\ n_3\frac{\|u\|_2^2}{2} + a(u_1n_2 - u_2n_1) \\ 0 \end{pmatrix} \qquad g_4 = \begin{pmatrix} 1 \\ u_1 + an_1 \\ u_2 + an_2 \\ u_3 + an_3 \\ H + aV \\ \frac{\tilde{\nu}}{\rho} \end{pmatrix}, \tag{A.6}$$

$$g_5 = \begin{pmatrix} 1 \\ u_1 - an_1 \\ u_2 - an_2 \\ u_3 - an_3 \\ H - aV \\ \frac{\tilde{\nu}}{\rho} \end{pmatrix}, \qquad g_6 = \begin{pmatrix} 0 \\ 0 \\ 0 \\ 0 \\ 0 \\ 1 \end{pmatrix}$$

And the inverse of G, i.e., J, by,

$$q_1 = \begin{pmatrix} \frac{\gamma-1}{a^2} n_1 \Big(H - \|u\|_2^2\Big) - \frac{1}{a}(u_2 n_3 - u_3 n_2) \\ \frac{\gamma-1}{a^2} n_1 u_1 \\ \frac{\gamma-1}{a^2} n_1 u_2 + \frac{1}{a} n_3 \\ \frac{\gamma-1}{a^2} n_1 u_3 - \frac{1}{a} n_2 \\ -\frac{\gamma-1}{a^2} n_1 \\ 0 \end{pmatrix}, \qquad q_2 = \begin{pmatrix} \frac{\gamma-1}{a^2} n_2 \Big(H - \|u\|_2^2\Big) - \frac{1}{a}(u_3 n_1 - u_1 n_3) \\ \frac{\gamma-1}{a^2} n_2 u_1 - \frac{1}{a} n_3 \\ \frac{\gamma-1}{a^2} n_2 u_2 \\ \frac{\gamma-1}{a^2} n_2 u_3 + \frac{1}{a} n_1 \\ -\frac{\gamma-1}{a^2} n_2 \\ 0 \end{pmatrix},$$

$$q_3 = \begin{pmatrix} \frac{\gamma-1}{a^2} n_3 \Big(H - \|u\|_2^2\Big) - \frac{1}{a}(u_1 n_2 - u_2 n_1) \\ \frac{\gamma-1}{a^2} n_3 u_1 + \frac{1}{a} n_2 \\ \frac{\gamma-1}{a^2} n_3 u_2 - \frac{1}{a} n_1 \\ \frac{\gamma-1}{a^2} n_3 u_3 \\ -\frac{\gamma-1}{a^2} n_3 \\ 0 \end{pmatrix}, \qquad q_4 = \frac{1}{2a^2} \begin{pmatrix} (\gamma-1)\frac{\|u\|_2^2}{2} - aV \\ -(\gamma-1)u_1 + an_1 \\ -(\gamma-1)u_2 + an_2 \\ -(\gamma-1)u_3 + an_3 \\ (\gamma-1) \\ 0 \end{pmatrix}^T,$$

$$q_5 = \frac{1}{2a^2} \begin{pmatrix} (\gamma-1)\frac{\|u\|_2^2}{2} + aV \\ -(\gamma-1)u_1 - an_1 \\ -(\gamma-1)u_2 - an_2 \\ -(\gamma-1)u_3 - an_3 \\ (\gamma-1) \\ 0 \end{pmatrix}^T, \qquad q_6 = \frac{\tilde{\nu}(\gamma-1)}{\rho a^2} \begin{pmatrix} -\frac{\|u\|_2^2}{2} \\ u_1 \\ u_2 \\ u_3 \\ -1, \\ \frac{\rho a^2}{\tilde{\nu}(\gamma-1)} \end{pmatrix}^T. \tag{A.7}$$

A.2. The implemented Roe matrix

For completeness we consider all entries of the Roe matrix given by equation (3.55),

$$\Big|A^{\mathrm{Roe}}\Big|_{\mathrm{ef}} = \begin{pmatrix} \Big|A^{\mathrm{Roe}}\Big|_{\mathrm{ef}_{(1,1)}} & \cdots & \Big|A^{\mathrm{Roe}}\Big|_{\mathrm{ef}_{(1,6)}} \\ \vdots & \ddots & \vdots \\ \Big|A^{\mathrm{Roe}}\Big|_{\mathrm{ef}_{(6,1)}} & \cdots & \Big|A^{\mathrm{Roe}}\Big|_{\mathrm{ef}_{(6,6)}} \end{pmatrix}, \tag{A.8}$$

$$\begin{aligned}
\Big|A^{\mathrm{Roe}}\Big|_{\mathrm{ef}_{(1,1)}} &= |V|_{\mathrm{ef}_1} - V M_0^{(1)} + \frac{1}{a}(\gamma-1)\frac{\|u\|_2^2}{2} M_0^{(2)}, \\
\Big|A^{\mathrm{Roe}}\Big|_{\mathrm{ef}_{(1,i+1)}} &= n_i M_0^{(1)} + (1-\gamma)\frac{u_i}{a} M_0^{(2)}, \qquad i = 1,2,3, \\
\Big|A^{\mathrm{Roe}}\Big|_{\mathrm{ef}_{(1,5)}} &= \frac{1}{a}(\gamma-1) M_0^{(2)}, \\
\Big|A^{\mathrm{Roe}}\Big|_{\mathrm{ef}_{(1,6)}} &= 0, \\
\Big|A^{\mathrm{Roe}}\Big|_{\mathrm{ef}_{(i+1,1)}} &= \frac{\|u\|_2^2}{2}(\gamma-1)\Big(\frac{1}{a} u_i M_0^{(2)} + n_i M_0^{(1)}\Big) - \\
&\qquad V\Big(a n_i M_0^{(2)} + u_i 1 M_0^{(1)}\Big), \qquad i = 1,2,3,
\end{aligned}$$

$$
\begin{aligned}
\left|A^{\mathrm{Roe}}\right|_{\mathrm{ef}_{(i+1,j+1)}} &= n_j u_i 1 M_0^{(1)} + \delta_{ij}|V|_{\mathrm{ef}_1} + n_i n_j M_0^{(2)} + \\
&\qquad (1-\gamma)u_j\Big(\frac{1}{a}u_i M_0^{(2)} + n_i 1 M_0^{(1)}\Big), \quad i,j = 1,2,3, \\
\left|A^{\mathrm{Roe}}\right|_{\mathrm{ef}_{(i+1,5)}} &= (\gamma-1)\Big(\frac{1}{a}u_i M_0^{(2)} + n_i 1 M_0^{(1)}\Big), \quad i = 1,2,3, \\
\left|A^{\mathrm{Roe}}\right|_{\mathrm{ef}_{(i+1,6)}} &= 0, \\
\left|A^{\mathrm{Roe}}\right|_{\mathrm{ef}_{(5,1)}} &= -V^2 a M_0^{(2)} - V H M_0^{(1)} + \frac{\|u\|_2^2}{2}(\gamma-1)\Big(V M_0^{(1)} + \frac{1}{a}H M_0^{(2)}\Big), \\
\left|A^{\mathrm{Roe}}\right|_{\mathrm{ef}_{(5,i+1)}} &= (1-\gamma)\Big(V M_0^{(1)} + \frac{1}{a}H M_0^{(2)}\Big) + n_i V a M_0^{(2)} + n_i H M_0^{(1)}, \qquad i = 1,2,3, \\
\left|A^{\mathrm{Roe}}\right|_{\mathrm{ef}_{(5,5)}} &= |V|_{\mathrm{ef}_1} + (\gamma-1)\Big(V M_0^{(1)} + \frac{1}{a}H M_0^{(2)}\Big), \\
\left|A^{\mathrm{Roe}}\right|_{\mathrm{ef}_{(5,6)}} &= 0, \\
\left|A^{\mathrm{Roe}}\right|_{\mathrm{ef}_{(6,1)}} &= \frac{1}{\rho}\Big[\frac{\tilde{\nu}}{a}(\gamma-1)\frac{\|u\|_2^2}{2}M_0^{(2)} - \tilde{\nu}V M_0^{(1)}\Big], \\
\left|A^{\mathrm{Roe}}\right|_{\mathrm{ef}_{(6,i+1)}} &= \frac{1}{\rho}\Big[\tilde{\nu}n_i M_0^{(1)} + \tilde{\nu}(1-\gamma)\frac{u_i}{a}M_0^{(2)}\Big], \qquad i = 1,2,3, \\
\left|A^{\mathrm{Roe}}\right|_{\mathrm{ef}_{(6,5)}} &= \frac{1}{\rho}\Big[\frac{1}{a}(\gamma-1)\tilde{\nu}M_0^{(2)}\Big], \\
\left|A^{\mathrm{Roe}}\right|_{\mathrm{ef}_{(6,6)}} &= |V|_{\mathrm{ef}_1}
\end{aligned}
$$

Appendix B

DERIVATIVE OF THE VISCOUS TERMS

In this section we will use the the superscripts "m" and "t" refer to the mean and turbulent systems of equations respectively.

We start the discussion by recalling the definition of the viscous terms for the mean flow equations, see equation (2.3). These equations do not depend on the turbulent variables W_{t}. As a consequence, its derivative with respect to the turbulent variable $\tilde{\nu}$ is straightforward,

$$\frac{\partial \langle f_v^{\mathrm{m}}, n\rangle}{\partial \tilde{\nu}} = 0. \tag{B.1}$$

On the one hand, to complete the derivative of the mean flow equations, we require the derivative of the viscous fluxes with respect to the mean flow variables $\frac{\partial \langle f_v^{\mathrm{m}}, n\rangle}{\partial W_{\mathrm{m}}}$. An exhaustive and detailed computation of these terms is provided in [5, Section 4.3] and [22]. Since these computations do not depend whether the turbulent equations are coupled or not to the mean flow, they are not explicitly written in here.

On the other hand, we additionally require the derivative of turbulent component $\left\langle f_v^{\mathrm{t}}, n\right\rangle$ with respect to both, the mean and the turbulent variables. It is the goal of this section to present such computations.

We recall that our conservative variables vector together with the turbulent variable is given by,

$$W = (W_{\mathrm{m}}, W_{\mathrm{t}})^T = (\rho, \rho u_1, \rho u_2, \rho u_3, \rho E, \tilde{\nu})^T.$$

Before defining the whole set of derivatives, we recall from section 3.1.3. that in order to discretize the viscous terms we use an averaging of the variables on the face. Thus, the following holds,

$$\nu_{l,ij} = \frac{1}{2}\big(\nu_{l,i} + \nu_{l,j}\big), \qquad \tilde{\nu}_{ij} = \frac{1}{2}(\tilde{\nu}_i + \tilde{\nu}_j). \tag{B.2}$$

For the Spalart-Allmaras model, the derivative of the viscous terms f_v for $\tilde{\nu} \geq 0$ yields to,

$$\frac{\partial \left\langle f_v^t, n\right\rangle}{\partial W_j} = \frac{\partial}{\partial W_j}\left(\frac{\nu_{l,ij} + \tilde{\nu}_{ij}}{\sigma}\right)\sum_{k=1}^{3} n_k \left(\frac{\partial \tilde{\nu}}{\partial x_k}\right)_{ij} + \frac{\nu_{l,ij} + \tilde{\nu}_{ij}}{\sigma}\frac{\partial}{\partial W_j}\left(\sum_{k=1}^{3} n_k \left(\frac{\partial \tilde{\nu}}{\partial x_k}\right)_{ij}\right). \tag{B.3}$$

The second derivative appearing on the right hand side of previous expression leads to,

$$\frac{\partial}{\partial W_j}\left(\sum_{k=1}^{3} n_k \left(\frac{\partial \tilde{\nu}}{\partial x_k}\right)_{ij}\right) = \sum_{k=1}^{3} n_k \frac{\partial}{\partial W_j}\left(\frac{\partial \tilde{\nu}}{\partial x_k}\right)_{ij}. \tag{B.4}$$

We use TSL approximation (see equation (3.17)) for the computation of the gradient $\frac{\partial\tilde{\nu}}{\partial x_k}$ on the face ij:

$$\frac{\partial}{\partial W_j}\left(\frac{\partial\tilde{\nu}}{\partial x_k}\right)_{ij} = \frac{n_k}{\Delta\left(p^{(j)},p^{(i)}\right)}\frac{\partial\tilde{\nu}_j}{\partial W_j}. \tag{B.5}$$

Substituting previous expression into equation (B.4) gives the result,

$$\frac{\partial}{\partial W_j}\left(\sum_{k=1}^{3} n_k\left(\frac{\partial\tilde{\nu}}{\partial x_k}\right)_{ij}\right) = \frac{1}{\Delta\left(p^{(j)},p^{(i)}\right)}\frac{\partial\tilde{\nu}_j}{\partial W_j}. \tag{B.6}$$

The first derivative appearing on the right hand side of equation (B.3) is formulated as:

$$\frac{\partial}{\partial W_j}\left(\frac{\nu_{l,ij}+\tilde{\nu}_{ij}}{\sigma}\right) = \frac{1}{\sigma}\left(\frac{\partial\nu_{l,ij}}{\partial W_j}+\frac{\partial\tilde{\nu}_{ij}}{\partial W_j}\right), \tag{B.7}$$

where the derivative of the laminar kinematic viscosity is given by,

$$\frac{\partial\nu_{l,ij}}{\partial W_j} = \frac{1}{2}\frac{1}{\rho_j^2}\left(\rho_j\frac{\partial\mu_{l,j}}{\partial W_j}-\mu_{l,j}\frac{\partial\rho_j}{\partial W_j}\right). \tag{B.8}$$

As was already stated in section 3.2.3., μ_l is assumed to be constant (rule 3)), and hence previous expression is reduced to:

$$\frac{\partial\nu_{l,ij}}{\partial W_j} = -\frac{1}{2}\frac{1}{\rho_j^2}\mu_{l,j}\frac{\partial\rho_j}{\partial W_j}. \tag{B.9}$$

The derivative of the turbulent kinematic viscosity is written as,

$$\frac{\partial\tilde{\nu}_{ij}}{\partial W_j} = \frac{1}{2}\frac{\partial\tilde{\nu}_j}{\partial W_j}. \tag{B.10}$$

Wrapping it up, equation (B.7) is reformulated as,

$$\frac{\partial}{\partial W_j}\left(\frac{\nu_{l,ij}+\tilde{\nu}_{ij}}{\sigma}\right) = \frac{1}{\sigma}\frac{1}{2}\left(\frac{\partial\tilde{\nu}_j}{\partial W_j}-\frac{1}{\rho_j^2}\mu_{l,j}\frac{\partial\rho_j}{\partial W_j}\right). \tag{B.11}$$

With equations (B.6) and (B.8), equation (B.3) reads,

$$\frac{\partial\left\langle f_v^t,n\right\rangle}{\partial W_j} = \frac{1}{\sigma}\frac{1}{2}\left(\frac{\partial\tilde{\nu}_j}{\partial W_j}-\frac{1}{\rho_j^2}\mu_{l,j}\frac{\partial\rho_j}{\partial W_j}\right)\sum_{k=1}^{3} n_k\frac{\partial\tilde{\nu}}{\partial x_k}+\frac{\nu_{l,ij}+\tilde{\nu}_{ij}}{\sigma}\frac{1}{\Delta\left(p^{(j)},p^{(i)}\right)}\frac{\partial\tilde{\nu}_j}{\partial W_j}. \tag{B.12}$$

The term $\sum_{k=1}^{3} n_k\left(\frac{\partial\tilde{\nu}}{\partial x_k}\right)_{ij}$ may be rewritten using TSL as,

$$\sum_{k=1}^{3} n_k\left(\frac{\partial\tilde{\nu}}{\partial x_k}\right)_{ij} = \frac{\tilde{\nu}_j-\tilde{\nu}_i}{\Delta\left(p^{(j)},p^{(i)}\right)}.$$

Finally, equation (B.12) can be rewritten as,

$$\frac{\partial\left\langle f_v^t, n\right\rangle}{\partial W_j} = \frac{1}{\Delta\left(p^{(j)}, p^{(i)}\right)} \frac{1}{\sigma}\left[\frac{1}{2}\left(\frac{\partial \tilde{\nu}_j}{\partial W_j} - \frac{1}{\rho_j^2}\mu_{l,j}\frac{\partial \rho_j}{\partial W_j}\right)\left(\tilde{\nu}_j - \tilde{\nu}_i\right) + \left(\nu_{l,ij} + \tilde{\nu}_{ij}\right)\frac{\partial \tilde{\nu}_j}{\partial W_j}\right]. \tag{B.13}$$

Previous derivation has been presented only for point j. The derivative on point i is straightforward. Analogously,

$$\frac{\partial\left\langle f_v^t, n\right\rangle}{\partial W_i} = \frac{1}{\Delta\left(p^{(j)}, p^{(i)}\right)} \frac{1}{\sigma}\left[\frac{1}{2}\left(\frac{\partial \tilde{\nu}_i}{\partial W_i} - \frac{1}{\rho_i^2}\mu_{l,i}\frac{\partial \rho_i}{\partial W_i}\right)\left(\tilde{\nu}_j - \tilde{\nu}_i\right) - \left(\nu_{l,ij} + \tilde{\nu}_{ij}\right)\frac{\partial \tilde{\nu}_i}{\partial W_i}\right]. \tag{B.14}$$

On the other hand, for $\tilde{\nu} < 0$ we have,

$$\frac{\partial\left\langle f_v^t, n\right\rangle}{\partial W_j} = \frac{\partial}{\partial W_j}\left(\frac{\nu_{l,ij} + f_{n,ij}\tilde{\nu}_{ij}}{\sigma}\right)\sum_{k=1}^{3} n_k\left(\frac{\partial \tilde{\nu}}{\partial x_k}\right)_{ij} + \frac{\nu_{l,ij} + f_{n,ij}\tilde{\nu}_{ij}}{\sigma}\frac{\partial}{\partial W_j}\left(\sum_{k=1}^{3} n_k\left(\frac{\partial \tilde{\nu}}{\partial x_k}\right)_{ij}\right). \tag{B.15}$$

The second derivative appearing on the right hands side of previous expression is already computed in equation (B.4). The first derivative appearing in equation (B.15) is formulated as:

$$\frac{\partial}{\partial W_j}\left(\frac{\nu_{l,ij} + f_{n,ij}\tilde{\nu}_{ij}}{\sigma}\right) = \frac{1}{\sigma}\left(\frac{\partial \nu_{l,ij}}{\partial W_j} + \frac{\partial\left(f_{n,ij}\tilde{\nu}_{ij}\right)}{\partial W_j}\right) = \frac{1}{\sigma}\left(\frac{\partial \nu_{l,ij}}{\partial W_j} + f_{n,ij}\frac{\partial \tilde{\nu}_{ij}}{\partial W_j} + \tilde{\nu}_{ij}\frac{\partial f_{n,ij}}{\partial W}\right). \tag{B.16}$$

The first two addends are computed in equations (B.8) and (B.10) respectively, meanwhile the last term in equation (B.16) is given by:

$$\frac{\partial f_{n,ij}}{\partial W_j} = \frac{2c_{n1}\frac{\partial \chi_{ij}^3}{\partial W_j}}{\left(c_{n1} - \chi_{ij}^3\right)^2}, \tag{B.17}$$

with

$$\begin{aligned}\frac{\partial \chi_{ij}^3}{\partial W_j} = \frac{\partial}{\partial W_j}\left[\frac{1}{2}\left(\chi_j^3 + \chi_i^3\right)\right] = \frac{1}{2}3\chi_j^2\frac{\partial\left(\frac{\rho_j\tilde{\nu}_j}{\mu_{l,j}}\right)}{\partial W_j} &= \frac{3\chi_j^2}{2}\frac{\mu_{l,j}\frac{\partial\left(\rho_j\tilde{\nu}_j\right)}{\partial W_j} - \rho_j\tilde{\nu}_j\frac{\partial \mu_{l,j}}{\partial W_j}}{\mu_{l,j}^2} \\ &= \frac{3\chi_j^2}{2}\frac{1}{\mu_{l,j}}\left(\frac{\partial\left(\rho_j\tilde{\nu}_j\right)}{\partial W_j} - \chi\frac{\partial \mu_{l,j}}{\partial W_j}\right).\end{aligned} \tag{B.18}$$

The laminar viscosity is considered constant and thus, previous expression is reduced to,

$$\frac{\partial \chi_{ij}^3}{\partial W_j} = \frac{1}{2}3\chi_j^2\frac{\rho_j}{\mu_{l,j}}\frac{\partial \tilde{\nu}_j}{\partial W_j}. \tag{B.19}$$

Thus, equation (B.17) is simplified to,

$$\frac{\partial f_{n,ij}}{\partial W_j} = \frac{3\chi_j^2 c_{n1}}{\left(c_{n1} - \chi_{ij}^3\right)^2}\frac{\rho_j}{\mu_{l,j}}\frac{\partial \tilde{\nu}_j}{\partial W_j}. \tag{B.20}$$

With equations (B.8), (B.10) and (B.20), equation (B.16) is rewritten as,

$$\frac{\partial}{\partial W_j}\left(\frac{\nu_{l,ij}+f_{n,ij}\tilde{\nu}_{ij}}{\sigma}\right)=-\frac{1}{2}\frac{1}{\rho_j^2}\mu_{l,j}\frac{\partial\rho_j}{\partial W_j}+f_{n,ij}\frac{1}{2}\frac{\partial\tilde{\nu}_j}{\partial W_j}+\tilde{\nu}_{ij}\frac{3\chi_j^2c_{n1}}{\left(c_{n1}-\chi_{ij}^3\right)^2}\frac{\rho_j}{\mu_{l,j}}\frac{\partial\tilde{\nu}_j}{\partial W_j}. \tag{B.21}$$

Finally, equation (B.15) is reformulated and written as,

$$\frac{\partial\left\langle f_v^t,n\right\rangle}{\partial W_j}=\left(-\frac{1}{2}\frac{1}{\rho_j^2}\mu_{l,j}\frac{\partial\rho_j}{\partial W_j}+f_{n,ij}\frac{1}{2}\frac{\partial\tilde{\nu}_j}{\partial W_j}+\tilde{\nu}_{ij}\frac{3\chi_j^2c_{n1}}{\left(c_{n1}-\chi_{ij}^3\right)^2}\frac{\rho_j}{\mu_{l,j}}\frac{\partial\tilde{\nu}_j}{\partial W_j}\right)\sum_{k=1}^{3}n_k\left(\frac{\partial\tilde{\nu}}{\partial x_k}\right)_{ij}+\frac{\nu_{l,ij}+f_{n,ij}\tilde{\nu}_{ij}}{\sigma}\frac{1}{\Delta\left(p^{(j)},p^{(i)}\right)}\frac{\partial\tilde{\nu}_j}{\partial W_j}, \tag{B.22}$$

which can be simplified and rewritten in the following form,

$$\frac{\partial\left\langle f_v^t,n\right\rangle}{\partial W_j}=\frac{1}{\Delta\left(p^{(j)},p^{(i)}\right)}\left[\left(-\frac{1}{2}\frac{\mu_{l,j}}{\rho_j^2}\frac{\partial\rho_j}{\partial W_j}+f_{n,ij}\frac{1}{2}\frac{\partial\tilde{\nu}_j}{\partial W_j}+\tilde{\nu}_{ij}\frac{3\chi_j^2c_{n1}}{\left(c_{n1}-\chi_{ij}^3\right)^2}\frac{\rho_j}{\mu_{l,j}}\frac{\partial\tilde{\nu}_j}{\partial W_j}\right)(\tilde{\nu}_j-\tilde{\nu}_i)+\frac{\nu_{l,ij}+f_{n,ij}\tilde{\nu}_{ij}}{\sigma}\frac{\partial\tilde{\nu}_j}{\partial W_j}\right]. \tag{B.23}$$

Analogously for point i,

$$\frac{\partial\langle f_v,n\rangle}{\partial W_i}=\frac{1}{\Delta\left(p^{(j)},p^{(i)}\right)}\left[\left(-\frac{1}{2}\frac{\mu_{l,i}}{\rho_i^2}\frac{\partial\rho_i}{\partial W_i}+f_{n,ij}\frac{1}{2}\frac{\partial\tilde{\nu}_i}{\partial W_i}+\tilde{\nu}_{ij}\frac{3\chi_i^2c_{n1}}{\left(c_{n1}-\chi_{ij}^3\right)^2}\frac{\rho_i}{\mu_{l,i}}\frac{\partial\tilde{\nu}_i}{\partial W_i}\right)(\tilde{\nu}_j-\tilde{\nu}_i)-\frac{\nu_{l,ij}+f_{n,ij}\tilde{\nu}_{ij}}{\sigma}\frac{\partial\tilde{\nu}_i}{\partial W_i}\right]. \tag{B.24}$$

DLR-IB-AS-BS-2020-25

Coupling strategies for solving the RANS equations

Guillermo Suárez Martínez

Verteiler:

Institutsbibliothek	1 Exemplar
Verfasser	5 Exemplare
Institutsleitung	1 Exemplar
Abteilungsleiter	1 Exemplar
Deutsche Bibliothek in Frankfurt/Main	2 Exemplare
Niedersächsische Landesbibliothek Hannover	1 Exemplar
Techn. Informationsbibliothek Hannover	1 Exemplar
Zentralbibliothek BS	2 Exemplare
Zentralarchiv GÖ	1 Exemplar
Reserve	5 Exemplare